

Symmetry restoration for TDiff scalar fields

Darío Jaramillo-Garrido,^{*} Antonio L. Maroto,[†] and Prado Martín-Moruno[‡]

*Departamento de Física Teórica and Instituto de Física de Partículas y del Cosmos (IPARCOS-UCM),
Universidad Complutense de Madrid, E-28040 Madrid, Spain*

(Dated: February 2024)

We explore the idea of restoring the full diffeomorphism (Diff) invariance in theories with only transverse diffeomorphisms (TDiff) by the introduction of additional fields. In particular, we consider in detail the case of a TDiff invariant scalar field and how Diff symmetry can be restored by introducing an additional vector field. We reobtain the corresponding dynamics and energy-momentum tensor from the covariantized action and analyze the potential and kinetic domination regimes. For the former, the theory describes a cosmological constant-type behaviour, while for the latter we show that the theory can describe an adiabatic perfect fluid whose equation of state and speed of sound is obtained in a straightforward way.

I. INTRODUCTION

Our current best description of gravitational phenomena is, and has been for over a century, the theory of General Relativity (GR). It is not a theory without weaknesses, however, and although it performs remarkably well in numerous tests on solar system scales, there is reason to believe that it is not the end of the story. For one, it is not a theory which serves to describe gravity in its most extreme regimes, where one expects quantum effects to gain importance, but it is also possible to find problems even while remaining classical. Indeed, the various tensions between theory and observations in cosmology are another hint at the possibility that the theory breaks down at such scales. Sparked by considerations of the sort, together with other theoretical issues such as the cosmological constant problem, modified theories of gravity have been a central object of study in this regard (see e.g. [1] for a review).

In particular, it proves worthwhile to reconsider the fundamental symmetries involved in GR, namely the diffeomorphism (Diff) invariance of the theory. This amounts to the assertion that the physical equations remain invariant under general coordinate transformations. The study of situations where such a symmetry is broken can in fact be traced back to Einstein himself in 1919 with the introduction of Unimodular Gravity [2], where the metric determinant is reduced to be a non-dynamical field fixed to the value $g = 1$. Unimodular Gravity is perhaps the most well-known example of a theory with broken Diff invariance, being the symmetry group in that case the union of transverse diffeomorphisms (TDiff) and Weyl rescalings (together dubbed WTDiff, see e.g. [3] for a review). The equations of motion of the theory are the trace-free Einstein equations (see e.g. [4] for a comprehensive introduction), in which any cosmological constant-type contribution does not gravitate, thus pro-

viding an elegant solution to the cosmological constant problem.

In more recent years, interest has grown in theories which present TDiff invariance. Simply put, transverse diffeomorphisms are general coordinate transformations in which the Jacobian determinant is required to be $J = 1$. Infinitesimally, if we consider the coordinate transformation $x^\mu \rightarrow \hat{x}^\mu = x^\mu + \xi^\mu(x)$ generated by a vector field $\xi^\mu(x)$, then what we do is require the condition $\partial_\mu \xi^\mu = 0$ (see [5] for a concise introduction to transverse diffeomorphisms). The fact that the Jacobian determinant equals unity means that objects which were tensor densities under Diff become actual tensors under TDiff. In particular, the metric determinant becomes a TDiff scalar field, and this has interesting implications. Indeed, on the one hand, the metric determinant becomes a scalar field to which one may endow dynamics. On the other hand, the invariant volume element we find in an action integral is no longer fixed by the symmetry to be $d\text{vol} = \sqrt{g} d^4x$, but can actually take on the more general form $d\text{vol} = f(g) d^4x$, with $f(g)$ an arbitrary function of the metric determinant, and this opens up an enormous range of possibilities for novel couplings. Field theories in which the gravitational sector is TDiff invariant are studied in references [6–10], where cosmological implications are also discussed. One can also study the consequences of breaking the symmetries in the matter sector. TDiff invariant theories with a scalar field were recently considered in references [5, 11–13]. Reference [5] considers general scalar field TDiff theories in cosmological contexts, reference [12] performs a general study for a scalar field without assuming any background geometry, and reference [13] provides a unified description for the dark sector using a particular theory, comparing the results with the latest cosmological observations and datasets.

Now, it is not an uncommon situation in physics to find several equivalent descriptions, or reformulations, of the same theory. Examples include, but are by no means limited to, the well-known equivalence between the Palatini and the metric approach to GR, the scalar-tensor perspective of $f(R)$ -gravity (see, for example, [1]), the correspondence between the field equations of non linear Ricci-based metric-affine theories of gravity coupled

^{*} djaramil@ucm.es

[†] maroto@ucm.es

[‡] pradomm@ucm.es

GW Backgrounds associated with PBHs

GUILLEM DOMÈNECH^{a,b}

^a*Institute for Theoretical Physics, Leibniz University Hannover,
Appelstraße 2, 30167 Hannover, Germany. and*

^b*Max-Planck-Institut für Gravitationsphysik,
Albert-Einstein-Institut, 30167 Hannover, Germany*

PBH formation requires high-density regions in the (random) density field filling the primordial universe. While only the largest (and so rarest) overdensities collapse to form PBHs, the rest cause large anisotropic stresses, which are the source of GWs. We provide an overview of the theoretical aspects of the GW backgrounds associated with PBHs from large primordial fluctuations. We consider GW backgrounds associated with PBH formation, PBH reheating and unresolved PBH binaries. We present several graphical summaries and illustrations for the busy reader.

I. INTRODUCTION

Whenever there are fluctuations on top of the isotropic and homogeneous primordial universe, there is a secondary generation of GWs. Kenji Tomita was the first to write about this effect in the '70s in Ref. [1], saying that “gravitational waves are induced by deformed density perturbations”. Our interpretation of Ref. [1] is that by “deformed density perturbations” Tomita meant the anisotropic stress resulting from the presence of density perturbations. This will be clear later from Fig. 1. This effect, which we will call induced GWs, was later studied in the '90s by Matarrese, Pantano and Saez [2, 3] and by Matarrese, Mollerach and Bruni [4]. Ten years later, in 2006, we find a glimpse of the potential of induced GWs by Ananda, Clarkson and Wands [5], where they considered an “excess power in a single mode” from the power spectrum measured by CMB observations (and also using a notation very similar to the current one). A very nice work by Baumann, Steinhardt, Takahashi and Ichiki [6] hinted that induced GWs could be enhanced during a matter-dominated phase (see also Refs. [7, 8]). But, it was not until 2008 that Saito and Yokoyama [9, 10] made the connection between induced GWs and PBHs. Their idea was quickly followed by Bugaev and Klimai [11–13]. For more details on the early history of induced GWs and recent developments, we refer the reader to Ref. [14] for a recent review on the topic by the author of this chapter. Other helpful reviews can be found in Refs. [15–18].

Induced GWs are a crucial observable for any PBH scenario. As it will be evident by the end of this chapter, an induced GW background must be present if there is (or was) a significant fraction of PBHs in the universe. Though the opposite is not always true, the induced GW background might suggest, or strongly exclude, PBHs as a significant fraction of DM. This chapter will aim to introduce the main formulas and predictions for the GW backgrounds associated with PBHs, focusing on a qualitative and intuitive understanding of the physics behind such GWs and the

* guillem.domenech@itp.uni-hannover.de

BSW phenomenon for near-fine-tuned particles with external force: general classification of scenarios

H.V.Ovcharenko

Department of Physics, V.N.Karazin Kharkov

National University, 61022 Kharkov, Ukraine and

*Institute of Theoretical Physics, Faculty of Mathematics and Physics,
Charles University, Prague, V Holesovickach 2, 180 00 Praha 8, Czech Republic*

O.B.Zaslavskii

Department of Physics and Technology,

Kharkov V.N. Karazin National University,

4 Svoboda Square, Kharkov 61022, Ukraine

Abstract

If two particles moving towards a black hole collide in the vicinity of the horizon, the energy $E_{c.m.}$ in the center of mass frame can grow indefinitely if one of particles is fine-tuned. This is the Bañados, Silk and West (BSW) effect. One of objections against this effect consists in that for some types of a horizon fine-tuned particles cannot reach the horizon. However, this difficulty can be overcome if instead of exact fine-tuning, one of particle is nearly fine-tuned, with the value of small detuning being adjusted to the distance to the horizon. Such particles are called near-fine-tuned. We give classification of such particles and describe possible high energy scenarios of collision in which they participate. We analyze the ranges of possible motion for each type of particle and determine under which condition such particles can reach the horizon. We analyze collision energy $E_{c.m.}$ and determine under which conditions it may grow indefinitely. We also include into consideration the forces acting on particles and find when the BSW effect with nearly-fine-tuned particles is possible with finite forces. We demonstrate that the BSW effect with particles under discussion is consistent with the principle of kinematic censorship. According to this principle, $E_{c.m.}$ cannot be literally infinite in any event of collision (if no singularity is present), although it can be made as large as one likes.

Correlated 0.01Hz - 40 Hz seismic and Newtonian noise and its impact on future gravitational-wave detectors

Kamiel Janssens^{1,2}, Guillaume Boileau³, Nelson Christensen², Nick van Remortel¹, Francesca Badaracco^{4,5}, Benjamin Canuel⁶, Alessandro Cardini⁷, Andrea Contu⁷, Michael W. Coughlin⁸, Jean-Baptiste Decitre⁹, Rosario De Rosa^{10,11}, Matteo Di Giovanni^{12,13}, Domenico D’Urso^{14,7}, Stéphane Gaffet⁹, Carlo Giunchi¹⁵, Jan Harms^{16,17}, Soumen Koley^{16,17}, Valentina Mangano¹³, Luca Naticchioni¹³, Marco Olivieri¹⁸, Federico Paoletti¹⁹, Davide Rozza^{14,7}, Dylan O. Sabulsky⁹, Shahar Shani-Kadmiel²⁰ and Lucia Trozzo¹¹

¹*Universiteit Antwerpen, Prinsstraat 13, 2000 Antwerpen, Belgium*

²*Université Côte d’Azur, Observatoire de la Côte d’Azur, CNRS, Artemis, 06304 Nice, France*

³*Université Côte d’Azur, Observatoire de la Côte d’Azur, CNRS, Laboratoire Lagrange, 06304 Nice, France*

⁴*Università degli studi di Genova, via Dodecaneso 33, 16146, Italy*

⁵*INFN, Sez. di Genova, via Dodecaneso 33, 16146, Italy*

⁶*LP2N, Laboratoire Photonique, Numérique et Nanosciences, Université Bordeaux–IOGS–CNRS:UMR 5298, rue F. Mitterrand, F-33400 Talence, France*

⁷*INFN, sezione di Cagliari, I-09042, Monserrato (Cagliari), Italy*

⁸*School of Physics and Astronomy, University of Minnesota, Minneapolis, Minnesota 55455, USA*

⁹*Laboratoire Souterrain à Bas Bruit (LSBB), CNRS: UAR3538, Avignon University, Rustrel F-84400, France*

¹⁰*Università Federico II Napoli, 80126 Napoli, Italy*

¹¹*INFN - sezione di Napoli, 80126 Napoli, Italy*

¹²*La Sapienza Università di Roma, I-00185 Roma, Italy*

¹³*INFN, Sezione di Roma, I-00185 Roma, Italy*

¹⁴*Department of Chemistry, Physics, Mathematics and Natural Science, Università degli Studi di Sassari, I-07100, Sassari, Italy*

¹⁵*Istituto Nazionale di Geofisica e Vulcanologia, Sezione di Pisa, Italy*

¹⁶*Gran Sasso Science Institute (GSSI), I-67100 L’Aquila, Italy*

¹⁷*INFN, Laboratori Nazionali del Gran Sasso, I-67100 Assergi, Italy*

¹⁸*Sezione di Bologna, Istituto Nazionale di Geofisica e Vulcanologia, Bologna, Italy*

¹⁹*INFN - sezione di Pisa, 56127 Pisa, Italy*

²⁰*R&D Department of Seismology and Acoustics, KNMI, De Bilt, The Netherlands*

(Dated: February 28, 2024)

We report correlations in underground seismic measurements with horizontal separations of several hundreds of meters to a few kilometers in the frequency range 0.01 Hz to 40 Hz. These seismic correlations could threaten science goals of planned interferometric gravitational-wave detectors such as the Einstein Telescope as well as atom interferometers such as MIGA and ELGAR. We use seismic measurements from four different sites, i.e. the former Homestake mine (USA) as well as two candidate sites for the Einstein Telescope, Sos Enattos (IT) and Euregio Maas-Rhein (NL-BE-DE) and the site housing the MIGA detector, LSBB (FR). At all sites, we observe significant coherence for at least 50% of the time in the majority of the frequency region of interest. Based on the observed correlations in the seismic fields, we predict levels of correlated Newtonian noise from body waves. We project the effect of correlated Newtonian noise from body waves on the capabilities of the triangular design of the Einstein Telescope’s to observe an isotropic gravitational-wave background (GWB) and find that, even in case of the most quiet site, its sensitivity will be affected up to ~ 20 Hz. The resolvable amplitude of a GWB signal with a negatively sloped power-law behaviour would be reduced by several orders of magnitude. However, the resolvability of a power-law signal with a slope of e.g. $\alpha = 0$ ($\alpha = 2/3$) would be more moderately affected by a factor ~ 6 -9 (~ 3 -4) in case of a low noise environment. Furthermore, we bolster confidence in our results by showing that transient noise features have a limited impact on the presented results.

I. INTRODUCTION

Searches for unmodeled and/or long duration gravitational-wave (GW) signals, such as the isotropic GW background (GWB) [1], are more susceptible to be biased by correlated noise. One such example are correlations in magnetic field fluctuations over Earth-scale distances, such as the Schumann resonances [2, 3]. Their potential effect on GWB searches with Earth-based GW

interferometers – LIGO [4], Virgo [5] and KAGRA [6] – has been extensively investigated [7–14]. Moreover, the effect of correlated lightning glitches on searches for GW bursts, such as core collapse supernova, was studied [14, 15]. Furthermore, the effect of Schumann resonances on the Einstein Telescope (ET) was investigated [16] and shown to be a limiting noise source for the search for a GWB below ~ 30 Hz, in case ET has a similar magnetic coupling as LIGO/Virgo.

ET is the European proposal for a third-generation,

Measuring kinematic anisotropies with pulsar timing arrays

N. M. Jiménez Cruz¹, Ameet Malhotra¹, Gianmassimo Tasinato^{1,2}, Ivonne Zavala¹

¹ *Physics Department, Swansea University, SA28PP, United Kingdom*

² *Dipartimento di Fisica e Astronomia, Università di Bologna,
INFN, Sezione di Bologna, I.S. FLAG, viale B. Pichat 6/2, 40127 Bologna, Italy*

Abstract

Recent Pulsar Timing Array (PTA) collaborations show strong evidence for a stochastic gravitational wave background (SGWB) with the characteristic Hellings-Downs inter-pulsar correlations. The signal may stem from supermassive black hole binary mergers, or early universe phenomena. The former is expected to be strongly anisotropic while primordial backgrounds are likely to be predominantly isotropic with small fluctuations. In case the observed SGWB is of cosmological origin, our relative motion with respect to the SGWB rest frame is a guaranteed source of anisotropy, leading to $\mathcal{O}(10^{-3})$ energy density fluctuations of the SGWB. These kinematic anisotropies are likely to be larger than the intrinsic anisotropies, akin to the cosmic microwave background (CMB) dipole anisotropy. We assess the sensitivity of current PTA data to the kinematic dipole anisotropy and also provide forecasts with which the magnitude and direction of the kinematic dipole may be measured in the future with an SKA-like experiment. We also discuss how the spectral shape of the SGWB and the location of pulsar observed affects the prospects of detecting the kinematic dipole with PTA. A detection of this anisotropy may even help resolve the discrepancy in the magnitude of the kinematic dipole as measured by CMB and large-scale structure observations.

1 Introduction

Various Pulsar Timing Array (PTA) collaborations recently reported the detection of a stochastic gravitational wave background (SGWB) of unknown origin [1–5]. Determining the sources of the SGWB – whether it is generated from the mergers of supermassive black hole binaries [6, 7], or via high energy processes in the early universe (see e.g. [8] for a review) – requires the detection of SGWB properties beyond the spectral shape and amplitude of the SGWB intensity. The anisotropy of the SGWB is one such key property that can discriminate among an astrophysical or cosmological origin of the observed signal. On the one hand, a strong level of anisotropy is expected for an astrophysical signal, due to the clustering of galaxies where the GW sources reside, as well as Poisson-type fluctuations in the source properties [9–18]. On the other hand, cosmological sources are expected to have a small ($\sim 10^{-5}$) level of intrinsic anisotropy (see e.g. [19–24], and [25] for a review). However, in addition to intrinsic anisotropies, cosmological SGWB are expected to be characterised by a level of kinematic Doppler anisotropies similar to what has been observed by cosmic microwave background (CMB) experiments. According to CMB observations, our velocity with respect to the cosmic rest frame has a magnitude

Constraining Asymmetric Dark Matter using Colliders and Direct Detection

Arnab Roy , ^{a,b} Basudeb Dasgupta , ^a and Monoranjan Guchait  ^a

^aTata Institute of Fundamental Research, Homi Bhabha Road, Colaba, Mumbai 400005, India

^bSchool of Physics and Astronomy, Monash University,
Wellington Road, Clayton, Victoria 3800, Australia

E-mail: arnab.roy1@monash.edu, bdasgupta@theory.tifr.res.in,
guchait@tifr.res.in

ABSTRACT: We reappraise the viability of asymmetric dark matter (ADM) realized as a Dirac fermion coupling dominantly to the Standard Model fermions. Treating the interactions of such a DM particle with quarks/leptons in an effective-interactions framework, we derive updated constraints using mono-jet searches from the Large Hadron Collider (LHC) and mono-photon searches at the Large Electron-Positron (LEP) collider. We carefully model the detectors used in these experiments, which is found to have significant impact. The constraint of efficient annihilation of the symmetric part of the ADM, as well as other observational constraints are synthesized to produce a global picture. Consistent with previous work, we find that ADM with mass in the range 1–100 GeV is strongly constrained, thus ruling out its best motivated mass range. However, we find that leptophilic ADM remains allowed for $\gtrsim 10$ GeV DM, including bounds from colliders, direct detection, and stellar heating. We forecast that the Future Circular Collider for electron-positron collisions (FCC-ee) will improve sensitivity to DM-lepton interactions by almost an order of magnitude.

Images Distortion Hypothesis*

K. S. Virbhadra[†]

Mathematics Department, Drexel University, 33rd and Market Streets, Philadelphia, PA 19104, USA

We recently hypothesized that a distortion parameter exists such that its signed sum for all images of singular gravitational lensing of a source vanishes identically [1]. We found a distortion parameter (the ratio of the tangential to radial magnifications) that satisfied the hypothesis for the images of Schwarzschild lensing. We now show that another distortion parameter (the difference between tangential and radial magnifications) also supports our hypothesis when we perform computations with the primary-secondary and relativistic images. The distortion parameters, which satisfy the aesthetically appealing hypothesis, will likely aid in developing gravitational lensing theory. Finally, we discuss the conservation of distortions of images in gravitational lensing.

PACS numbers: 95.30.sf, 04.20.Dw, 04.70.Bw, 98.62.Sb

I. INTRODUCTION

In 1958 (around two decades before the first gravitationally lensed images were observed), Sir Charles Darwin [2] pioneered gravitational lensing (GL) research due to the light deflection in the vicinity of a Schwarzschild *photohole* [3]. He found that those images were too demagnified to be observed, and it seems that he referred to them as “ghosts” because of this. Research on GL due to light deflection in a very strong gravitational field remained almost stagnant for nearly four decades until we [4] obtained a new gravitational lens equation. This equation enables the study of light deflection in weak and strong gravitational fields, including those near photon spheres. Unaware of Darwin’s work, we studied GL due to light deflection near the photon sphere of Schwarzschild “black hole”. Like Darwin, we also found images that were very demagnified and termed them “relativistic images” (lensed images due to light deflection $\hat{\alpha} > 3\pi/2$). Despite the discouraging theoretical results of very demagnified relativistic images, our work revived theoretical research on gravitational lensing by massive compact objects, such as black holes and other compact esoteric objects (see in [5–19] and references therein.) The monumental success of the Event Horizon Telescope (*EHT*) project in 2019 (surprisingly around one hundred years after the first light deflection was observed under the leadership of Eddington) [20] as well as the ongoing development of the Next Generation Event Horizon Telescope *ngEHT* [21, 22] project have generated significant theoretical interest in GL due to black holes and their mimickers (see [23–66] and references therein.)

The theory of GL and its implications for astrophysics and cosmology are well discussed in [67, 68]. We [5] proved important theorems on photon surfaces that have significant implications for GL. In our recent paper [1],

we hypothesized that a distortion parameter exists such that its signed sum for all images of a singular GL of a source identically vanishes. We provided a distortion parameter and demonstrated that our hypothesis is valid. Toward the end of the paper, we proposed another distortion parameter. We now show that the second distortion parameter also satisfies the distortion hypothesis with all images, including relativistic images, and this is the plan for this paper. Similar to our previous paper on the distortion hypothesis [1], we use the geometrized units so that the ADM mass parameter $M \equiv MG/c^2$, where G is the universal gravitational constant and c is the speed of light in vacuum.

II. LENS EQUATION AND DISTORTION HYPOTHESIS

A gravitational lens equation that allows arbitrarily large as well as small deflection angles of light rays is given by [4]

$$\tan \beta = \tan \theta - \alpha, \quad (1)$$

where

$$\alpha = \mathcal{D} [\tan \theta + \tan (\hat{\alpha} - \theta)] \quad (2)$$

with a dimensionless *distance parameter*

$$\mathcal{D} = \frac{D_{ds}}{D_s} \in (0, 1). \quad (3)$$

The symbols have the same meaning as in our previous paper [1]: D_s , D_{ds} , and D_d , represent, respectively, the observer-source, deflector (lens)-source, and observer-deflector angular diameter distances, whereas β and θ stand for the angular source and image positions, respectively. For $0.5 < \mathcal{D} < 1$, the source is farther (from the lens) compared to the observer, and for $0 < \mathcal{D} < 0.5$, it is nearer. For $\mathcal{D} = 0.5$, the lens is halfway between the observer and the source.

* This paper is dedicated to my first *guru* of general relativity Professor Ram Bahadur Singh of Patna University. (In Sanskrit, *gu* means darkness and *ru* means one who dispels.)

[†] Email address : shwetket@yahoo.com

Direct Detection of Dark Photon Dark Matter with the James Webb Space Telescope

Haipeng An,^{1,2,3,4,*} Shuailiang Ge,^{3,5,†} Jia Liu,^{5,3,‡} and Zhiyao Lu^{5,§}

¹*Department of Physics, Tsinghua University, Beijing 100084, China*

²*Center for High Energy Physics, Tsinghua University, Beijing 100084, China*

³*Center for High Energy Physics, Peking University, Beijing 100871, China*

⁴*Frontier Science Center for Quantum Information, Beijing 100084, China*

⁵*School of Physics and State Key Laboratory of Nuclear Physics and Technology, Peking University, Beijing 100871, China*

(Dated: February 28, 2024)

Abstract

In this study, we propose an investigation into dark photon dark matter (DPDM) within the infrared frequency band, utilizing highly sensitive infrared light detectors commonly integrated into space telescopes, such as the James Webb Space Telescope (JWST). The presence of DPDM induces electron oscillations in the reflector of these detectors. Consequently, these oscillating electrons can emit monochromatic electromagnetic waves with a frequency almost equivalent to the mass of DPDM. By employing the stationary phase approximation, we can demonstrate that when the size of the reflector significantly exceeds the wavelength of the electromagnetic wave, the contribution to the electromagnetic wave field at a given position primarily stems from the surface unit perpendicular to the relative position vector. This simplification results in the reduction of electromagnetic wave calculations to ray optics. By applying this concept to JWST, our analysis of observational data demonstrates the potential to establish constraints on the kinetic mixing between the photon and dark photon within the range [10, 500] THz. Despite JWST not being optimized for DPDM searches, our findings reveal constraints comparable to those obtained from the XENON1T experiment in the laboratory, as well as astrophysical constraints from solar emission. Additionally, we explore strategies to optimize future experiments specifically designed for DPDM searches.

* anhp@mail.tsinghua.edu.cn

† sge@pku.edu.cn

‡ jialiu@pku.edu.cn

§ 2000011457@stu.pku.edu.cn

Mind The Gap: Nonlocal Cascades and Preferential Heating in High- β Alfvénic Turbulence

Waverly Gorman,^{1*} Kristopher G. Klein,¹

¹University of Arizona, Tucson, AZ, USA

Accepted XXX. Received YYY; in original form ZZZ

ABSTRACT

Characterizing the thermodynamics of turbulent plasmas is key to decoding observable signatures from astrophysical systems. In magnetohydrodynamic (MHD) turbulence, nonlinear interactions between counter-propagating Alfvén waves cascade energy to smaller spatial scales where dissipation heats the protons and electrons. When the thermal pressure far exceeds the magnetic pressure, linear theory predicts a spectral gap at perpendicular scales near the proton gyroradius where Alfvén waves become non-propagating. For simple models of an MHD turbulent cascade that assume only local nonlinear interactions, the cascade halts at this gap, preventing energy from reaching smaller scales where electron dissipation dominates, leading to an overestimate of the proton heating rate. In this work, we demonstrate that nonlocal contributions to the cascade, specifically large scale shearing and small scale diffusion, can bridge the non-propagating gap, allowing the cascade to continue to smaller scales. We provide an updated functional form for the proton-to-electron heating ratio accounting for this nonlocal energy transfer by evaluating a nonlocal weakened cascade model over a range of temperature and pressure ratios. In plasmas where the thermal pressure dominates the magnetic pressure, we observe that the proton heating is moderated compared to the significant enhancement predicted by local models.

Key words: turbulence – (magnetohydrodynamics) MHD – accretion discs – plasmas

1 INTRODUCTION AND BACKGROUND

The presence of kinetic-scale plasma processes can be indirectly inferred in astrophysical systems through their influence on measurable quantities. One such example is the indirect detection of black holes through electron radiation from the turbulent plasma in the surrounding accretion disks (Event Horizon Telescope Collaboration et al. 2019, 2022). Understanding electron heating is critical to calibrate the expected radiation output and allow for the comparison of models to measurements (Ressler et al. 2015).

In general relativistic magnetohydrodynamic (GRMHD) simulations of accretion disks, the total proton-to-electron heating ratio Q_p/Q_e directly affects the energy accessible to electrons. The energy deposited on the electrons is then distributed between various thermodynamic and radiative processes evolved in the simulations. Xie & Yuan (2012) showed that the fraction of dissipation that heats the electrons strongly influences the radiative efficiency for a hot accretion flow. As an example, a comparison of Q_p/Q_e prescriptions from the Howes (2011) model for a Landau damped turbulent cascade and a model for heating from magnetic reconnection by Werner et al. (2018) showed significant qualitative differences in properties of accretion flow as well as in simulated spectra and images between the two prescriptions when applied to simulations of Sgr A* (Chael et al. 2018) and jets around M87 (Chael et al. 2019). Relative heating rates can be extracted from other heating mechanisms such as

ion-cyclotron heating (Squire et al. 2023; Cranmer & van Ballegoijen 2012) and stochastic heating (Chandran et al. 2010; Hoppock et al. 2018; Cerri et al. 2021) although Q_p/Q_e prescriptions are not readily available. A review of the parametric dependencies of these mechanisms can be found in Howes (2024). The current approach is to compare relative heating prescriptions with known dissipation mechanisms against observations to probe for the underlying physical mechanisms; see for example Dexter et al. (2020) and Yao et al. (2021).

The motivation for the present work is to modify the Q_p/Q_e prescription for a critically-balanced Landau-damped turbulent cascade, increasing its application to a wider variety of astrophysical plasmas, specifically for systems where the proton thermal pressure dominates the magnetic pressure ($\beta_p \gg 1$) with $\beta_p \equiv \frac{2\mu_0 n_p T_p}{B^2}$ (with μ_0 the vacuum permeability, n_p the proton number density, T_p the proton temperature, and B the magnetic field amplitude). The cascade model (described in Howes et al. 2008) follows the magnetic energy in a Landau-damped turbulent cascade as it transitions from magnetohydrodynamic (MHD) Alfvén waves to wavevector anisotropic low-frequency kinetic Alfvén waves, spanning inertial and dissipation ranges. The previous Q_p/Q_e prescription (Howes 2010) is a parametric study and fit of the Howes et al. (2008) model for varying β_p and proton-to-electron temperature ratios ($\tau \equiv T_p/T_e$). Solutions to the linear dispersion relation of a collisionless gyrokinetic plasma in the high- β_p limit ($\beta_p \gg 1$) develop a finite spectral gap where the real frequency ω approaches zero and the damping rate γ reaches its local maximum around the proton gyroscale, $k_{\perp} \rho_p \sim 1$ where ρ_p

* E-mail: waverlyg@arizona.edu

Bare mass effects on the reheating process after inflation

Simon Clery^{a,*}, Marcos A. G. Garcia^{b,†}, Yann Mambrini^{a,‡}, Keith A. Olive^{c,§}

^a *Université Paris-Saclay, CNRS/IN2P3, IJCLab, 91405 Orsay, France*

^b *Departamento de Física Teórica, Instituto de Física,*

Universidad Nacional Autónoma de México, Ciudad de México C.P. 04510, Mexico

^c *William I. Fine Theoretical Physics Institute, School of Physics and Astronomy,
University of Minnesota, Minneapolis, MN 55455, USA*

(Dated: February 28, 2024)

We consider the effects of a bare mass term for the inflaton, when the inflationary potential takes the form $V(\phi) = \lambda\phi^k$ about its minimum with $k \geq 4$. We concentrate on $k = 4$, but discuss general cases as well. Further, we assume $\lambda\phi_{\text{end}}^2 \gg m_\phi^2$, where ϕ_{end} is the inflaton field value when the inflationary expansion ends. We show that the presence of a mass term (which may be present due to radiative corrections or supersymmetry breaking) can significantly alter the reheating process, as the equation of state of the inflaton condensate changes from $w_\phi = \frac{1}{3}$ to $w_\phi = 0$ when $\lambda\phi^2$ drops below m_ϕ^2 . We show that for a mass $m_\phi \gtrsim T_{\text{RH}}/250$, the mass term will dominate at reheating. We compute the effects on the reheating temperature for cases where reheating is due to inflaton decay (to fermions, scalars, or vectors) or to inflaton scattering (to scalars or vectors). For scattering to scalars and in the absence of a decay, we derive a strong upper limit to the inflaton bare mass $m_\phi < 350 \text{ MeV} (T_{\text{RH}}/10^{10} \text{ GeV})^{3/5}$, as there is always a residual inflaton background which acts as cold dark matter. We also consider the effect of the bare mass term on the fragmentation of the inflaton condensate.

I. INTRODUCTION

The hypothesis of a violent inflationary phase during the first moments of the Universe makes it possible to address several cosmological issues, ranging from the flatness of the Universe to the horizon or entropy problem [1]. However, a complete inflationary model requires above all a mechanism for a graceful exit. Indeed, the prolonged period of exponential expansion must end with a sufficiently efficient transfer of the oscillation modes of the inflaton condensate ϕ to a thermal bath [2, 3], i.e. reheating, that ensures a temperature $\gtrsim 2 \text{ MeV}$ to allow for standard big bang nucleosynthesis. Moreover, the density fluctuation spectrum produced during inflation should agree with observations of the CMB anisotropy spectrum [4], which in turn constrains the parameters of the inflaton potential $V(\phi)$.

The process of transferring the energy stored in inflaton oscillations to Standard Model particles is not instantaneous [5–8]. Rather, in many models, an oscillating inflaton condensate decays or scatters progressively producing a bath of relativistic particles. The efficiency of the reheating process depends on the rate of the energy transfer as well as on the shape of the inflaton potential, $V(\phi)$, about its minimum [9, 10]. Even if the exact shape of the potential at the end of inflation is unknown

it can often be approximated about its minimum by a polynomial function of ϕ .

In many models of inflation, the inflaton potential can be approximated about its minimum by a quadratic term, $V(\phi) = \frac{1}{2}m_\phi^2\phi^2$. The Starobinsky model [11] is one example. In this case, only one Fourier mode of the inflaton oscillation contributes to the reheating process. The energy density in radiation, ρ_R , grows rapidly at first, and redshifts as $\rho_R \propto a^{-\frac{3}{2}}$ where a is the cosmological scale factor, as decays continue to add to the radiation bath. Because $\rho_\phi \propto a^{-3}$, eventually, the radiation bath comes to dominate the total energy density, at which time we can define a reheating temperature. This occurs when the cosmological scale factor, a_{RH} satisfies $\rho_R(a_{\text{RH}}) = \rho_\phi(a_{\text{RH}})$. This occurs (up to a numerical factor) when $H(a_{\text{RH}}) \simeq \Gamma_\phi$, or $T_{\text{RH}} \simeq \sqrt{\Gamma_\phi M_P}$, where H is the Hubble parameter, Γ_ϕ is the width of the inflaton condensate, and $M_P = 1/\sqrt{8\pi G_N} \simeq 2.4 \times 10^{18} \text{ GeV}$ is the reduced Planck mass.

For a potential whose expansion about its minimum is $V(\phi) = \lambda\phi^k$, with $k \geq 4$, the exercise is more subtle, and requires a more involved analysis [9, 10]. The reheating process will in general depend on the spin of the final state particles in either inflaton decays or scatterings. In fact, in some cases reheating does not occur. For example, for $k = 4$, the evolution of $\rho_\phi \propto a^{-4}$ is the same as the evolution of $\rho_R \propto a^{-4}$ for inflaton decays or scatterings to vector bosons [12], precluding the condition $\rho_\phi(a_{\text{RH}}) = \rho_R(a_{\text{RH}})$ to occur. However, we cannot exclude the presence of a bare mass term $\frac{1}{2}m_\phi^2\phi^2$, which may be subdominant at the end of inflation, and during

* simon.clery@ijclab.in2p3.fr

† marcos.garcia@fisica.unam.mx

‡ yann.mambrini@ijclab.in2p3.fr

§ olive@umn.edu

Slow electron holes in the Earth's magnetosheath

Z. I. Shaikh¹, I. Y. Vasko¹, I. H. Hutchinson², S. R. Kamaletdinov³, J. C. Holmes⁴, D. L. Newman^{5,6}, and F. S. Mozer¹

¹Space Sciences Laboratory, University of California at Berkeley, USA

²Massachusetts Institute of Technology, Cambridge, USA

³University of California, Los Angeles, USA

⁴Los Alamos National Laboratory, Los Alamos, New Mexico, USA

⁵Center for Integrated Plasma Studies, University of Colorado, Boulder, CO, USA

⁶Laboratory for Atmospheric and Space Physics, Boulder, CO, USA

Key Points:

- Statistical analysis of 645 solitary waves in the Earth's magnetosheath revealed that 630 of them are electron holes.
- The electron holes are associated with quasi-Maxwellian ion velocity distribution functions.
- The electron hole velocities are comparable with those of the bulk of ions and well below electron thermal speed.

Corresponding author: Zubair I. Shaikh, zshaikh@berkeley.edu

–1–

Abstract

We present a statistical analysis of electrostatic solitary waves observed aboard Magnetospheric Multiscale spacecraft in the Earth's magnetosheath. Applying single-spacecraft interferometry to several hundred solitary waves collected in about two minute intervals, we show that almost all of them have the electrostatic potential of positive polarity and propagate quasi-parallel to the local magnetic field with plasma frame velocities of the order of 100 km/s. The solitary waves have typical parallel half-widths from 10 to 100 m that is between 1 and 10 Debye lengths and typical amplitudes of the electrostatic potential from 10 to 200 mV that is between 0.01 and 1% of local electron temperature. The solitary waves are associated with quasi-Maxwellian ion velocity distribution functions, and their plasma frame velocities are comparable with ion thermal speed and well below electron thermal speed. We argue that the solitary waves of positive polarity are slow electron holes and estimate the time scale of their acceleration, which occurs due to interaction with ions, to be of the order of one second. The observation of slow electron holes indicates that their lifetime was shorter than the acceleration time scale. We argue that multi-spacecraft interferometry applied previously to these solitary waves is not applicable because of their too-short spatial scales. The source of the slow electron holes and the role in electron-ion energy exchange remain to be established.

Plain Language Summary

Earth's magnetosheath is a highly turbulent medium and an ideal natural laboratory for the analysis of plasma turbulence. Spacecraft measurements showed that high-frequency electric field fluctuations in the Earth's magnetosheath are predominantly electrostatic and consist, particularly, of electrostatic solitary waves with bipolar parallel electric fields. The properties of these electrostatic fluctuations have been largely unaddressed and, moreover, the results of previous studies were inconsistent. In this paper, we present a statistical analysis of electrostatic solitary waves observed aboard Magnetospheric Multiscale in the Earth's magnetosheath. We revealed that most of the solitary waves are Debye-scale structures with the electrostatic potential of positive polarity and typical amplitudes between 0.01 and 1% of local electron temperature. We demonstrated that the solitary waves must be electron holes, purely kinetic structures produced in a nonlinear stage of various electron-streaming instabilities. Even more critical is that these structures are *slow*; their plasma frame velocities are well below electron thermal speed but coincide with the velocities of the bulk of ions. While the source of electrostatic fluctuations in Earth's magnetosheath could not be revealed, the finding that these fluctuations can be slow implies they can facilitate efficient energy exchange between ions and electrons.

1 Introduction

High-resolution electric field measurements aboard modern spacecraft in numerous regions of the near-Earth space revealed the presence of electrostatic solitary waves, localized electrostatic structures with typically bipolar electric field parallel to local magnetic field [Mozer *et al.*, 2015; Pickett, 2021; Hansel *et al.*, 2021]. Prior to the high-resolution measurements, only a signature of solitary waves, broadband electrostatic fluctuations in spectral measurements, was observed [Gurnett *et al.*, 1976, 1979; Gurnett, 1985]. Broadband electrostatic fluctuations and corresponding solitary waves have been observed in the solar wind [Mangeney *et al.*, 1999; Mozer *et al.*, 2021], interplanetary shock waves [Williams *et al.*, 2005; Wilson *et al.*, 2007, 2010], lunar environment [Hashimoto *et al.*, 2010; Malaspina and Hutchinson, 2019; Chu *et al.*, 2021], Earth's bow shock [Vasko *et al.*, 2018a, 2020; Wang *et al.*, 2021; Kamaletdinov *et al.*, 2022], magnetopause [Cattell *et al.*, 2002; Graham *et al.*, 2015], auroral region [Temerin *et al.*, 1982; Ergun *et al.*, 1998; Muschietti *et al.*, 1999], inner magnetosphere [Franz *et al.*, 2005; Malaspina *et al.*, 2014; Vasko *et al.*, 2017a; Tong *et al.*, 2018], and plasma sheet [Matsumoto *et al.*, 1994; Cattell *et al.*, 2005; Lotekar *et al.*, 2020]. We have learned that solitary waves can provide efficient electron heating [Vasko *et al.*, 2018b; Norgren *et al.*, 2020; Chu *et al.*, 2021] and pitch-angle scattering [Vasko *et al.*, 2017b; Shen *et al.*, 2021; Kamaletdinov *et al.*, 2022] and also serve as tracers of instabilities not resolvable by particle instruments [Khotyaintsev

–2–

Field-Aligned Current Structures during the Terrestrial Magnetosphere's Transformation into Alfvén Wings and Recovery

J. M. H. Beedle^{1,2,3}, L.-J. Chen², J. R. Shuster¹, H. Gurrām^{2,4}, D. J. Gershman², Y. Chen⁵, R. C. Rice^{2,4}, B. L. Burkholder^{2,6}, A. S. Ardakani³, K. J. Genestreti⁷, R. B. Torbert¹

¹Space Science Center, University of New Hampshire, Durham, NH, USA

²NASA Goddard Space Flight Center, Greenbelt, MD, USA

³Department of Physics, The Catholic University of America, Washington D.C., USA

⁴Department of Physics, University of Maryland, College Park, MD USA

⁵Center for Space Physics and Department of Astronomy, Boston University, Boston, MA, USA

⁶University of Maryland, Baltimore County, MD, USA

⁷Earth Oceans and Space, Southwest Research Institute, Durham, NH, USA

Key Points:

- On April 24th, 2023, sub-Alfvénic solar wind conditions from a CME caused the Earth's magnetosphere to form an Alfvén Wing formation.
- The MMS spacecraft observed the dawn-flank wing of the formation, enabling the first in situ measurements of Alfvén Wing current structures.
- These current structures were found to be primarily anti-field-aligned, electron-driven, and filamentary.

Corresponding author: Jason M. H. Beedle, jason.beedle@unh.edu

–1–

manuscript submitted to *Geophysical Research Letters*

Abstract

On April 24th, 2023, a CME event caused the solar wind to become sub-Alfvénic, leading to the development of an Alfvén Wing configuration in the Earth's Magnetosphere. Alfvén Wings have previously been observed as cavities of low flow in Jupiter's magnetosphere, but the observing satellites did not have the ability to directly measure the Alfvén Wings' current structures. Through in situ measurements made by the Magnetospheric Multiscale (MMS) spacecraft, the April 24th event provides us with the first direct measurements of current structures during an Alfvén Wing configuration. We have found two distinct types of current structures associated with the Alfvén Wing transformation as well as the magnetosphere recovery. These structures are observed to be significantly more anti-field-aligned and electron-driven than typical magnetopause currents, indicating the disruptions caused to the magnetosphere current system by the Alfvén Wing formation.

Plain Language Summary

The solar wind applies pressure on the Earth's magnetic field, distorting it from a dipole into its compressed dayside and stretched tail configuration. However, this typical structure can be disrupted by eruptive solar events such as Coronal Mass Ejections or CMEs, which may cause the solar wind's pressure to drop low enough that it is no longer able to push the magnetosphere back to form a single unified tail. When this occurs, the tail splits into two separate structures, called Alfvén Wings. While this configuration is rare at Earth, it is common at the outer planets and their moons, where Alfvén Wing configurations have been studied and modeled. However, because the observing spacecraft lacked the necessary instrumentation, we have not yet directly observed the Alfvén Wing current structures. On April 24th, 2023, a CME event led to the creation of Alfvén Wing formations in the Earth's magnetosphere. We observed this event using the Magnetospheric Multiscale (MMS) spacecraft, which enabled us to make the first direct observations of Alfvén Wing current structures. These currents were found to be mainly parallel to the local magnetic field, in contrast to typical magnetopause currents, indicating the complex nature of the disrupted magnetosphere's current system.

1 Introduction

Coronal Mass Ejections (CMEs) are events that project fast moving solar wind plasma and magnetic field lines into the interplanetary medium, creating disturbances and interacting with the background solar wind to create shocks - see Beedle, Rura, et al. (2022) and sources therein. Upon reaching Earth, these events cause significant disruptions to the magnetosphere's systems through magnetic reconnection on the dayside magnetopause, and the loading of energy into the tail. CMEs are also able to introduce the magnetosphere system to an environment with very low density and high magnetic field strength - e.g. Ridley (2007). Because of these low density conditions, CMEs can cause the solar wind to become sub-Alfvénic where the solar wind mach number drops below 1, a significant decrease from the typical solar wind mach number of ~ 11 (Schunk & Nagy, 2000). During such times, as the solar wind pressure collapses, the bow shock may disappear and Alfvén Wings form in the magnetosphere, dividing the once unified magnetotail into a dual configuration such as modeled in the simulations of Chané et al. (2015) etc. Note, the Alfvén Wings form above the poles of a body when the IMF is dominantly B_Z orientated, while the wings instead form along the flanks when IMF B_Y becomes more dominant.

The current structure associated with the formation of an Alfvén Wing configuration has been modeled and explored in studies for Jupiter, Saturn, and their associated moons - see Neubauer (1980), Kivelson et al. (2004), Jia et al. (2010) and the as-

–2–

Images and flares of geodesic hotspots around a Kerr black hole

Jiewei Huang¹, Zhenyu Zhang², Minyong Guo^{1,3*}, Bin Chen^{2,4,5}

¹ *Department of Physics, Beijing Normal University, Beijing 100875, P. R. China*

² *Department of Physics, Peking University, No.5 Yiheyuan Rd, Beijing 100871, P.R. China*

³ *Key Laboratory of Multiscale Spin Physics, Ministry of Education, Beijing 100875, P. R. China*

⁴ *Center for High Energy Physics, Peking University, No.5 Yiheyuan Rd, Beijing 100871, P. R. China*

⁵ *Collaborative Innovation Center of Quantum Matter, No.5 Yiheyuan Rd, Beijing 100871, P. R. China*

Abstract

In this study, we develop a numerical method to generate images on an observer's screen, formed by radiation from hotspots on any timelike orbits outside a black hole. This method uses the calculation of fractional numbers, enabling us not only to produce the overall image but also to distinguish between primary, secondary, and higher-order images. Building upon this, we compute the images of hotspots from eight potential types of geodesic timelike orbits outside a Kerr black hole, summarizing the properties of both the overall and individual order images. Furthermore, we calculate the centroid motion and lightcurve. Notably, we observe flare phenomena across all orbit types and classify these flares into three categories based on the Doppler and gravitational redshift effects.

* Corresponding author: minyongguo@bnu.edu.cn

General predictions of neutron star properties using unified relativistic mean-field equations of state

Luigi Scurto,^{1,*} Helena Pais,^{1,†} and Francesca Gulminelli^{2,‡}

¹*CFisUC, Department of Physics, University of Coimbra, 3004-516 Coimbra, Portugal*

²*Normandie Univ., ENSICAEN, UNICAEN, CNRS/IN2P3, LPC Caen, F-14000 Caen, France*

In this work we present general predictions for the static observables of neutron stars (NSs) under the hypothesis of a purely nucleonic composition of the ultra-dense baryonic matter, using Bayesian inference on a very large parameter space conditioned by both astrophysical and nuclear physics constraints.

The equation of states are obtained using a unified approach of the NS core and inner crust within a fully covariant treatment based on a relativistic mean-field Lagrangian density with density dependent couplings. The posterior distributions are well compatible with the ones obtained by semi-agnostic meta-modelling techniques based on non-relativistic functionals, that span a similar portion of the parameter space in terms of nuclear matter parameters, and we confirm that the hypothesis of a purely nucleonic composition is compatible with all the present observations.

We additionally show that present observations do not exclude the existence of very massive neutron stars with mass compatible with the lighter partner of the gravitational event GW190814 measured by the LIGO-Virgo collaboration. Some selected representative models, that respect well all the constraints taken into account in this study, and approximately cover the residual uncertainty in our posterior distributions, will be uploaded in the COMPOSE database for use by the community.

I. INTRODUCTION

The analysis of multi-messenger data on compact stars require models for the equation of state (EoS) of dense matter that are sufficiently flexible to account for the present uncertainties of the theoretical modelling, thus avoiding artificial bias in the parameter estimation, see refs.[1, 2] for recent reviews on the EoS modelling.

A paramount - though not unique - example of this statement is given by the estimation of neutron star radii from gravitational wave (GW) signals observed by ground based interferometers from the merging of compact binaries [3]. Indeed, given the mass of a neutron star, its tidal deformability under the gravitational field of the companion in the late inspiral dynamics is one-to-one correlated to the star radius, for a given equation of state model. Even if the leading order adiabatic tidal effects enter the phase of the waveform only at the fifth post-Newtonian order[4, 5] and can therefore be extracted only from loud signals with a high signal-to-noise ratio, important constraints on the tidal parameter were already obtained by the LVK collaboration, particularly from the famous GW170817 event [6]. New observations from the ongoing O4 and upcoming O5 run, and next generation detectors such as Einstein Telescope Cosmic Explorer are expected to further tighten the tidal deformability constraint through more precise and more numerous observations [7]. A precise estimation of the correlation between the tidal polarizability parameter Λ and the star mass M can therefore lead to radius eval-

uations that can be more precise than estimations from X-ray bursts or pulse timing measurements [8–11], at the same time providing precious information on the behavior of ultra-dense matter in a regime that is completely inaccessible to laboratory experiments.

The most model-independent approach in this respect is given by agnostic (parametric or non-parametric) EoS modelling, such as piecewise polytropes [12], spectral parameterization [13–15], Gaussian process-based sampling [16–19], or neural networks[20] that do not impose a specific form of the EoSs and are only restricted by the requirement of causality and thermodynamic stability. Although very powerful for EoS inference from astrophysical data, the common drawback of these agnostic models is that they do not provide information on the internal composition of neutron stars, and more generally on the properties of the strong interaction in the non-perturbative domain of QCD. For this reason, semi-agnostic models have been proposed [21–27], that do not directly model the functional relation between pressure and energy density, but infer this quantity by imposing the equilibrium of weak interactions to a flexible parametrisation of the energy density of an electrically neutral system composed of leptons and baryons. In this meta-modelling approach, the parameters of the energy functional are chosen such as to explore the full uncertainty domain of microscopic models of dense matter, with minimal hypotheses on the relevant degrees of freedom. The simplest realization of this approach consists in considering only nucleonic (neutron and proton) degrees of freedom for the baryonic part, and express the interaction part of the energy density as a polynomial expansion around the equilibrium density of symmetric nuclear matter, where the behavior is best constrained by laboratory experiments [28–32]. Alternatively, expansions around pure neutron matter have been proposed, where

*Electronic address: lscurto@student.uc.pt

†Electronic address: hpais@uc.pt

‡Electronic address: gulminelli@lpccaen.in2p3.fr

The In-Out Formalism for In-In Correlators

Yaniv Donath* and Enrico Pajer†

*Department of Applied Mathematics and Theoretical Physics, University of Cambridge,
Wilberforce Road, Cambridge, CB3 0WA, UK*

Abstract Cosmological correlators, the natural observables of the primordial universe, have been extensively studied in the past two decades using the in-in formalism pioneered by Schwinger and Keldysh for the study of dissipative open systems. Ironically, most applications in cosmology have focused on non-dissipative closed systems. We show that, for non-dissipative systems, correlators can be equivalently computed using the in-out formalism with the familiar Feynman rules. In particular, the myriad of in-in propagators is reduced to a single (Feynman) time-ordered propagator and no sum over the labelling of vertices is required. In de Sitter spacetime, this requires extending the expanding Poincaré patch with a contracting patch, which prepares the bra from the future. Our results are valid for fields of any mass and spin but assuming the absence of infrared divergences.

We present three applications of the in-out formalism: a representation of correlators in terms of a sum over residues of Feynman propagators in the energy-momentum domain; an algebraic recursion relation that computes Minkowski correlators in terms of lower order ones; and the derivation of cutting rules from Veltman's largest time equation, which we explicitly develop and exemplify for two-vertex diagrams to all loop orders.

The in-out formalism leads to a natural definition of a de Sitter scattering matrix, which we discuss in simple examples. Remarkably, we show that our scattering matrix satisfies the standard optical theorem and the positivity that follows from it in the forward limit.

*yaniv@donath-zafir.com

†enrico.pajer@gmail.com

Testing the isotropy of cosmic acceleration with Pantheon+SH0ES: A cosmographic analysis

Carlos A. P. Bengaly* and Jailson S. Alcaniz†

Observatório Nacional, 20921-400, Rio de Janeiro - RJ, Brazil

Cássio Pigozzo‡

Instituto de Física, Universidade Federal da Bahia, 40210-340, Salvador - BA, Brazil

(Dated: February 28, 2024)

We use a recent Pantheon+SH0ES compilation of Type Ia Supernova distance measurements at low-redshift, i.e., $0.01 \leq z \leq 0.10$, in order to investigate the directional dependency of the deceleration parameter (q_0) in different patches (60° size) across the sky, as a probe of the statistical isotropy of the Universe. We adopt a cosmographic approach to compute the cosmological distances, fixing H_0 and M_B to reference values provided by the collaboration. By looking at 500 different patches randomly taken across the sky, we find a maximum $\sim 3\sigma$ CL anisotropy level for q_0 , whose direction points orthogonally to the CMB dipole axis, i.e., $(RA^{\text{SN}}, DEC^{\text{SN}}) = (267^\circ, 6^\circ)$ vs $(RA^{\text{CMB}}, DEC^{\text{CMB}}) = (167^\circ, -7^\circ)$. We assessed the statistical significance of those results, finding that such a signal is expected due to the limitations of the observational sample. These results support that there is no significant evidence for a departure from the cosmic isotropy assumption, one of the pillars of the standard cosmological model.

* carlosbengaly@on.br

† alcaniz@on.br

‡ cpigozzo@ufba.br

Automated Scheduling of Doppler Exoplanet Observations at Keck Observatory

LUKE B. HANDLEY ¹, ERIK A. PETIGURA ¹, VELIBOR V. MIŠIĆ ², JACK LUBIN ¹ AND HOWARD ISAACSON ^{3,4}

¹*Department of Physics & Astronomy, University of California Los Angeles, Los Angeles, CA 90095, USA*

²*Anderson School of Management, University of California Los Angeles, Los Angeles, CA 90095, USA*

³*501 Campbell Hall, University of California at Berkeley, Berkeley, CA 94720, USA*

⁴*Centre for Astrophysics, University of Southern Queensland, Toowoomba, QLD, Australia*

ABSTRACT

Precise Doppler studies of extrasolar planets require fine-grained control of observational cadence, i.e. the timing of and spacing between observations. We present a novel framework for scheduling a set of Doppler campaigns with different cadence requirements at the W. M. Keck Observatory (WMKO). For a set of observing programs and allocated nights on an instrument, our software optimizes the timing and ordering of ~ 1000 observations within a given observing semester. We achieve a near-optimal solution in real-time using a hierarchical Integer Linear Programming (ILP) framework. Our scheduling formulation optimizes over the roughly 10^{3000} possible orderings. A top level optimization finds the most regular sequence of allocated nights by which to observe each host star in the request catalog based on a frequency specified in the request. A second optimization scheme minimizes the slews and downtime of the instrument. We have assessed our algorithms performance with simulated data and with the real suite of Doppler observations of the California Planet Search in 2023.

Keywords: methods: observational

1. INTRODUCTION

The discovery and characterization of extrasolar planets with the Doppler technique requires careful attention to the observational ‘cadence’ defined as the *timing of and spacing between* observations of a given target. The census of known Doppler extrasolar planets have orbital periods ranging from only a few hours to several decades (Howard et al. 2012; Fulton et al. 2021). Thus, Doppler surveys must be tuned to appropriately sample the orbital periods of interest.

Moreover, time-variable surface features produce shifts in the stellar spectra that register as Doppler shifts, yet have nothing to do with the star’s motion around the star-planet barycenter (Luhn et al. 2020). The amplitude of activity RVs ranges from tens of cm/s for the very quietest stars to hundreds of m/s for young and active stars. The timescale of this stellar variability ranges from minutes (acoustic modes) (Chaplin et al. 2019) to hours (granulation), to days (rotation), to years (magnetic cycles) (Fulton et al. 2015).

Over the last few years, a number of spectrometers have been commissioned that are stable at the level of several tens of cm/s. Some noteworthy examples include ESPRESSO (Pepe et al. 2021), MAROON-X (Seifahrt

et al. 2018), EXPRES (Blackman et al. 2020), NEID (Schwab et al. 2016), and KPF (Gibson et al. 2020). For such instruments, stellar activity is the dominant noise source for nearly all target stars. Several strategies have been developed for mitigating stellar activity. Most require dense sampling of RVs over timescales relevant to planetary and activity signals. Therefore, control of observational cadence has become even more critical as the community attempts to detect planetary signals below 1 m/s in the presence of stellar activity (Anglada-Escudé et al. 2016).

Achieving the desired observational cadence at any Doppler facility is a complex scheduling challenge. Most facilities support a number of active Doppler programs with different targets, observational priorities, and cadence requirements. In addition, most Doppler instruments share the telescope with other instruments with their own scheduling constraints (e.g. dark time for extra-galactic observations). Finally, weather losses are guaranteed but the set of impacted nights is not known in advance.

Today, the task of scheduling Doppler observations is performed almost entirely by humans. This is a challenging and time-consuming task. Schedulers must determine the sequence of observations that favor high pro-

Attention-based Neural Network Emulators for Multi-Probe Data Vectors Part I: Forecasting the Growth-Geometry split

Kunhao Zhong,^{1,2*} Evan Saraivanov¹, James Caputi¹, Vivian Miranda³, Supranta S. Boruah⁴, Tim Eifler⁴, Elisabeth Krause^{4,5}

¹*Department of Physics and Astronomy, Stony Brook University, Stony Brook, NY 11794, USA*

²*Department of Physics and Astronomy, University of Pennsylvania, Philadelphia, PA 19104, USA*

³*C. N. Yang Institute for Theoretical Physics, Stony Brook University, Stony Brook, NY 11794, USA*

⁴*Department of Astronomy and Steward Observatory, University of Arizona, 933 N Cherry Ave, Tucson, AZ 85719, USA*

⁵*Department of Physics, University of Arizona, 1118 E Fourth Str, Tucson, AZ, 85721-0065, USA*

Accepted XXX. Received YYY; in original form ZZZ

ABSTRACT

We present a new class of machine-learning emulators that accurately model the cosmic shear, galaxy-galaxy lensing, and galaxy clustering real space correlation functions in the context of Rubin Observatory year one simulated data. To illustrate its capabilities in forecasting models beyond the standard Λ CDM, we forecast how well LSST Year 1 data will be able to probe the consistency between geometry Ω_m^{geo} and growth Ω_m^{growth} dark matter densities in the so-called split Λ CDM parameterization. When trained with a few million samples, our emulator shows uniform accuracy across a wide range in an 18-dimensional parameter space. We provide a detailed comparison of three neural network designs, illustrating the importance of adopting state-of-the-art Transformer blocks. Our study also details their performance when computing Bayesian evidence for cosmic shear on three fiducial cosmologies. The transformers-based emulator is always accurate within POLYCHORD’s precision. As an application, we use our emulator to study the degeneracies between dark energy models and growth geometry split parameterizations. We find that the growth-geometry split remains to be a meaningful test of the smooth dark energy assumption.

1 INTRODUCTION

Markov Chain Monte Carlo (MCMC) is a common and effective technique for inferring cosmological parameters, as it enables the exploration of high-dimensional likelihoods from a wide range of data sets. These include space and ground-based measurements of the Cosmic Microwave Background (CMB) (Planck Collaboration et al. 2020a; Aiola et al. 2020; Dutcher et al. 2021), type Ia supernova (Scolnic et al. 2018, 2022), Baryon Acoustic Oscillations (BAO) (Ross et al. 2015; Alam et al. 2017; Raichoor et al. 2020; Alam et al. 2021; Zhao et al. 2022), and lensing and clustering of optical galaxies (Hikage et al. 2019; Hamana et al. 2020; Nicola et al. 2020; Asgari et al. 2021; Heymans et al. 2021; Abbott et al. 2022).

Forthcoming stage-IV surveys will observe the lensing and clustering of optical galaxies with unparalleled precision. These experiments include the Dark Energy Spectroscopic Instrument (DESI Collaboration et al. 2023), the Large Synoptic Survey Telescope (LSST) (Ivezić et al. 2019), the Euclid mission (Laureijs et al. 2011), and the Roman Space Telescope (Dore et al. 2019). They all aim to provide a more ambitious investigation into the nature of dark energy and dark matter, with a corresponding increase in the model complexity of nuisance physics. For example, new analyses will consider parameterizations for galaxy biases and intrinsic alignments that are better-motivated from an effective field theory perspective (Kokron et al. 2021; Mergulhão et al. 2022; Bakx et al. 2023; Chen & Kokron 2023; Nicola et al. 2023; Rubira & Schmidt 2023). The dark sector may simultaneously include new physics in the early (Carrillo González et al. 2021; Benevento et al. 2022; Hill et al. 2022; Buen-Abad et al. 2023; Berryman et al. 2023; Franco Abellán et al. 2023; McDonough et al. 2023; Niedermann & Sloth 2023;

Poulin et al. 2023; Ramadan et al. 2023), intermediate (Simon et al. 2022; Holm et al. 2022; Alvi et al. 2022; Anchordoqui et al. 2022; Ashoorioon & Davari 2023; Bucko et al. 2023; Holm et al. 2023; Nygaard et al. 2023; Rubira et al. 2023), and late Universes (Gleyzes et al. 2015; Zumalacárregui et al. 2017; Nesseris et al. 2017; Peirone et al. 2018; Espejo et al. 2019; Sakr & Martinelli 2022; Amon & Efstathiou 2022; Berghaus et al. 2023; Lin et al. 2023; Wang et al. 2023; Zhong et al. 2023), as simple alternatives to Λ CDM is shown to be ineffective in explaining current tensions (Schöneberg et al. 2022).

Future investigations into the dark sector and nuisance physics are expected to have higher dimensionality of the parameter space and larger execution time per model. For example, CMB constraints from the damping tail of the temperature power spectrum at multipoles $\ell \gtrsim 3000$ will soon require additional parameters related to baryonic physics (McCarthy et al. 2022). The stiff increase in computational costs associated with running MCMC simulations is inevitable as the precision of theory predictions must align with the reduced uncertainties of new experiments.

Indeed, the current computational costs associated with evaluating some statistical metrics that assess tension and goodness-of-fit are already slowing the research progress. Currently, MCMCs aimed at constraining early dark energy scenarios, often employing a combination of CMB data measured by Planck and ACT experiments (Hill et al. 2022), can take weeks to satisfy the stringent $R - 1 \approx 0.005$ Gelman-Rubin convergence threshold (Gelman & Rubin 1992). This criterion is necessary for robustly assessing goodness-of-fit (Raveri & Hu 2019). Moreover, the marginalization of Early Dark Energy predictions over general late-time dark energy equations of state further

Testing approximate infrared scattering radiative-transfer methods for hot Jupiter atmospheres

ELSPETH K.H. LEE ¹

¹Center for Space and Habitability, University of Bern, Gesellschaftsstrasse 6, CH-3012 Bern, Switzerland

(Received YY; Revised YY; Accepted YY)

Submitted to ApJ

ABSTRACT

The calculation of internal atmospheric (longwave) fluxes is a key component of any model of exoplanet atmospheres that requires radiative-transfer (RT) calculations. For atmospheres containing a strong scattering component such as cloud particles, most 1D multiple-scattering RT methods typically involve numerically expensive matrix inversions. This computational bottleneck is exacerbated when multitudes of RT calculations are required, such as in general circulation models (GCMs) and retrieval methods. In an effort to increase the speed of RT calculations without sacrificing too much accuracy, we investigate the applicability of approximate longwave scattering methods developed for the Earth science community to hot Jupiter atmospheres. We test the absorption approximation (AA) and variational iteration method (VIM) applied to typical cloudy hot Jupiter scenarios, using 64 stream DISORT calculations as reference solutions. We find the four-stream VIM variant is a highly promising method to explore using for hot Jupiter GCM and retrieval modelling, showing excellent speed characteristics, with typical errors $\sim 1\%$ for outgoing fluxes and within $\sim 50\%$, but with larger errors in the deep cloud layer test case, for vertical heating rates. Other methods explored in this study were found to typically produce similar error characteristics in vertical heating rates.

Keywords: Radiative transfer(1335) – Exoplanet atmospheres(487)

1. INTRODUCTION

The calculation of thermal internal atmospheric fluxes, traditionally called ‘longwave’ radiation, is a key part of investigating the emission properties of exoplanet atmospheres. This type of calculation is critical to modelling and fitting secondary eclipse (dayside) spectral data of tidally locked exoplanets (e.g. [Crouzet et al. 2014](#); [Kreidberg et al. 2014](#); [Coulombe et al. 2023](#)) as well as full orbit thermal spectral phase curves of exoplanets (e.g. [Stevenson et al. 2014](#); [Arcangeli et al. 2019](#); [Mikal-Evans et al. 2022](#)).

With the advent of JWST, exoplaneteers now have access to an expansive wavelength range, unparalleled sensitivity and continuous staring time for these types of observations than previous keystone observatories. However, this comes with an increase in the challenge

of appropriately modelling this data for both forward and retrieval efforts. The wavelength dependent opacity and scattering properties of potential clouds and hazes in these atmospheres can have a large impact on an objects spectra and interpretation of observational data.

Several recent studies have shown the importance of incorporating longwave scattering when modelling cloud properties. [Kitzmann et al. \(2013\)](#) compare a 24-stream DISORT calculation with a two-stream method to investigate the longwave greenhouse effect of CO₂ clouds on exoplanet atmospheres. They find large deviations between the DISORT and two-stream methods alters the strength of the longwave greenhouse effect, impacting the climate of potential worlds containing CO₂ clouds. [Taylor et al. \(2021\)](#) provide analytical expectations for the impact of a scattering component on the outgoing flux of hot Jupiter atmospheres. They show that degeneracies and biases in retrieval results can occur when the longwave scattering is not taken into account and propose a method to retrieve optical constants of the

LETTER TO THE EDITOR

Evidence for extended [CII] and dust emission in local dwarf galaxies

M. Romano^{*1,2}, D. Donevski^{1,3,4}, Junais¹, A. Nanni^{1,5}, M. Ginolfi⁶, G. C. Jones⁷, I. Shivaei⁸, G. Lorenzon¹, M. Hamed¹, D. Salak^{9,10}, and P. Sawant¹

¹ National Centre for Nuclear Research, ul. Pasteura 7, 02-093 Warsaw, Poland

² INAF - Osservatorio Astronomico di Padova, Vicolo dell'Osservatorio 5, I-35122, Padova, Italy

³ SISSA, Via Bonomea 265, Trieste, Italy

⁴ IFPU - Institute for fundamental physics of the Universe, Via Beirut 2, 34014 Trieste, Italy

⁵ INAF - Osservatorio astronomico d'Abruzzo, Via Maggini SNC, 64100, Teramo, Italy

⁶ Dipartimento di Fisica e Astronomia, Università di Firenze, Via G. Sansone 1, 50019, Sesto Fiorentino (Firenze), Italy

⁷ Department of Physics, University of Oxford, Denys Wilkinson Building, Keble Road, Oxford OX1 3RH, UK

⁸ Centro de Astrobiología (CAB), CSIC-INTA, Ctra. de Ajalvir km 4, Torrejón de Ardoz, E-28850, Madrid, Spain

⁹ Institute for the Advancement of Higher Education, Hokkaido University, Kita 17 Nishi 8, Kita-ku, Sapporo, Hokkaido 060-0817, Japan

¹⁰ Department of Cosmosciences, Graduate School of Science, Hokkaido University, Kita 10 Nishi 8, Kita-ku, Sapporo, Hokkaido 060-0810, Japan

February 28, 2024

ABSTRACT

Aims. The evolution of dwarf galaxies is dramatically affected by gaseous and dusty outflows, as they can easily deprive their interstellar medium of the material needed for the formation of new stars, simultaneously enriching their surrounding circumgalactic medium (CGM). In this Letter, we present the first evidence for extended [CII] 158 μm line and dust continuum emission in local dwarf galaxies hosting star-formation-driven outflows.

Methods. By stacking the [CII], far-infrared and near-UV (NUV) emission obtained from *Herschel* and GALEX data, we derive the average radial profiles, and compare the spatial extension of gas, dust, and stellar activity in dwarf galaxies.

Results. We find that [CII] and dust emissions are comparable to each other, and more extended than the NUV continuum. The [CII] size is in agreement with that measured for $z > 4$ star-forming galaxies, suggesting that similar mechanisms could be at the origin of the observed atomic carbon reservoir around local and high- z sources. The cold dust follows the [CII] emission, going beyond the stellar continuum as opposed to what is typically observed in the early Universe where measurements can be affected by the poor sensitivity and faintness of dust emission in the CGM of high- z galaxies.

Conclusions. We attribute the extended [CII] and dust continuum emission to the presence of galactic outflows. As local dwarf galaxies are considered analogs of primordial sources, we could expect that comparable feedback processes can be at the origin of the observed [CII] halos at $z > 4$, dominating over other possible formation mechanisms.

Key words. Galaxies: dwarf - Galaxies: evolution - Galaxies: ISM - Galaxies: starburst - ISM: jets and outflows

1. Introduction

The evolution of galaxies is regulated by the tangled interplay between gas, stars, and dust in their interstellar medium (ISM). This picture is further complicated by a continuous exchange of material with the surrounding circumgalactic medium (CGM) that can be driven by merging activity, inflow, and outflow of gas, giving rise to the so-called baryon cycle (see e.g., Tumlinson et al. 2017; Péroux & Howk 2020 for a review). Typically, the CGM can extend up to several kiloparsec, hosting a large reservoir of cosmic web-accreted gas and/or processed material ejected from galaxies, that can be used as fuel for future star formation.

Gas can be expelled from the ISM and injected into the CGM (or even further into the intergalactic medium, IGM) through high-velocity winds produced by stellar feedback (e.g., Gallerani et al. 2018; Ginolfi et al. 2020b; Romano et al. 2023) and ac-

tive galactic nuclei (AGNs, e.g., Cicone et al. 2015; Rupke et al. 2017; Jones et al. 2023). The ejected material can be made of dust, and ionized, atomic, and molecular gas that can be explored with different tracers and methods, including indirect observations of UV absorption lines along quasars lines of sight (e.g., Werk et al. 2016; Guo et al. 2020), or direct detections of emission lines such as HI 21 cm, Ly α , [CII] 158 μm , or CO transitions (e.g., Fujimoto et al. 2020; Sanderson et al. 2021; Ianjamasimanana et al. 2022; Jones et al. 2023).

Particularly, the [CII] line has gained a prominent role in the field of galaxy evolution, as it is a major coolant of the ISM and can provide precious information on the gas kinematics and morphology, star-formation activity, stellar feedback, and CGM enrichment (e.g., Ginolfi et al. 2020a; Jones et al. 2021; Romano et al. 2021). Due to its low ionization potential (i.e., 11.3 eV, as compared to the 13.6 eV of neutral hydrogen), [CII] can trace different gas phases (e.g., Pineda et al. 2013; Zanella et al. 2018; Heintz et al. 2021), although many studies suggest that

* E-mail: michael.romano@ncbj.gov.pl

A Spectropolarimetric Study of Pictor A Radio Galaxy with MeerKAT

Lexy A. L. Andati^{1*}, Lerato M. Baidoo^{1,2}, Athanaseus J. T. Ramaila^{1,3}, Oleg M. Smirnov^{1,3},
Sphesihle Makhathini^{4,1}, and Richard A. Perley^{5,1}

¹Centre for Radio Astronomy Techniques and Technologies, Department of Physics and Electronics, Rhodes University, PO Box 94, Makhanda 6140, South Africa

²Dunlap Institute for Astronomy and Astrophysics, University of Toronto, Toronto, ON M5S 3H4, Canada

³South African Radio Astronomy Observatory, 2 Fir Street, Black River Park, Observatory, 7925, South Africa

⁴School of Physics, University of the Witwatersrand, 1 Jan Smuts Avenue, Johannesburg 2000, South Africa

⁵National Radio Astronomy Observatory, Socorro, NM 87801, USA

Accepted XXX. Received YYY; in original form ZZZ

ABSTRACT

We present the results of a polarimetric study from our new high-sensitivity L-band (0.8–1.7 GHz) observation of Pictor A with the MeerKAT radio telescope. We confirm the presence of the radio jet extending from the nucleus to the western hotspot of this source. Additionally, we show the radio emission expected to be coincident with previously observed X-ray emission in the radio lobes, confirming that the emission mechanism is of inverse Compton origin, as suggested by a previous study. Our spectropolarimetric analysis using the RM-Synthesis technique reveals a relatively uniform mean RM distribution across the lobes of Pictor A, with most lines-of-sight exhibiting single-peaked Faraday spectra. However, a number of the lines-of-sight exhibit single peaked spectra with a wide base or multiple peaks, suggesting the presence of multiple Faraday components or a Faraday thick structure along Pictor A’s lines-of-sight. We also confirm the asymmetry in RM variability and depolarization between the two lobes of this source which were reported in a previous study.

Key words: Polarization – galaxies:magnetic fields – galaxies: interactions – galaxies: individual Pictor A

1 INTRODUCTION

Pictor A is the fifth-brightest discrete radio source in the Southern sky. It has a radio power of $3.79 \times 10^{26} \text{ W Hz}^{-1}$ (Robertson 1973) and is a FR-II galaxy (Fanaroff & Riley 1974), with structure consisting of two radio lobes, hotspots at the edge of each lobe, a core at its centre, and radio jets. Its host galaxy is centred at right ascension (RA, J2000) $5^{\text{h}}19^{\text{m}}50^{\text{s}}$ and declination (Dec) $-45^{\circ}46'44''$, and is identified as a broad-line galaxy (Halpern & Eracleous 1994; Lewis et al. 2010), with disc-like morphology (Inskip et al. 2010) of either Sa (Lauberts 1982) or S0 (Loveday 1996) type. Pictor A is at a redshift of 0.035 (Schmidt 1965), such that $1''$ angular scale corresponds to 0.697 kpc in linear scale.¹ This radio source has an angular size of ~ 8 arcmin in the East-West (EW) direction, and ~ 4 arcmin in the North-South (NS) direction, which corresponds to ~ 340 kpc EW and ~ 170 kpc NS in linear size, respectively (e.g. see fig. 3 of Perley et al. 1997).

The radio lobes of Pictor A are known for their remarkably round shape – with ellipticity > 0.9 (Perley et al. 1997), which is unusual for FR-II galaxies. The lobes of FR-II galaxies are usually found to be elongated along a specific direction (e.g. the direction of jet propagation). Thus, Perley et al. (1997) supposes that the lobes of Pictor A may be relaxed in a uniform environment – hence its uniform expansion in all directions. Moreover, these lobes showed no

edge brightening, except for filamentary structures particularly in the western lobe consisting of enhanced surface brightness of $0.5 \text{ mJy arcsec}^{-2}$. The presence of such filamentary structure is common in radio galaxies; for example, they are seen in the lobes of Cygnus A (Perley et al. 1984), Fornax A (Fomalont et al. 1989; Anderson et al. 2018), 4C 12.03, CGCG 044-046 and CGCG 021-063 (Fanaroff et al. 2021).

The X-ray emission spectra of Pictor A’s lobes are best modelled using a power-law model with a photon index of 1.57 ± 0.04 (Hardcastle et al. 2016), indicating that the dominant source of emission is the inverse Compton scattering of CMB photons off the relativistic electron population. Fitting a two-component model (power-law and thermal) to the region absent of radio emission, the authors found a ‘soft thermal emission’ component of temperature $0.33 \pm 0.07 \text{ keV}$ (also noted by Zirbel 1997) and a rather steep photon index of 2.07. The results were inconclusive, with no compelling evidence for including a thermal component.

The western hotspot (WHS hereon) is one of the brightest radio and X-ray hotspots known (Wilson et al. 2001; Hardcastle et al. 2004; Tingay et al. 2008). The radio hotspot is identified to be coincident with a compact, very bright (magnitude of 19.5) and highly polarized (> 30 per cent) source of optical emission (Roeser & Meisenheimer 1987), and with an extremely bright X-ray hotspot (Wilson et al. 2001). In the X-ray, Hardcastle et al. (2016) determined this hotspot to be variable on scales of months to a year. The eastern lobe has two hotspots (Prestage 1985; Perley et al. 1997).

The western radio jet was first observed by Perley et al. (1997), with no evidence of a counter-jet (the eastern jet). In the X-ray,

* E-mail: andatilexy@gmail.com

¹ Assuming a Λ CDM cosmological model, with $H_0 = 70 \text{ km s}^{-1} \Omega_m = 0.3$ and $\Omega_\Lambda = 0.7$.

Modelling LAEs in the Epoch of Reionization with OBELISK

The Connection Between Lyman- α Spectra and Lyman-Continuum Escape

Emma Giovinazzo¹, Maxime Trebitsch², Valentin Mauerhofer², Pratika Dayal², and Pascal A. Oesch^{1,3}

¹ Department of Astronomy, University of Geneva, Chemin Pegasi 51, 1290 Versoix, Switzerland

² Kapteyn Astronomical Institute, University of Groningen, P.O. Box 800, 9700 AV Groningen, The Netherlands

³ Cosmic Dawn Center (DAWN), Niels Bohr Institute, University of Copenhagen, Jagtvej 128, København N, DK-2200, Denmark

Received —; accepted —

ABSTRACT

Context. Lyman- α emitters (LAEs) are particularly useful objects for the study of the Epoch of Reionization. Lyman- α profiles can be used to estimate the amount of ionizing photons that are able to escape the galaxies, and therefore to understand what objects contributed to reionization. However, Lyman- α is a resonant line and its complex radiative transfer effects make the interpretation of the line challenging and require the use of appropriate radiative transfer methods for anything but the simplest gas distributions, such as uniform gaseous spheres, slabs or cubes.

Aims. With this work we aim to study the properties of simulated LAEs, and the robustness of these inferred properties under a change in the dust model. We also explore the Lyman Continuum (LyC) escape fraction of these galaxies and compare our results with observationally calibrated methods to infer this quantity from the Lyman- α spectrum.

Methods. We use the radiative transfer code `RASCAS` to perform synthetic observations of 13 flux-selected galaxies from the OBELISK simulation at redshift $z = 6$, towards the end of the Epoch of Reionization. Each galaxy was observed in Lyman- α , ionizing and non-ionizing continuum from 48 different viewing angles.

Results. We show that the Lyman- α profiles emitted from a galaxy present large variations with a change in viewing angle and that the relation between peak separation and Lyman- α escape fraction is not as strong as previously found, as we find lines of sight with both low peak separation and low escape fraction, due to their dust content. We also show that the properties of the Lyman- α line are reasonably robust under a change in dust model. Lastly, we compare the Lyman continuum escape fractions we derive from the simulation to three observationally calibrated methods of inferring this quantity. We determine that none of these relations reproduce the scatter that we find in our sample, and that high escape fraction lines of sight have both low peak separation and low dust extinction in the UV.

Key words. galaxies: high-redshift – reionization – Radiative transfer – Line: profiles

1. Introduction

The Epoch of Reionization (EoR) marks the last phase transition of the Universe, during which the initially cold and neutral intergalactic medium (IGM) became ionized. This period also marks the formation of the first luminous objects, which formed at the center of collapsed halos and produced sufficient amounts of ionizing radiation to drive the reionization process (e.g. Barkana & Loeb 2001, Dayal & Ferrara 2018).

Current constraints from quasar spectra place the end of the Epoch of Reionization around $z \sim 5.5 - 6$ (e.g., Wyithe et al. 2005; Fan et al. 2006; Eilers et al. 2018; Schroeder et al. 2012; Becker et al. 2021; Bosman et al. 2022), but it is still unclear which sources are responsible for the emission of the majority of the ionizing photons. It is commonly believed that the main driver of the reionization of hydrogen in the Universe is massive star formation in galaxies (e.g. Robertson et al. 2015; Bouwens et al. 2015; Finkelstein et al. 2019; Naidu et al. 2020; Trebitsch et al. 2022), as young and massive stars emit copious amounts of Lyman Continuum (LyC) radiation ($\lambda < 912 \text{ \AA}$). This scenario implicates a very patchy process (e.g. D’Aloisio et al. 2015; Davies & Furlanetto 2016; Eilers et al. 2018), where galaxies are able to ionize gas in their surroundings, forming growing bubbles of ionized gas around themselves until these

bubbles overlap and the entirety of the intergalactic medium is ionized. Another potentially important source of ionizing photons are Active Galactic Nuclei (AGNs) (e.g., Madau & Haardt 2015; Giallongo et al. 2015). However, studies of the AGN luminosity function in the EoR have shown that AGNs are only minor contributors of reionization and fail to solely reionize the universe by $z \sim 6$ (e.g. Onoue et al. 2017; Parsa et al. 2017; Matsuoka et al. 2023), although according to theoretical models, AGNs could dominate the ionizing photon production at the highest masses (Dayal et al. 2020).

To properly understand this process it is necessary to determine which galaxies leak the most ionizing photons, which depends on large scale properties of the IGM such as clumping, and on properties of the galaxies such as their star formation rate and the escape fraction of Lyman Continuum photons $f_{\text{esc}}(\text{LyC})$. This last parameter quantifies the fraction of ionizing photons that are able to escape the galaxy and therefore ionize the surrounding medium. Determining this quantity through observations is challenging, as it is only possible to observe the escaped radiation. Only recently have surveys been able to accumulate large numbers of direct detection of escaping ionizing photons (e.g. Bergvall et al. 2006, Shapley et al. 2006, Heckman et al. 2011, Leitert et al. 2013, Izotov et al. 2016a,b, Izotov et al. 2018a,b, Fletcher et al. 2019, Davis et al. 2021, Izotov et al.

Recovered SN Ia rate from simulated LSST images

V. Petrecca^{*1,2}, M. T. Botticella¹, E. Cappellaro³, L. Greggio³, B. O. Sánchez⁴, A. Möller⁵, M. Sako⁶, M. L. Graham⁷, M. Paolillo^{2,1,8}, F. Bianco^{9,10}, and the LSST Dark Energy Science Collaboration

¹ INAF - Osservatorio Astronomico di Capodimonte, Salita Moiariello 16, 80131 Napoli, Italy

² Department of Physics, University of Napoli “Federico II”, via Cinthia 9, 80126 Napoli, Italy

³ INAF – Osservatorio Astronomico di Padova, Vicolo dell’Osservatorio 5, Padova 35122, Italy

⁴ Aix Marseille Univ, CNRS/IN2P3, CPPM, Marseille, France

⁵ Centre for Astrophysics and Supercomputing, Swinburne University of Technology, Mail Number H29, PO Box 218, 31122 Hawthorn, VIC, Australia

⁶ Department of Physics and Astronomy, University of Pennsylvania, Philadelphia, PA 19104, USA

⁷ DIRAC Institute, Department of Astronomy, University of Washington, 3910 15th Avenue NE, Seattle, WA 98195, USA

⁸ INFN — Sezione di Napoli, via Cinthia 9, 80126, Napoli, Italy

⁹ University of Delaware, 210 South College Ave., Newark, DE 19716, USA

¹⁰ Vera C. Rubin Observatory, Tucson, AZ 85719, USA

Received 19 December 2023 / Accepted 23 February 2024

ABSTRACT

Aims. The Vera C. Rubin Observatory’s Legacy Survey of Space and Time (LSST) will revolutionize Time Domain Astronomy by detecting millions of different transients. In particular, it is expected to increment the number of type Ia supernovae (SN Ia) of a factor of 100 compared to existing samples up to redshift ~ 1.2 . Such a high number of events will dramatically reduce statistical uncertainties in the analysis of SN Ia properties and rates. However, the impact of all other sources of uncertainty on the measurement of the SN Ia rate must still be evaluated. The comprehension and reduction of such uncertainties will be fundamental both for cosmology and stellar evolution studies, as measuring the SN Ia rate can put constraints on the evolutionary scenarios of different SN Ia progenitors.

Methods. We use simulated data from the Dark Energy Science Collaboration (DESC) Data Challenge 2 (DC2) and LSST Data Preview 0 to measure the SN Ia rate on a 15 deg^2 region of the Wide-Fast-Deep area. We select a sample of SN candidates detected on difference images, associate them to the host galaxy with a specially developed algorithm, and retrieve their photometric redshifts. Then, we test different light curves classification methods, with and without redshift priors (albeit ignoring contamination from other transients, as DC2 contains only SN Ia). We discuss how the distribution in redshift measured for the SN candidates changes according to the selected host galaxy and redshift estimate.

Results. We measure the SN Ia rate analyzing the impact of uncertainties due to photometric redshift, host galaxy association and classification on the distribution in redshift of the starting sample. We found a 17% average lost fraction of SN Ia with respect to the simulated sample. As 10% of the bias is due to the uncertainty on the photometric redshift alone (which also affects classification when used as a prior), it results to be the major source of uncertainty. We discuss possible reduction of the errors in the measurement of the SN Ia rate, including synergies with other surveys, which may help using the rate to discriminate different progenitor models.

Key words. Stars: supernovae – Galaxies: stellar content: surveys

1. Introduction
















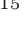





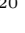
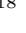
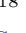











Type Ia supernovae (SN Ia) are violent explosions characterized by a peak in luminosity correlated to the duration of the event, which makes them standardizable candles (Phillips 1993; Tripp & Branch 1999) and fundamental cosmological probes (Riess et al. 1998; Perlmutter et al. 1999). There is general consensus that SN Ia are the result of a thermonuclear explosion of a carbon-oxygen White Dwarf (WD) with two possible progenitor channels: a WD accreting mass from a non-degenerate star (single degenerate scenario SD; Whelan & Iben 1973) or two WD spiraling together and eventually merging (double degenerate scenario DD; Webbink 1984; Iben & Tutukov 1984). However, the exact nature of their progenitors and the details of the explosion mechanism are not yet clear (see Livio & Mazzali 2018 for a recent review). Direct observations of both pre- and post-

explosion images do not provide unambiguous evidence for either SN Ia progenitor systems (e.g., Kelly et al. 2014; Graur & Woods 2019), or surviving companions (e.g., Schaefer & Pagnotta 2012; Kerzendorf et al. 2019). Similarly, detailed spectral analyses of SN Ia and their remnants are not able to clearly identify the companion star in the binary system (e.g., Badenes et al. 2007; Foley et al. 2012; Dhawan et al. 2016). The diversity of the SN Ia light curves and their correlation with the host galaxy properties are also not able to exclude any progenitor scenario, hence both of them might be at play.

An alternative way of putting constraints on the SN Ia progenitors system is the analysis of the delay times distribution (DTD), which is the time between the formation of the binary system and the SN Ia explosion. Different progenitor scenarios imply a different DTD from population synthesis models (Wang & Han 2012). As the SN Ia rate results from the convolution of the host galaxy star formation rate (SFR) and the DTD (Greggio 2005; Greggio 2010), measuring the SN Ia rate and the SFR for

* vincenzo.petrecca@inaf.it

Three Warm Jupiters around Solar-analog stars detected with *TESS**

JAN EBERHARDT ¹, MELISSA J. HOBSON ^{1,2}, THOMAS HENNING ¹, TRIFON TRIFONOV ^{1,3,4}, RAFAEL BRAHM ^{5,2},
NESTOR ESPINOZA ⁶, ANDRÉS JORDÁN ^{5,2}, DANIEL THORNGREN ⁷, REMO BURN ¹, FELIPE I. ROJAS ^{8,2},
PAULA SARKIS ¹, MARTIN SCHLECKER ^{9,1}, MARCELO TALA PINTO ^{5,10}, KHALID BARKAOUI ^{11,12,13},
RICHARD P. SCHWARZ ¹⁴, OLGA SUAREZ ¹⁵, TRISTAN GUILLOT ¹⁵, AMAURY H.M.J. TRIAUD ¹⁶,
MAXIMILIAN N. GÜNTHER ¹⁷, LYU ABE ¹⁵, GAVIN BOYLE ^{18,19}, RODRIGO LEIVA ^{2,20}, VINCENT SUC ^{5,18},
PHIL EVANS ¹⁸, NICK DUNCKEL ¹⁸, CARL ZIEGLER ²¹, BEN FALK ⁶, WILLIAM FONG ²², ALEXANDER RUDAT ²²,
AVI SHPORER ²², STEPHANIE STRIEGEL ²³, DAVID WATANABE ²⁴, JON M. JENKINS ²⁵, SARA SEAGER ^{22,12,26},
AND JOSHUA N. WINN ²⁷

¹Max-Planck-Institut für Astronomie, Königstuhl 17, D-69117 Heidelberg, Germany

²Millennium Institute for Astrophysics, Chile

³Department of Astronomy, Sofia University “St Kliment Ohridski”, 5 James Bourchier Blvd, BG-1164 Sofia, Bulgaria

⁴Landessternwarte, Zentrum für Astronomie der Universität Heidelberg, Königstuhl 12, D-69117 Heidelberg, Germany

⁵Facultad de Ingeniería y Ciencias, Universidad Adolfo Ibáñez, Av. Diagonal las Torres 2640, Peñalolén, Santiago, Chile

⁶Space Telescope Science Institute, 3700 San Martin Drive, Baltimore, MD 21218, USA

⁷Department of Physics & Astronomy, Johns Hopkins University, Baltimore, MD, USA

⁸Instituto de Astrofísica, Facultad de Física, Pontificia Universidad Católica de Chile, Chile

⁹Department of Astronomy/Steward Observatory, The University of Arizona, 933 North Cherry Avenue, Tucson, AZ 85721, USA

¹⁰Millennium Institute of Astrophysics, Santiago, Chile

¹¹Astrobiology Research Unit, Université de Liège, Allée du 6 Août 19C, B-4000 Liège, Belgium

¹²Department of Earth, Atmospheric and Planetary Sciences, Massachusetts Institute of Technology, Cambridge, MA 02139, USA

¹³Instituto de Astrofísica de Canarias (IAC), E-38200 La Laguna, Tenerife, Spain

¹⁴Center for Astrophysics | Harvard & Smithsonian, 60 Garden St, Cambridge, MA 02138, USA

¹⁵Université Côte d’Azur, Observatoire de la Côte d’Azur, CNRS, Laboratoire Lagrange, Bd de l’Observatoire, CS 34229, F-06304 Nice cedex 4, France

¹⁶School of Physics & Astronomy, University of Birmingham, Edgbaston, Birmingham B15 2TT, United Kingdom

¹⁷European Space Agency (ESA), European Space Research and Technology Centre (ESTEC), Keplerlaan 1, 2201 AZ Noordwijk, The Netherlands

¹⁸El Sauce Observatory, Coquimbo Province, Chile

¹⁹Cavendish Laboratory, J J Thomson Avenue, Cambridge, CB3 0HE, UK

²⁰Instituto de astrofísica de Andalucía, CSIC, Glorieta de la Astronomía s/n, E-18008 Granada, Spain

²¹Department of Physics, Engineering and Astronomy, Stephen F. Austin State University, 1936 North Street, Nacogdoches, TX 75962

²²Department of Physics and Kavli Institute for Astrophysics and Space Research, Massachusetts Institute of Technology, Cambridge, MA 02139, USA

²³SETI Institute, Mountain View CA 94043 USA/NASA Ames Research Center, Moffett Field CA 94035 USA

²⁴Planetary Discoveries, Valencia CA, USA

²⁵NASA Ames Research Center, Moffett Field, CA 94035, USA

²⁶Department of Aeronautics and Astronautics, MIT, 77 Massachusetts Avenue, Cambridge, MA 02139, USA

²⁷Department of Astrophysical Sciences, Princeton University, NJ 08544, USA

(Revised February 28, 2024; Accepted —)

Abstract

We report the discovery and characterization of three giant exoplanets orbiting solar-analog stars, detected by the *TESS* space mission and confirmed through ground-based photometry and radial velocity (RV) measurements taken at La Silla observatory with *FEROS*. TOI-2373 b is a warm Jupiter orbiting its host star every ~ 13.3 days, and is one of the two most massive known exoplanet with a precisely determined mass and radius around a star similar to the Sun, with an estimated mass of m_p

* Based on observations collected at the European Organization for Astronomical Research in the Southern Hemisphere under MPG programmes 0104.A-9007(A) and 0106.A-9014(A)

Extrapolating the projected potential of gravitational lens models: property-preserving degeneracies

Jori Liesenborgs^{1*}, Derek Perera² and Liliya L.R. Williams²

¹ *UHasselt – Flanders Make, Expertisecentrum voor Digitale Media, Wetenschapspark 2, B-3590, Diepenbeek, Belgium*

² *School of Physics and Astronomy, University of Minnesota, 116 Church Street SE, Minneapolis, MN 55455, USA*

ABSTRACT

While gravitational lens inversion holds great promise to reveal the structure of the light-deflecting mass distribution, both light and dark, the existence of various kinds of degeneracies implies that care must be taken when interpreting the resulting lens models. This article illustrates how thinking in terms of the projected potential helps to gain insight into these matters. Additionally it is shown explicitly how, when starting from a discretised version of the projected potential of one particular lens model, the technique of quadratic programming can be used to create a multitude of equivalent lens models that preserve all or a subset of lens properties. This method is applied to a number of scenarios, showing the lack of grasp on the mass outside the strong lensing region, revisiting mass redistribution in between images and applying this to a recent model of the SDSS J1004+4112 cluster, as well as illustrating the generalised mass sheet degeneracy and source-position transformation. In the case of J1004 we show that this mass redistribution did not succeed at completely eliminating a dark mass clump recovered by GRALE near one of the quasar images.

Key words: gravitational lensing: strong – gravitational lensing: weak – methods: data analysis – galaxies: clusters: individual: SDSS J1004+4112

1 INTRODUCTION

Apart from causing beautiful observations, the light deflection caused by the gravitational lens effect holds the promise of providing insight into the distribution of the matter responsible for this deflection, as well as for probing parameters of the cosmological model. To make this possible, one typically needs to try to invert the lens effect, e.g. try to reconstruct a model for the gravitational lens that is compatible with the observations.

Over the years, several techniques for doing so have been developed, differing in the kinds of observations they use as input as well as in how the matter distribution it tries to reconstruct, is modeled. This ranges from statistical analyses of small deformations of background galaxies, i.e. weak lensing data, to the use of multiple, possibly highly deformed images, also referred to as a strong lensing scenario. The cause of the deflection, the matter distribution of the lens itself, can be modelled by a relatively small number of density profiles, typically aligned with the visible matter (e.g. LENS_{TOOL}, Jullo et al. (2007)), by a large set of basis functions, intended to be capable of modelling a wide variety of distributions (e.g. PIXE_{LENS}, Saha & Williams (2004), Coles (2008)), or even by both of these options, in a more hybrid approach (e.g. WSLAP+, Sendra et al. (2014)). Others still do not model the mass distribution directly, but instead model the lens’

gravitational potential (e.g. RELENSING, Torres-Ballesteros & Castañeda (2023)).

Irrespective of the procedure and input data that are used, it is important to realize that a solution to the inversion problem is not uniquely determined, that there exist various kinds of degenerate solutions that are able to explain the observations equally well. Some of these are exact by nature, others differ in principle but only cause changes that still lie within the known observational uncertainties. Depending on how the mass distribution is modelled, these degeneracies can manifest themselves in different ways. It may even seem that there are no such degeneracies present, if the inversion technique used does not provide the freedom needed to describe equivalent solutions. The existence of multiple, equally compatible solutions is fundamental however, so care must be taken when interpreting inversion results.

In this article we illustrate how thinking about lens inversion not on the level of the mass distribution itself, but the potential causing it, can help gain additional insight into which properties can actually be constrained well. Assuming that one solution to the lens inversion problem is known, a tool is introduced that uses quadratic programming to search for lens models that are equally compatible with the observed data.

After briefly reiterating the gravitational lensing formalism in section 2, a toy model will be introduced in section 3 to study an effect that is often encountered when performing lens inversions with our own method GRALE, namely mass density peaks outside of the region covered by the multiple

* Corresponding author: jori.liesenborgs@uhasselt.be

Double, double, toil, and trouble:

The tails, bubbles, and knots of the local compact obscured nucleus galaxy NGC 4418

C. F. Wethers¹*, S. Aalto¹, G. C. Privon^{2,3,4}, F. Stanley⁵, J. Gallagher⁶, M. Gorski¹, S. König¹, K. Onishi¹, M. Sato¹, C. Yang¹, R. Beswick⁷, L. Barcos-Munoz⁸, F. Combes⁹, T. Diaz-Santos¹⁰, A. S. Evans^{11,8}, I. Garcia-Bernete¹², C. Henkel^{13,14}, M. Imanishi¹⁵, S. Martín^{16,17}, S. Müller¹, Y. Nishimura¹⁸, C. Ricci^{19,20}, D. Rigopoulou², and S. Viti^{21,22};

(Affiliations can be found after the references)

Received ????: accepted ????

ABSTRACT

Context. Compact obscured nuclei (CONs) are an extremely obscured ($N_{\text{H}_2} > 10^{25} \text{ cm}^{-2}$) class of galaxy nuclei thought to exist in 20-40 per cent of nearby (ultra-)luminous infrared galaxies. While they have been proposed to represent a key phase of the active galactic nucleus (AGN) feedback cycle, the nature of these CONs – what powers them, their dynamics, and their impact on the host galaxy – remains unknown.

Aims. This work analyses the galaxy-scale optical properties of the local CON NGC 4418 ($z=0.00727$). The key aims of the study are to understand the impact of nuclear outflows on the host galaxy and infer the power source of its CON. Through the mapping of the galaxy spectra and kinematics, we seek to identify new structures in NGC 4418 to ultimately reveal more about the CON's history, its impact on the host, and, more generally, the role CONs play in galaxy evolution.

Methods. We present new, targeted integral field unit observations of the galaxy with the Multi-Unit Spectroscopic Explorer (MUSE). For the first time, we mapped the ionised and neutral gas components of the galaxy, along with their dynamical structure, to reveal several previously unknown features of the galaxy.

Results. We confirm the presence of a previously postulated, blueshifted outflow along the minor axis of NGC 4418. We find this outflow to be decelerating and, for the first time, show it to extend in both directions from the nucleus. We report the discovery of two further outflow structures: a redshifted southern outflow connected to a tail of ionised gas surrounding the galaxy and a blueshifted bubble to the north. In addition to these features, we find the [O III] emission reveals the presence of knots across the galaxy, which are consistent with regions of the galaxy that have been photoionised by an AGN.

Conclusions. We identify several new features in NGC 4418, including a bubble structure, a reddened outflow, and [O III] knot structures throughout the galaxy. We additionally confirm the presence of a bilateral blueshifted outflow along the minor axis. Based on the properties of these features, we conclude that the CON in NGC 4418 is most likely powered by AGN activity.

Key words. galaxies: nuclei – galaxies: kinematics and dynamics – galaxies: evolution – galaxies: active

1. Introduction

Compact obscured nuclei (CONs) have been shown to exist in as many as 40 per cent of nearby (ultra-)luminous infrared galaxies ((U)LIRGs; e.g. Falstad et al. 2021; García-Bernete et al. 2022). These compact (<100 pc) nuclear structures are characterised by their extreme nuclear column densities, $N_{\text{H}_2} > 10^{25} \text{ cm}^{-2}$ (e.g. Sakamoto et al. 2013), which make them almost invisible at mid-IR, optical, and even X-ray wavelengths due to the heavy attenuation (e.g. Treister et al. 2010; Lusso et al. 2013; Roche et al. 2015). Currently, the only way to identify CONs is through the rare $\nu_2 = 1$ transition of vibrationally excited HCN (HCN-VIB), which is usually radiatively excited by intense mid-IR emission from hot dust at high column densities (Aalto et al. 2015). While a handful of alternative identification methods are being developed (e.g. Donnan et al. 2023), including using the 1 millimetre surface brightness (Falstad et al. 2021) and the silicate absorption slope (García-Bernete et al. 2022), no CONs have yet been confirmed via these methods.

Although the exact nature of CONs remains unknown, they likely play a critical role in the evolution of galaxies as an early, obscured starburst phase in which remnant material is being expelled from the centre of the galaxy via, for example, active galactic nucleus (AGN) driven outflows. Such a phase could represent the early stages of a feedback cycle, where a fraction of the expelled gas will eventually fall back into the galactic plane. Indeed, while only a handful of CONs have been confirmed in the nearby Universe ($z < 0.05$), all show signatures of molecular outflows in HCN and/or CO, and several host molecular gas inflows (Falstad et al. 2021). Even in the CONs with no obvious inflow signatures, the CO outflows appear to be slow ($V < 400 \text{ km s}^{-1}$), meaning this gas will likely remain within the galaxy. This inflow and outflow feedback cycle provides a key mechanism by which a super-massive black hole (SMBH) affects its host galaxy on scales larger than its sphere of influence. Thus, identifying these CON outflows, understanding what drives them, and quantifying their effect on the larger-scale galaxy properties is critical in building a co-evolutionary model of galaxies.

* e-mail: wethers@chalmers.se

CosmoMIA: Cosmic Web-based redshift space halo distribution

D. Forero Sánchez,¹ F.-S. Kitaura,^{2,3} F. Sinigaglia,^{4,5,2,3} J.M. Coloma-Nadal,^{6,2} J.-P. Kneib¹

¹Institute of Physics, Laboratory of Astrophysics, École Polytechnique Fédérale de Lausanne (EPFL), Observatoire de Sauverny, CH-1290 Versoix, Switzerland

²Instituto de Astrofísica de Canarias, Calle Via Láctea s/n, E-38205, La Laguna, Tenerife, Spain

³Departamento de Astrofísica, Universidad de La Laguna, E-38206, La Laguna, Tenerife, Spain

⁴Département d'Astronomie, Université de Genève, Chemin Pegasi 51, CH-1290 Versoix, Switzerland

⁵Institut für Astrophysik, Universität Zürich, Winterthurerstrasse 190, CH-8057 Zürich, Switzerland

⁶Institute of Space Sciences (ICE, CSIC), Campus UAB, Carrer de Can Magrans, s/n, 08193 Barcelona, Spain

E-mail: daniel.forerosanchez@epfl.ch, fkitaura@iac.es

Abstract. Modern galaxy surveys demand extensive survey volumes and resolutions surpassing current dark matter-only simulations' capabilities. To address this, many methods employ effective bias models on the dark matter field to approximate object counts on a grid. However, realistic catalogs necessitate specific coordinates and velocities for a comprehensive understanding of the Universe. In this research, we explore sub-grid modeling to create accurate catalogs, beginning with coarse grid number counts at resolutions of approximately $5.5, h^{-1}$ Mpc per side. These resolutions strike a balance between modeling nonlinear damping of baryon acoustic oscillations and facilitating large-volume simulations. Augmented Lagrangian Perturbation Theory (ALPT) is utilized to model the dark matter field and motions, replicating the clustering of a halo catalog derived from a massive simulation at $z = 1.1$. Our approach involves four key stages: Tracer Assignment: Allocating dark matter particles to tracers based on grid cell counts, generating additional particles to address discrepancies. Attractor Identification: Defining attractors based on particle cosmic web environments, acting as gravitational focal points. Tracer Collapse: Guiding tracers towards attractors, simulating structure collapse. Redshift Space Distortions: Introducing redshift space distortions to simulated catalogs using ALPT and a random dispersion term. Results demonstrate accurate reproduction of monopoles and quadrupoles up to wave numbers of approximately $k = 0.6, h$ Mpc⁻¹. This method holds significant promise for galaxy surveys like DESI, EUCLID, and LSST, enhancing our understanding of the cosmos across scales.

¹daniel.forerosanchez@epfl.ch

²fkitaura@iac.es

Optimization of foreground moment deprojection for semi-blind CMB polarization reconstruction

A. Carones,^{a,b} M. Remazeilles^c

^aDipartimento di Fisica, Università di Roma “Tor Vergata”, via della Ricerca Scientifica 1, I-00133, Roma, Italy

^bSezione INFN Roma 2, via della Ricerca Scientifica 1, I-00133, Roma, Italy

^cInstituto de Física de Cantabria (CSIC-UC), Avda. los Castros s/n, 39005 Santander, Spain

E-mail: alessandro.carones@roma2.infn.it, remazeilles@ifca.unican.es

Abstract. Upcoming Cosmic Microwave Background (CMB) experiments, aimed at measuring primordial CMB polarization B -modes, require exquisite control of instrumental systematics and Galactic foreground contamination. Blind minimum-variance techniques, like the Needlet Internal Linear Combination (NILC), have proven effective in reconstructing the CMB polarization signal and mitigating foregrounds and systematics across diverse sky models without suffering from foreground mismodelling errors. Still, residual foreground contamination from NILC may bias the recovered CMB polarization at large angular scales when confronted with the most complex foreground scenarios. By adding constraints to NILC to deproject statistical moments of the Galactic emission, the Constrained Moment ILC (cMILC) method has been demonstrated to further enhance foreground subtraction, albeit with an associated increase in overall noise variance. Faced with this trade-off between foreground bias reduction and overall variance minimization, there is still no recipe on which moments to deproject and which are better suited for blind variance minimization. To address this, we introduce the optimized cMILC (ocMILC) pipeline, which performs full automated optimization of the required number and set of foreground moments to deproject, pivot parameter values, and deprojection coefficients across the sky and angular scales, depending on the actual sky complexity, available frequency coverage, and experiment sensitivity. The optimal number of moments for deprojection, before paying significant noise penalty, is determined through a data diagnosis inspired by the Generalized NILC (GNILC) method. Validated on B -mode simulations of the *PICO* space mission concept with four challenging foreground models, ocMILC exhibits lower Galactic foreground contamination compared to NILC and cMILC at all angular scales, with limited noise penalty. This multi-layer optimization enables the ocMILC pipeline to achieve unbiased posteriors of the tensor-to-scalar ratio, regardless of foreground complexity.

Keywords: CMBR polarization – CMBR experiments

Ph.D. Dissertation

BRNO 2015

PETR KURFÜRST

Bibliographic Entry

Author: Petr Kurfürst
Faculty of Science, Masaryk University
Department of Theoretical Physics and Astrophysics

Title of Thesis: Models of hot star decretion disks

Degree Programme: Physics

Field of Study: Theoretical Physics and Astrophysics

Supervisor: Prof. Mgr. Jiří Krtička, Ph.D.
Faculty of Science, Masaryk University
Department of Theoretical Physics and Astrophysics

Academic Year: 2015/2016

Number of Pages: 20 + 167

Keywords: stars: mass-loss – stars: evolution – stars: rotation – hydrodynamics

SYREN-HALOFIT: A fast, interpretable, high-precision formula for the Λ CDM nonlinear matter power spectrum

Deaglan J. Bartlett^{*1}, Benjamin D. Wandelt^{1,2}, Matteo Zennaro³, Pedro G. Ferreira³, and Harry Desmond⁴

¹ CNRS & Sorbonne Université, Institut d'Astrophysique de Paris (IAP), UMR 7095, 98 bis bd Arago, F-75014 Paris, France

² Center for Computational Astrophysics, Flatiron Institute, 162 5th Avenue, New York, NY 10010, USA

³ Astrophysics, University of Oxford, Denys Wilkinson Building, Keble Road, Oxford OX1 3RH, UK

⁴ Institute of Cosmology & Gravitation, University of Portsmouth, Dennis Sciama Building, Portsmouth, PO1 3FX, UK

Received XXX; accepted YYY

ABSTRACT

Context. Rapid and accurate evaluation of the nonlinear matter power spectrum, $P(k)$, as a function of cosmological parameters and redshift is of fundamental importance in cosmology. Analytic approximations provide an interpretable solution, yet current approximations are neither fast nor accurate relative to black-box numerical emulators.

Aims. To accelerate symbolic approximations to $P(k)$ by removing the requirement to perform integrals, instead using short symbolic expressions to compute all variables of interest. We also wish to make such expressions more accurate by re-optimising the parameters of these models (using a larger number of cosmologies and focusing on cosmological parameters of more interest for present-day studies) and providing correction terms.

Methods. We use symbolic regression to obtain simple analytic approximations to the nonlinear scale, k_σ , the effective spectral index, n_{eff} , and the curvature, C , which are required for the HALOFIT model. We then re-optimize the coefficients of HALOFIT to fit a wide range of cosmologies and redshifts. We then again exploit symbolic regression to explore the space of analytic expressions to fit the residuals between $P(k)$ and the optimised predictions of HALOFIT. All methods are validated against N -body simulations.

Results. We find symbolic expressions for k_σ , n_{eff} and C which have root mean squared fractional errors of 0.8%, 0.2% and 0.3%, respectively, for redshifts below 3 and a wide range of cosmologies. We provide re-optimised HALOFIT parameters, which reduce the root mean squared fractional error from 3% to below 2% for wavenumbers $k = 9 \times 10^{-3} - 9 h\text{Mpc}^{-1}$. We introduce SYREN-HALOFIT (symbolic-regression-enhanced HALOFIT), an extension to HALOFIT containing a short symbolic correction which improves this error to 1%. Our method is 2350 and 3170 times faster than current HALOFIT and HMCODE implementations, respectively, and 2680 and 64 times faster than EUCLIDEMULATOR2 (which requires running CLASS) and the BACCO emulator. We obtain comparable accuracy to EUCLIDEMULATOR2 and the BACCO emulator when tested on N -body simulations.

Conclusions. Our work greatly increases the speed and accuracy of symbolic approximations to $P(k)$, making them significantly faster than their numerical counterparts without loss of accuracy.

Key words. Cosmology: theory, Cosmology: cosmological parameters, Cosmology: large-scale structure of Universe, Methods: numerical

1. Introduction

Under the current cosmological paradigm, the large scale structure of the Universe evolved under gravity and cosmic expansion from highly Gaussian density fluctuations in the distant past to the present-day cosmic web. Despite the remarkable simplicity of the standard model (Λ CDM), which contains just six parameters, the nonlinear equations of motion necessitate the computationally non-trivial task of simulating this evolution, which is typically done through expensive N -body simulations. The nonlinear evolution has a dramatic effect on the matter power spectrum, $P(k)$, greatly enhancing the small-scale power compared to linear theory, and thus these effects cannot be neglected. Even linear theory – which is valid on large scales – requires solving a hierarchy of coupled, linear differential equations (Lewis et al. 2000; Blas et al. 2011; Hahn et al. 2023), demonstrating the difficulty in obtaining accurate predictions for $P(k)$.

Given the importance of the power spectrum in cosmological analyses, much effort has been put into by-passing these expensive simulations and directly predicting the matter power spec-

trum as a function of time and cosmological parameters. Speed and differentiability of surrogate models are particularly attractive features. For example, the first high-precision emulator for the linear outputs of Boltzmann codes, `PICO` (Fendt & Wandelt 2007a,b) enabled the first use of Hamiltonian Monte Carlo methods for cosmological parameter inference (Hajian 2007) due to these properties.

Approximations to the linear matter power spectrum are well-established, notably those of Eisenstein & Hu (1998, 1999), which are accurate to a few percent, and the earlier work of Bardeen et al. (1986), which provided a less accurate approximation. More recently, simple expressions which obtain a similar accuracy to Eisenstein & Hu were obtained by Bayron Orjuela-Quintana et al. (2022, 2023), although these do not have the same physical motivation as the earlier works. However, these symbolic expressions are insufficiently accurate for modern uses. This led Bartlett et al. (2023) to propose a simple extension to the Eisenstein & Hu expressions which gives a root mean squared fractional error of just 0.2% across a wide range of cosmologies, which is more than sufficient for current analyses (Taylor et al. 2018).

* deaglan.bartlett@iap.fr

Collisional excitation of propyne (CH₃CCH) by He atoms

M. Ben Khalifa* B. Darna and J. Loreau

KU Leuven, Department of Chemistry, Celestijnenlaan 200F, B-3001 Leuven, Belgium.
e-mail: malek.benkhalfifa@kuleuven.be, jerome.loreau@kuleuven.be

February 28, 2024

ABSTRACT

Context. A detailed interpretation of the detected emission lines of environments in which propyne (or methyl acetylene, CH₃CCH) is observed requires a knowledge of its collisional rate coefficients with the most abundant species in the interstellar medium, He or H₂.

Aims. We present the first three-dimensional potential energy surface (3D-PES) for the CH₃CCH-He molecular complex, study the dynamics of the collision, and report the first set of rate coefficients for temperatures up to 100 K for the collisional excitation of the lowest 60 *ortho* rotational levels and 60 *para* rotational levels of CH₃CCH by He atoms.

Methods. We computed the 3D-PES with the explicitly correlated coupled-cluster with single-, double-, and perturbative triple-excitation method, in conjunction with the augmented correlation-consistent triple zeta basis set (CCSD(T)-F12a/aug-cc-pVTZ). The 3D-PES was fitted to an analytical function. Scattering computations of pure rotational (de-)excitation of CH₃CCH by collision with He atoms were performed and the state-to-state cross sections were computed using the close coupling method for total energies up to 100 cm⁻¹ and with the coupled states approximation at higher energy for both *ortho* and *para* symmetries of CH₃CCH.

Results. The PES obtained is characterized by a large anisotropy and a potential well depth of 51.04 cm⁻¹. By thermally averaging the collisional cross sections, we determined quenching rate coefficients for kinetic temperatures up to 100 K. A strong even Δj propensity rule at almost all collision energies exists for CH₃CCH-He complex. To evaluate the impact of rate coefficients in the analysis of observations, we carried out non-LTE radiative transfer computations of the excitation temperatures and we demonstrate that LTE conditions are typically not fulfilled for the propyne molecule.

Key words. scattering – ISM: molecules – astrochemistry

1. Introduction

Over the past decades, methyl acetylene (or propyne, CH₃CCH) has received significant attention from the astrophysical and astrochemistry communities due to its important role in astrochemical processes (Mebel et al. 2017; Herbst 2017) such as its role as a precursor in the formation of several polycyclic aromatic hydrocarbons (PAHs) (Parker & Kaiser 2017).

The earliest tentative detection of propyne in the interstellar medium (ISM) was reported toward the Sgr B2 molecular cloud by Buhl & Snyder (1973). Later, propyne was observed by Lovas et al. (1976) towards Orion A and Sagittarius B2 through the 5₀ → 4₀ rotational line at 85 GHz. In the following years, CH₃CCH was identified in various astronomical environments: low mass star-forming regions (van Dishoeck et al. 1995), photodissociation regions through the Horsehead nebula with fractional abundances of 10⁻⁹ with respect to molecular hydrogen (Gratier et al. 2013; Guzmán et al. 2014; Hickson et al. 2016), massive young stellar objects (Fayolle et al. 2015), circumstellar envelopes of evolved stars (Agúndez et al. 2008) and even toward extragalactic sources such as M82, NGC 253, and NGC 1068 (Mauersberger et al. 1991; Qiu et al. 2020). It has also been detected in cold and dense cores (Vastel et al. 2014; Gratier et al. 2016) and even toward a planetary nebula, as recently reported by Schmidt & Ziurys (2019). As a matter of fact, the widespread detection of propyne even extends to planetary atmospheres: in our solar system, CH₃CCH has also been detected on Jupiter, Saturn, Uranus as well as in the atmosphere of Titan (Fouchet

et al. 2000; De Graauw et al. 1997; Burgdorf et al. 2006; Teanby et al. 2009).

The formation pathways of propyne in the gas phase have been widely studied and it has been demonstrated that there are no efficient synthetic pathways in gas-phase available to reproduce the abundances of CH₃CCH in the cold molecular clouds (Hickson et al. 2016). It was proposed that the principal source of propyne in the gas phase is via ion-molecule reactions with C₂H₂⁺ as a precursor (Schiff & Bohme 1979), neutral-neutral reactions such as CCH + CH₄ → CH₃CCH + H (Turner et al. 1999) as well as dissociative recombination reactions involving larger hydrocarbons (Calcutt et al. 2019).

Those pathways were not capable to reproduce the observed abundance of CH₃CCH in the astrophysical media. For this reason, surface reactions occurring on interstellar grains were additionally studied (Hickson et al. 2016; Guzmán et al. 2018). Propyne molecules are believed to adhere to the cold dust grains and then undergo hydrogenation at cold molecular cloud temperature of about 10 K. CH₃CCH was demonstrated to form through the hydrogenation of C₃ radical which could be further hydrogenated to propene. Nevertheless, the model including grain surface and gas phase reactions was not able to reproduce the observed methyl acetylene abundance by more than one order of magnitude. This failure to reproduce the abundance of propyne demonstrate that more crucial formation pathways are still unknown at low temperatures (Hickson et al. 2016; Guzmán et al. 2014; Öberg et al. 2013).

CH₃CCH is a symmetric top molecule and among the most efficient thermometers available. For a given j , the rotational levels

* ,

Peeling Back the Layers of Extinction of Dusty Galaxies in the Era of JWST: Modelling Joint NIRSpec + MIRI Spectra at rest-frame 1.5 - 28 μm

F. R. Donnan,^{1*} I. García-Bernete,¹ D. Rigopoulou,^{1,2} M. Pereira-Santaella,³ P. F. Roche,¹ A. Alonso-Herrero⁴

¹*Department of Physics, University of Oxford, Keble Road, Oxford, OX1 3RH, UK*

²*School of Sciences, European University Cyprus, Diogenes street, Engomi, 1516 Nicosia, Cyprus*

³*Instituto de Física Fundamental, CSIC, Calle Serrano 123, E-28006, Madrid, Spain*

⁴*Centro de Astrobiología (CAB), CSIC-INTA, Camino Bajo del Castillo s/n, E-28692 Villanueva de la Cañada, Madrid, Spain*

Accepted XXX. Received YYY; in original form ZZZ

ABSTRACT

We present an analysis of the combined NIRSpec and MIRI spectra of dusty galaxies between 1.5 - 28 μm restframe by implementing a differential extinction model, where the strength of extinction varies across the spectrum as different layers of the obscuring dust are probed. Our model is able to recover a 2D distribution of dust temperature and extinction which allows inference of the physical nature of the dust in these environments. We show that differential extinction is necessary to reproduce the spectra of 4 highly obscured Luminous Infrared Galaxies observed with NIRSpec IFU and MIRI MRS, where simple screen or uniformly mixed dust distributions fail to fit the data. We additionally compare the extinction of HII regions in these galaxies via hydrogen recombination lines, the extinction of molecular gas via the H₂ lines, Polycyclic Aromatic Hydrocarbons via the 12.7/11.3 PAH ratio and the stellar continuum. We find that the molecular gas is deeply buried with the HII regions in star-forming regions, with a similar extinction to the hottest dust components. However we find the cooler dust to be less obscured, at a similar extinction to the stellar continuum and PAHs. The nuclei show a complex dust distribution with VV114 NE, NGC 3256 S, IIZw96 SW showing a deeply buried continuum source relative to the molecular gas/HII regions. Additionally, NGC 3256 S, NGC 7469 and VV114 SW show an isolated hot dust component, indicative of AGN heating, where NGC 3256 S and NGC 7469 are previously known AGN.

Key words: galaxies: nuclei – galaxies: evolution – techniques: spectroscopic

1 INTRODUCTION

Luminous Infrared Galaxies (LIRGs, $L_{\text{IR}} > 10^{11}L_{\odot}$) and Ultraluminous Infrared Galaxies (ULIRGs, $L_{\text{IR}} > 10^{12}L_{\odot}$) are dust and gas rich galaxies, with dust enshrouded star formation and AGN activity (e.g. Sanders & Mirabel 1996; Rigopoulou et al. 1999; Lonsdale et al. 2006). These galaxies play a key role in the evolution of galaxies, making up the bulk of the star formation rate density at cosmic noon (e.g. Le Floc’h et al. 2005; Magnelli et al. 2011). In addition $\sim 40\%$ of local ULIRGs contain Compact Obscured Nuclei (CONs; Falstad et al. 2021; García-Bernete et al. 2022b; Donnan et al. 2023b), which hide rapid, active supermassive black hole growth and/or extremely compact starbursts (e.g. Veilleux et al. 2009; Aalto et al. 2015, 2019; Pereira-Santaella et al. 2021).

As a consequence of the vast quantities of dust, emission in the optical is absorbed and reprocessed in the infrared. Therefore observations in the infrared are required to accurately measure properties of these galaxies such as the star-formation rate, properties of the ISM etc. In particular, the mid-infrared is a feature rich region of the spectrum, with dust emission and absorption signatures, Polycyclic

Aromatic Hydrocarbons (PAHs), and numerous emission lines from ionised and molecular gas.

With all these emission/absorption features, the mid-IR spectra of galaxies can be extremely complex, therefore extracting the emission features and determining accurately the level of the continuum emission is a challenge. As the PAH features are broad and blended they create a pseudo-continuum, under which the true continuum lies (e.g. Brandl et al. 2006; Smith et al. 2007; Gallimore et al. 2010; Li 2020; Rigopoulou et al. 2021). This means a simple, local continuum around emission features is often not sufficient to obtain accurate PAH fluxes, particularly around the 7.7 μm band. This problem is compounded in more obscured sources, where strong absorption features from water ice ($\sim 6\mu\text{m}$), CH ($\sim 7\mu\text{m}$) and silicates ($\sim 9.8\mu\text{m}$) create a complex continuum (e.g. Spoon et al. 2007, 2022; Veilleux et al. 2009; García-Bernete et al. 2024a).

In highly obscured environments it becomes difficult to reproduce the continuum, particularly over a large wavelength range. This may be a consequence of differential extinction, where multiple regions of different dust densities all contribute within a single aperture. The resulting spectrum is therefore a combination of different intrinsic spectra with varying levels of obscuration. Such environments have been mapped in the Milky Way (e.g. Lallement et al. 2022). Differential extinction has an impact on the shape of the observed continuum, such as changing the ratio of the 18 μm to 9.8 μm sili-

* E-mail: fergus.donnan@physics.ox.ac.uk

Modeling effects of starspots on stellar magnetic cycles

Zebin Zhang^{1,2}, Jie Jiang^{1,2}, and Leonid Kitchatinov^{3,4}

¹ School of Space and Environment, Beihang University, Beijing, China
e-mail: jiejiang@buaa.edu.cn

² Key Laboratory of Space Environment monitoring and Information Processing of MIIT, Beijing, China

³ Institute of Solar-Terrestrial Physics, Irkutsk, Russia

⁴ Pulkovo Astronomical Observatory, St. Petersburg, Russia

Received xx, 2023; accepted xx, 2023

ABSTRACT

Context. Observations show that faster-rotating stars tend to have stronger magnetic activity and shorter magnetic cycles. The cyclical magnetic activity of the Sun and stars is believed to be driven by the dynamo process. The success of the Babcock-Leighton (BL) dynamo in understanding the solar cycle suggests an important role that starspots could play in stellar magnetic cycles.

Aims. We aim at extending the BL mechanism to solar-mass stars with various rotation rates and explore the effects of emergence properties of starspots in latitudes and tilt angles on stellar magnetic cycles.

Methods. We adopt a kinematic BL-type dynamo model operating in the bulk of the convection zone. The profiles of the large-scale flow fields are from the mean-field hydrodynamical model for various rotators. The BL source term in the model is constructed based on the rotation dependence of starspots emergence. That is, faster rotators have starspots at higher latitudes with larger tilt angles.

Results. Faster rotators have poloidal flux appearing closer to about $\pm 55^\circ$ latitudes, where the toroidal field generation efficiency is the strongest because of the strongest latitudinal differential rotation there. It takes a shorter time for faster rotators to transport the surface poloidal field from their emergence latitude to the $\pm 55^\circ$ latitudes of efficient Ω -effect thus shortening their magnetic cycles. The faster rotators operate in a more supercritical regime due to a stronger BL α -effect relating to the tilt angles, which leads to stronger saturated magnetic fields and a coupling of the poloidal field between two hemispheres more difficult. Thus the magnetic field parity shifts from the hemispherically asymmetric mixed mode to quadrupole, and further to dipole when a star spins down.

Conclusions. The emergence of starspots plays an essential role in the large-scale stellar dynamo.

Key words. dynamo – stars: activity – stars: magnetic field – stars: starspots – stars: rotation

1. Introduction

The solar large-scale magnetic fields show the quasi-11-yr cyclic variations manifested by the sunspots (Hathaway 2015). Starspots and magnetic cycles are ubiquitous among cool stars (Strassmeier 2009; Boro Saikia et al. 2018). The progress in solar magnetism paves the way for the understanding of stellar activity (Brun et al. 2015).

The cyclical magnetic activity of stars is usually studied through the chromospheric emission, e.g., Ca II H&K emission (Wilson 1978) or photospheric brightness variations (e.g., Reinhold et al. 2017; Montet et al. 2017). These studies show a general $P_{rot}-P_{cyc}$ relation, that is the magnetic cycle period P_{cyc} tends to be longer for stars having longer rotation period P_{rot} (Noyes et al. 1984b). Some studies show two branches of this relation, active and inactive ones corresponding to high and low activity, respectively (Saar & Brandenburg 1999; Böhm-Vitense 2007; Wright et al. 2011), while the existence of the active branch is still controversial (Boro Saikia et al. 2018). Past efforts on stellar activity also reveal the dependence of magnetic activity amplitude on the rotation period, hereafter called the $P_{rot}-A_{cyc}$ relation. That is, younger and faster rotating stars tend to have higher magnetic activity amplitude A_{cyc} . When rotators are fast enough, magnetic activity amplitude tends to saturate at some level (Hempelmann et al. 1996; Güdel 2004; Wright & Drake 2016; Zhang et al. 2020).

The $P_{rot}-P_{cyc}$ relation of stellar magnetism provides an important observational test for dynamo models. In kinematic α - Ω mean-field dynamo, the decreasing trend of the cycle period along the rotation period is a general property, because the cycle period is determined by the dynamo number related to the rotation period (Tobias 1998). During the past decades, the flux transport dynamo (FTD, Wang et al. 1991; Durney 1995; Choudhuri et al. 1995) works as the paradigm in understanding the solar cycle. In the framework of the FTD, the cycle period is controlled by the rate of meridional flow (Dikpati & Charbonneau 1999; Jouve & Brun 2007). If extending the FTD model to stars, the $P_{rot}-P_{cyc}$ relation requires an increase of meridional flow as the rotation rate increases (Nandy 2004). But magnetohydrodynamic (MHD) simulations show that the strength of meridional flow decreases as stars rotate faster (Brown et al. 2008; Augustson et al. 2012). Thus the faster rotators host longer magnetic cycles (Jouve et al. 2010; Karak et al. 2014b), which is contrary to what is observed. Kitchatinov (2022) suggests that the effective temperature is the essential parameter in understanding stellar magnetic cycles. Hotter stars sustain shorter cycles and they rotate faster on average. Brun & Browning (2017) introduce multi-cell meridional flows to reconcile the discrepancy. Do Cao & Brun (2011) consider the effect of magnetic turbulent pumping, and found the magnetic cycle shortens when the pumping effect becomes stronger with the increase of rotation rate. Pipin & Kosovichev (2016) include the dynamical quenching of magnetic buoyancy and magnetic helicity and Hazra et al.

TOI-1135 b: A young hot Saturn-size planet orbiting a solar-type star

M. Mallorquín^{1,2}, N. Lodieu^{1,2}, V. J. S. Béjar^{1,2}, M. R. Zapatero Osorio³, J. Sanz-Forcada³, M. R. Alarcon^{1,2}, H. M. Tabernero⁴, E. Nagel⁵, K. A. Collins⁶, D. R. Ciardi⁷, M. Serra-Ricart^{8,1,2}, J. Orell-Miquel^{1,2}, K. Barkaoui^{9,10,1}, A. Burdanov¹⁰, J. de Wit¹⁰, M. E. Everett¹¹, M. Gillon⁹, E. L. N. Jensen¹², L. G. Murphy¹³, P. A. Reed¹³, B. Safonov¹⁴, I. A. Strakhov¹⁴, C. Ziegler¹⁵

¹ Instituto de Astrofísica de Canarias (IAC), Calle Vía Láctea s/n, 38205 La Laguna, Tenerife, Spain, e-mail: mmd@iac.es

² Departamento de Astrofísica, Universidad de La Laguna (ULL), 38206 La Laguna, Tenerife, Spain

³ Centro de Astrobiología (CAB), CSIC-INTA, ESAC Campus, Camino bajo del castillo s/n, 28692, Villanueva de la Cañada, Madrid, Spain

⁴ Departamento de Física de la Tierra y Astrofísica and IPARCOS-UCM (Instituto de Física de Partículas y del Cosmos de la UCM), Facultad de Ciencias Físicas, Universidad Complutense de Madrid, 28040, Madrid, Spain

⁵ Institut für Astrophysik und Geophysik, Georg-August-Universität Göttingen, Friedrich-Hund-Platz 1, 37077 Göttingen, Germany

⁶ Center for Astrophysics, Harvard & Smithsonian, 60 Garden Street, Cambridge, MA 02138, USA

⁷ NASA Exoplanet Science Institute - Caltech/IPAC, Pasadena, CA USA

⁸ Light Bridges S. L., Avda. Alcalde Ramírez Bethencourt 17, 35004 Las Palmas de Gran Canaria, Canarias, Spain

⁹ Astrobiology Research Unit, Université de Liège, 19C Allée du 6 Août, 4000 Liège, Belgium

¹⁰ Department of Earth, Atmospheric and Planetary Science, Massachusetts Institute of Technology, 77 Massachusetts Avenue, Cambridge, MA 02139, USA

¹¹ NSF's National Optical-Infrared Astronomy Research Laboratory, 950 N. Cherry Ave., Tucson, AZ 85719, USA

¹² Department of Physics & Astronomy, Swarthmore College, Swarthmore PA 19081, USA

¹³ Department of Physical Sciences, Kutztown University, Kutztown PA 19530, USA

¹⁴ Sternberg Astronomical Institute Lomonosov Moscow State University

¹⁵ Department of Physics, Engineering and Astronomy, Stephen F. Austin State University, 1936 North St, Nacogdoches, TX 75962, USA

Received 19 December 2023 / Accepted 15 February 2024

ABSTRACT

Despite the thousands of planets in orbit around stars known to date, the mechanisms of planetary formation, migration, and atmospheric loss remain unresolved. In this work, we confirm the planetary nature of a young Saturn-size planet transiting a solar-type star every 8.03 d, TOI-1135 b. The age of the parent star is estimated to be in the interval of 125–1000 Myr based on various activity and age indicators, including its stellar rotation period of 5.13 ± 0.27 d and the intensity of photospheric lithium. We obtained follow-up photometry and spectroscopy, including precise radial velocity measurements using the CARMENES spectrograph, which together with the TESS data allowed us to fully characterise the parent star and its planet. As expected for its youth, the star is rather active and shows strong photometric and spectroscopic variability correlating with its rotation period. We modelled the stellar variability using Gaussian process regression. We measured the planetary radius at $9.02 \pm 0.23 R_{\oplus}$ ($0.81 \pm 0.02 R_{\text{Jup}}$) and determined a 3σ upper limit of $< 51.4 M_{\oplus}$ ($< 0.16 M_{\text{Jup}}$) on the planetary mass by adopting a circular orbit. Our results indicate that TOI-1135 b is an inflated planet less massive than Saturn or Jupiter but with a similar radius, which could be in the process of losing its atmosphere by photoevaporation. This new young planet occupies a region of the mass-radius diagram where older planets are scarce, and it could be very helpful to understanding the lower frequency of planets with sizes between Neptune and Saturn.

Key words. planetary systems – planets and satellites: individual: TOI-1135 b – planets and satellites: gaseous planets – methods: radial velocity – techniques: spectroscopic – stars: solar-type

1. Introduction

Close gas giants represent approximately 10% of the total population of known exoplanets.¹ However, how short-period gas giants form remains an open question. Although the family of gas giants is large, their occurrence rate is relatively low, with $\lesssim 1\%$ orbiting a solar-type star and even less for later stars (Wright et al. 2012). This contradiction is explained because they are the easiest exoplanets to detect by both transit and radial velocity (RV) methods.

Different formation mechanisms for these planets have been proposed (Dawson & Johnson 2018), including in situ formation (Batygin et al. 2016); disc migration (Lin et al. 1996); and high eccentricity tidal migration. The migration theory provides a reasonable explanation for the existence of short-orbit gas giants. According to this theory, these planets are believed to form farther out from their host stars (beyond the snowline), where the protoplanetary discs are rich in gas and dust. Through various mechanisms, such as gravitational interactions with other planets or interactions with the gas disc, these planets undergo a process of inwards migration towards the star until ending up

¹ <http://exoplanet.eu/>

Constraining the average magnetic field in galaxy clusters with current and upcoming CMB surveys

Vyoma Muralidhara^{a,b} and Kaustuv Basu,^b

^aMax-Planck-Institut für Astrophysik, Karl-Schwarzschild Str. 1, 85741 Garching, Germany

^bArgelander-Institut für Astronomie, Universität Bonn, D-53121 Bonn, Germany

E-mail: vmura@mpa-garching.mpg.de, kbasu@uni-bonn.de

Abstract. Galaxy clusters that host radio halos indicate the presence of population(s) of non-thermal electrons. These electrons can scatter low-energy photons of the Cosmic Microwave Background, resulting in the non-thermal Sunyaev-Zeldovich (ntSZ) effect. We measure the average ntSZ signal from 62 radio-halo hosting clusters using the *Planck* multi-frequency all-sky maps. We find no direct evidence of the ntSZ signal in the *Planck* data. Combining the upper limits on the non-thermal electron density with the average measured synchrotron power collected from the literature, we place lower limits on the average magnetic field strength in our sample. The lower limit on the volume-averaged magnetic field is $0.1-0.01 \mu\text{G}$, depending on the assumed power-law distribution of electron energies. We further explore the potential improvement of these constraints from the upcoming Simons Observatory and Fred Young Submillimeter Telescope (FYST) of the CCAT-prime collaboration. We find that combining these two experiments, the constraints will improve by a factor of 3–4, which can be sufficient to rule out some power-law models.

Aeolian erosion in protoplanetary discs: How impactful it is on dust evolution?

Stéphane Michoulier¹, Jean-François Gonzalez¹, Evgeni Grishin², and Clément Petetin¹

¹ Université Claude Bernard Lyon 1, CRAL UMR5574, ENS de Lyon, CNRS, Villeurbanne, F-69622, France
e-mail: jean-francois.gonzalez@ens-lyon.fr

² Monash Centre for Astrophysics (MoCA) and School of Physics and Astronomy, Monash University, Vic. 3800, Australia

Received 13 November 2023; accepted 26 February 2024

ABSTRACT

Context. Many barriers prevent dust to form planetesimals via coagulation in protoplanetary discs, such as bouncing, collisional fragmentation or aeolian erosion. Modelling dust and the different phenomena that can alter its evolution is therefore needed. Multiple solutions have been proposed, but still need to be confirmed.

Aims. In this paper, we explore the role aeolian erosion plays in the evolution of dust.

Methods. We use a monodisperse model to account for dust growth and fragmentation, implemented in a 1D model to compute the evolution of single grains and a 3D SPH code to compute the global evolution of dust and gas. We test the erosion model in our code and ensured it matches previous results.

Results. With a model of disc reproducing observations, we show with both 1D and 3D studies that erosion is not significant during the evolution of dust when we take fragmentation into consideration. With a low-viscosity disc, fragmentation is less of a problem, but grain growth is also less important, preventing the formation of large objects anyway. In dust traps, close to the star, erosion is also not impactful, even when fragmentation is turned off.

Conclusions. We show in this paper that aeolian erosion is negligible when radial drift, fragmentation and dust traps are taken into account and does not alter the dust evolution in the disc. However, it can have an impact on later stages, i.e. when the streaming instability forms large clumps close to the star, or when planetesimals are captured.

Key words. methods: numerical – planets and satellites: formation – protoplanetary discs

1. Introduction

Protoplanetary discs consist of gas and dust that orbit young stars and provide the necessary material for the agglomeration and growth of planetesimals, the building blocks of planets. The dynamical and physical processes occurring within these discs play a crucial role in shaping the characteristics and composition of planetary systems. Among these processes, aeolian erosion of large dust particles might influence the dynamics and evolution of the dust in the inner regions of protoplanetary discs (Blum & Wurm 2000; Wurm et al. 2001).

Aeolian erosion is a process where dust particles are ejected from a larger object due to the combined action of gas drag and turbulent motions within the disc. It has been studied by Blum & Wurm (2000); Wurm et al. (2001); Paraskov et al. (2006), and more recently by Rozner et al. (2020) and Grishin et al. (2020) (hereafter R20 and G20). They showed that large aggregates can be eroded in a short time, typically ranging from a few years to a few thousand years, with sizes going from several hundred metres down to a couple of centimetres (R20; G20). This process is therefore believed to destroy large boulders very efficiently and impact the evolution of grains in the inner region of the disc. Hence, erosion is another barrier to dust growth from small sizes to kilometeric objects.

In addition to aeolian erosion, fragmentation of dust particles is a process that can destroy grains in the inner regions of protoplanetary discs. When dust particles collide at high velocities, they may experience catastrophic disruptions, leading to the

so-called fragmentation barrier (Weidenschilling & Cuzzi 1993; Dominik & Tielens 1997; Blum & Wurm 2008). Fragmentation thresholds or material properties to model collisions are still not fully understood, with many uncertainties remaining. Moreover, dust experiences radial drift during its growth in the disc due to gas drag. Grains of a few centimetres to metres drift very efficiently, due to marginal coupling to the gas, and are accreted onto the star (Whipple 1972), which defines the radial drift barrier (Weidenschilling 1977). In order to prevent radial drift and the loss of material onto the star, several solutions have been proposed in order to help the formation of planetesimals. Some rely on the capture of dust in pressure maxima, others bypass the barriers to dust growth. For instance, vortices have been explored (Barge & Sommeria 1995; Meheut et al. 2012; Loren-Aguilar & Bate 2015) to trap dust and form clumps directly from gravitational collapse. Snow lines (Kretke & Lin 2007; Brauer et al. 2008; Drażkowska et al. 2014; Vericel & Gonzalez 2020) and self-induced dust traps (Gonzalez et al. 2017; Vericel & Gonzalez 2020; Vericel et al. 2021) form local pressure maxima, stopping the radial drift and helping grain growth by the increase of the local dust density. Other properties of dust have also been investigated like grain porosity (Ormel et al. 2007; Suyama et al. 2008; Okuzumi et al. 2009, 2012; Kataoka et al. 2013; Garcia & Gonzalez 2020), allowing grains to grow faster and to larger sizes, while being less sensitive to fragmentation. Additionally, other processes related to instabilities have been under investigation these recent years, mostly with the streaming instability (Youdin & Goodman 2005; Youdin & Johansen 2007;

Ultraviolet and Chromospheric activity and Habitability of M stars

XUE LI,^{1,2} SONG WANG,^{1,3} HENGGENG HAN,¹ HUIQIN YANG,^{1,3} CHUANJIE ZHENG,^{1,2} YANG HUANG,^{2,1} AND
JIFENG LIU^{1,2,3,4}

¹Key Laboratory of Optical Astronomy, National Astronomical Observatories, Chinese Academy of Sciences, Beijing 100101, China

²College of Astronomy and Space Sciences, University of Chinese Academy of Sciences, Beijing 100049, China

³Institute for Frontiers in Astronomy and Astrophysics, Beijing Normal University, Beijing 102206, China

⁴New Cornerstone Science Laboratory, National Astronomical Observatories, Chinese Academy of Sciences, Beijing 100012, People's Republic of China

ABSTRACT

M-type stars are crucial for stellar activity studies since they cover two types of magnetic dynamos and particularly intriguing for habitability studies due to their abundance and long lifespans during the main-sequence stage. In this paper, we used the LAMOST DR9 catalog and the GALEX UV archive data to investigate the chromospheric and UV activities of M-type stars. All the chromospheric and UV activity indices clearly show the saturated and unsaturated regimes and the well-known activity-rotation relation, consistent with previous studies. Both the FUV and NUV activity indices exhibit a single-peaked distribution, while the H α and Ca II H&K indices show a distinct double-peaked distribution. The gap between these peaks suggests a rapid transition from a saturated population to an unsaturated one. The smoothly varying distributions of different subtypes suggest a rotation-dependent dynamo for both early-type (partly convective) to late-type (fully convective) M stars. We identified a group of stars with high UV activity above the saturation regime ($\log R'_{\text{NUV}} > -2.5$) but low chromospheric activity, and the underlying reason is unknown. By calculating the continuously habitable zone and the UV habitable zone for each star, we found about 70% stars in the total sample and 40% stars within 100 pc are located in the overlapping region of these two habitable zones, indicating a number of M stars are potentially habitable. Finally, we examined the possibility of UV activity studies of M stars using the China Space Station Telescope.

Keywords: stars: activity, ultraviolet emission, stars: chromospheres, stars: flare

1. INTRODUCTION

M-type stars are thought to exhibit stronger magnetic activity compared to other types of stars. Numerous studies have been conducted to investigate the stellar activities of M-type stars, by using X-ray (e.g., Stelzer et al. 2013; Wright & Drake 2016), H α emission (e.g., Douglas et al. 2014; Newton et al. 2017), Ca II H&K emission (e.g., Astudillo-Defru et al. 2017; Boro Saikia et al. 2018; Lehtinen et al. 2020), UV emission (e.g., Stelzer et al. 2013; Schneider & Shkolnik 2018; Richey-Yowell et al. 2023), and optical flare (e.g., Yang et al. 2017), etc. These investigations aim to understand the manifestations of stellar activity and its connection to the stellar dynamo. For early M stars, they typically fol-

low the solar-type dynamo mechanism (α - Ω dynamo or tachocline dynamo). The generation of magnetic fields occurs in their deep convection zones due to the interior radial differential rotation, and the magnetic fields are then amplified through the interaction between magnetic flux tubes and convection processes (e.g., Parker 1975; Reid & Hawley 2000). On the other hand, late M stars, which are fully convective, lack a tachocline and exhibit a different dynamo mechanism, such as the α^2 dynamo. Therefore, M-type stars offer a unique opportunity to study two different magnetic dynamos within a single stellar type.

Since M-type stars constitute approximately 70% of the total stellar population in the Milky Way (Bochanski et al. 2009), there is significant interest in investigating the habitable zones and potentially habitable planets around M stars. Thanks to recent space missions like Kepler and TESS, several habitable planets have

Detection of a cyclotron line in the Be X-ray pulsar IGR J06074+2205

Kinjal Roy,* Rahul Sharma, Hemanth Manikantan, and Biswajit Paul

Raman Research Institute, C. V. Raman Avenue, Sadashivanagar, Bengaluru - 560 080, India.

ABSTRACT

Context. IGR J0607.4+2205 is a transient Be X-ray binary discovered two decades ago. IGR J0607.4+2205 underwent an outburst in 2023 during which it was observed twice with *NuSTAR*.

Aims. The main goal of this work is to model the broadband X-ray spectrum of IGR J0607.4+2205 during the outburst and to study the variations of the spectral and timing features at different intensities.

Methods. We extracted the light curve and spectrum of the source from the two *NuSTAR* observations carried out during the recent outburst in the energy range of 3–78 keV. We used the epoch folding technique to find pulsation from the source and to study the changes in emission characteristics from the source with energy across an order of magnitude variation in source luminosity.

Results. IGR J0607.4+2205 shows pulsations with a period of ~ 347.6 s during both the observations, with a pulse fraction of $\geq 50\%$. The broadband spectrum of the source was modelled using a power-law continuum with a high-energy cutoff. During the first observation, a cyclotron absorption line at ~ 51 keV was also present in the source with an optical depth of ~ 1.3 . However, no cyclotron line feature was detected in the second observation when the source was an order of magnitude fainter. Additionally, soft excess was detected in the second observation, which was modelled with a black body component emerging from close to the neutron star (NS).

Conclusions. We report the first ever detection of a cyclotron line in the broadband spectrum of IGR J0607.4+2205 centred at 51 ± 1 keV. The magnetic field strength of the NS is estimated to be $\sim 4 \times 10^{12}$ G from the centroid energy of the absorption line. A significant change is observed in the pulse profile with luminosity during the decay of the outburst, indicating an associated change in the beaming pattern.

Key words. pulsars: individual (IGR J0607.4+2205) — X-rays: binaries — X-rays: bursts

1. Introduction

Transient X-ray binary pulsars (XRPs) with a Be-type main sequence companion (BeXRPs) are useful for studying accretion onto highly magnetised neutron stars (NSs). The BeXRPs are known to exhibit a wide range of luminosity, ranging from 10^{37-38} erg s $^{-1}$ during the peak of the outburst to 10^{32-34} erg s $^{-1}$ during the quiescence phase (Tsygankov et al. 2017). Many BeXRPs have been detected since the launch of the first X-ray telescopes (Malacaria et al. 2020). Pioneered by the highly successful *RXTE*-ASM (Levine et al. 1996), the practice of initiating observations soon after the onset of an outburst has become standard. Recent advancements in sensitive, wide-viewing-angle X-ray instruments such as *MAXI*/GSC (Matsuoka et al. 2009), *Swift*/BAT (Krimm et al. 2013), and *Fermi*/GBM (Malacaria et al. 2020) enable the prompt identification of transients entering an outburst. Subsequent follow-up observations with sensitive broadband instruments like *NuSTAR* (Harrison et al. 2013) allow comprehensive studies of the source characteristics across a wide range of energy.

In highly magnetised ($B \geq 10^{12}$ G) high-mass X-ray binary (HMXB) systems, the accreted matter gets channelled along the magnetic field lines to the poles of the NS. A hot spot is produced in the accretion mound near the magnetic poles of the NS, producing soft X-rays that undergo inverse-Compton scattering by electrons in the accretion column giving rise to strong

X-ray emissions (Becker & Wolff 2007). The presence of strong magnetic fields at the polar regions leads to the quantisation of electron energy levels (E_n) in accordance with the Landau levels (Meszaros 1992) given by $E_n \sim 11.6 \times n \times B_{12}$ keV, where B_{12} is the magnetic field strength in units of 10^{12} G and $n=1,2,3,4,\dots$ denotes the different levels. The cyclotron resonant scattering feature (CRSF) is the absorption feature in the spectra of pulsars due to interactions between photons and quantised electrons present in the line-forming region of the NS. CRSFs are the best diagnostic tool for studying the magnetic field strength of a NS. The CRSF is detected in the hard X-ray regime and is observed as absorption-like features (Staubert et al. 2019).

The source IGR J0607.4+2205 was discovered by the *JEM-X* instrument on board *INTEGRAL* (Chenevez et al. 2004). A follow-up *Chandra* observation of the source was performed to localise the source (Tomsick et al. 2006). Subsequent observations of the source using *XMM-Newton* (Reig & Zezas 2018) revealed pulsations at a period of 347.2 s, establishing the compact object as a NS. The companion of IGR J0607.4+2205 was found to be a B0.5Ve star establishing the source as a BeXRP, and the distance to the source was estimated to be 4.5 kpc (Reig et al. 2010). The source IGR J0607.4+2205 underwent an outburst in the beginning of October 2023 with coherent pulsation detected at 2.6700(2) mHz from *Fermi*/GBM (Malacaria et al. 2023). The source underwent three outbursts during 2022–2023 as observed with *MAXI*/GSC, and based on the assumption that the outbursts were type-I outbursts, the orbital period was cal-

* kinjal@rriemail.rii.res.in

A search for radio pulsars in supernova remnants using FAST with one pulsar discovered

Zhen Zhang^{1,2}, Wenming Yan^{1,3,4*}, Jianping Yuan^{1,3,4}, Na Wang^{1,3,4}, Juntao Bai^{1,2}, Zhigang Wen^{1,3,4}, Baoda Li⁵, Jintao Xie⁶, De Zhao^{1,7}, Yubin Wang⁸ and Nannan Zhai^{1,2}

¹Xinjiang Astronomical Observatory, CAS, 150 Science 1-Street, Urumqi, Xinjiang 830011, China

²University of Chinese Academy of Sciences, Beijing 100049, China

³Key Laboratory of Radio Astronomy and Technology (Chinese Academy of Sciences),
A20 Datun Road, Chaoyang District, Beijing, 100101, P. R. China

⁴Xinjiang Key Laboratory of Radio Astrophysics, 150 Science 1-Street, Urumqi, Xinjiang 830011, China

⁵GuiZhou University, Guizhou 550025, People's Republic of China

⁶Research Center for Intelligent Computing Platforms, Zhejiang Laboratory, Hangzhou 311100, China

⁷School of Physical Science and Technology, Xinjiang University, Urumqi, Xinjiang, 830046, China

⁸School of Physics and Electronic Engineering, Sichuan University of Science & Engineering, Zigong 643000, China.

(Received xxx; accepted manuscript online xxx)

We report on the results of a search for radio pulsars in five supernova remnants (SNRs) with FAST. The observations were made using the 19-beam receiver in the Snapshot mode. The integration time for each pointing is 10 min. We discovered a new pulsar PSR J1845–0306 which has a spin period of 983.6 ms and a dispersion measure of $444.6 \pm 2.0 \text{ cm}^{-3} \text{ pc}$ in observations of SNR G29.6+0.1. To judge the association between the pulsar and the SNR, further verification is needed. We also re-detected some known pulsars in the data from SNRs G29.6+0.1 and G29.7–0.3. No pulsars were detected in observations of other three SNRs.

PACS: 97.60.Gb, 97.60.Jd, 97.60.Bw

DOI: [10.1088/0256-307X/39/x/xxxxxx](https://doi.org/10.1088/0256-307X/39/x/xxxxxx)

Before the discovery of pulsars, Baade & Zwicky proposed that supernova explosions could produce neutron stars^[1]. Currently, it is generally believed that pulsars are fast-spinning, highly magnetized neutron stars. According to the standard model of pulsar evolution^[2], pulsars are born in supernova explosions, so young pulsars with fast rotation are highly likely to be surrounded by SNR material. The two best examples supporting this model are the famous Vela pulsar and Crab pulsar. The Vela pulsar was discovered in 1968 at the edge of the Vela SNR^[3]. It is at the same distance and age as the SNR. Also in 1968, the Crab pulsar was discovered at the center of the Crab Nebula^[4], which was subsequently shown to be associated with the Crab Nebula. The confirmation of the association of the Vela and Crab pulsars with the SNRs provides important observational evidence for the model of neutron stars produced by supernova explosions.

Finding pulsars in their parent SNRs is vital to study pulsar formation and the supernova explosion mechanism. Attempts to search for pulsars in SNRs with large radio telescopes have been ongoing since the 1990s. Gorham et al.^[5] searched for pulsars in 18 SNRs using the Arecibo 305-m telescope at 430 and 1420 MHz, but did not find any new pulsars. Kaspi et al.^[6] conducted a pulsar search in 40 SNRs using the Parkes 64-m radio telescope at three frequencies of 436, 660 and 1520 MHz, and discovered two new pulsars. Biggs et al.^[7] used the Lovell 76-m radio telescope to search for pulsars in 29 SNRs at 610 MHz, and found no new pulsars. Lorimer et al.^[8] searched for pulsars in 33 SNRs using the Lovell 76-m radio telescope at 606 MHz and discovered two new pulsars. Camilo et al.^[9] detected a 136-ms pulsar in SNR G54.1+0.3 using the Arecibo radio telescope. Gupta et al.^[10] used the GMRT radio telescope to discover a 61.86-ms pulsar in SNR G21.5-0.9. Zhang et al. (2018) employed the Parkes 64-m radio telescope to search for pulsars in SNR 1987A, but no new pulsars were detected. Straal and van Leeuwen^[11] conducted a search for steep-spectrum pulsars in eight SNRs and pulsar wind nebulae using the LOFAR telescope, and discovered a pulsar candidate. Sett et al.^[12] searched five SNRs for pulsars using the Green Bank radio telescope at 820 MHz, but no new pulsars were found. In the Pulsar Galactic Surface Survey (GPPS) project, Han et al.^[13] discovered several pulsars in three known SNRs using the FAST telescope. Further verification is needed to determine whether these pulsars are associated with SNRs.

FAST has the unprecedented search sensitivity, it is expected to make breakthroughs in searching for pulsars in SNRs. In this Letter, we report on the search for radio pulsars in a sample of five SNRs (see Table 1 for

*Corresponding author. Email: yanwm@xao.ac.cn

© 2023 Chinese Physical Society and IOP Publishing Ltd

Search for neutrino emission from the Cygnus Bubble based on LHAASO γ -ray observations

WENLIAN LI[†] ¹, TIAN-QI HUANG[†] ^{2,3}, DONGLIAN XU ^{1,4} AND HUIHAI HE ^{2,3,5}

¹*Tsung-Dao Lee Institute, Shanghai Jiao Tong University, 201210 Shanghai, China*

²*Key Laboratory of Particle Astrophysics and Experimental Physics Division and Computing Center, Institute of High Energy Physics, Chinese Academy of Sciences, 100049 Beijing, China*

³*TIANFU Cosmic Ray Research Center, Chengdu, Sichuan, China*

⁴*School of Physics and Astronomy, Shanghai Jiao Tong University, Key Laboratory for Particle Astrophysics and Cosmology (MoE), Shanghai Key Laboratory for Particle Physics and Cosmology, 200240 Shanghai, China*

⁵*University of Chinese Academy of Sciences, 100049 Beijing, China*

ABSTRACT

The Cygnus region, which contains massive molecular and atomic clouds and young stars, is a promising Galactic neutrino source candidate. Cosmic rays transport in the region can produce neutrinos and γ -rays. Recently, the Large High Altitude Air Shower Observatory (LHAASO) detected an ultrahigh-energy γ -ray bubble (Cygnus Bubble) in this region. Using publicly available track events detected by the IceCube Neutrino Observatory in 7 years of full detector operation, we conduct searches for correlated neutrino signals from the Cygnus Bubble with neutrino emission templates based on LHAASO γ -ray observations. No significant signals were found for any employed templates. With the 7 TeV γ -ray flux template, we set a flux upper limit of 90% confidence level (C.L.) for the neutrino emission from the Cygnus Bubble to be $5.7 \times 10^{-13} \text{ TeV}^{-1} \text{ cm}^{-2} \text{ s}^{-1}$ at 5 TeV.

Keywords: Neutrino astronomy (1100), Gamma-ray astronomy (628), Galactic cosmic rays (567)

1. INTRODUCTION

Cosmic rays are high-energy astrophysical particles, primarily protons and atomic nuclei, while their origins have been a mystery for a century. Under the confinement of the Galactic magnetic field, the observed cosmic rays with energies up to several PeV are believed to originate from Galactic sources, called PeVatrons. Cosmic rays interact with the interstellar medium or the radiation field, generating both neutrinos (e.g., $\pi^+ \rightarrow \mu^+ + \nu_\mu$) and γ -rays (e.g., $\pi^0 \rightarrow 2\gamma$). High energy electrons can also produce γ -rays through inverse Compton scattering. However, the cross section suffers more stringent Klein–Nishina suppression for γ -rays with energies above 100 TeV. Therefore, the coincidence between neutrinos or γ -rays (> 100 TeV) and gas clumps will provide critical evidence for the identification of hadronic PeVatrons.

The Cygnus region is an active star forming area in our Galaxy and hosts various astrophysical sources, including massive young star clusters (YMCs, e.g., Cygnus OB2), pulsar wind nebulae (PWNe, e.g., TeV J2032+4130), and supernova remnants (SNRs, e.g., γ -Cygni). Fermi-LAT detected an excess of γ -ray emission (1-100 GeV) from the direction of the Cygnus region after subtracting the interstellar background and all known sources (Ackermann et al. 2011). The hard γ -ray spectrum points to freshly accelerated cosmic rays, whether they are cosmic ray electrons or nuclei. This $\sim 2^\circ$ extended γ -ray source, known as Cygnus Cocoon, has been further observed at TeV energies by ARGO-YBJ (Bartoli et al. 2014) and HAWC (Abeysekara et al. 2021). In the latest observation of the Cygnus region, LHAASO reported the Cygnus Bubble at ultra-high energy (LHAASO Collaboration 2024), extending to more than 6° from the core, which is much larger than the Cygnus Cocoon. The γ -ray brightness follows the distribution of the

Corresponding author: D.L. Xu
donglianxu@sjtu.edu.cn

[†] These authors contributed equally to this work

An Opacity-Free Method of Testing the Cosmic Distance Duality Relation Using Strongly Lensed Gravitational Wave Signals

Shun-Jia Huang,^{1,2,*} En-Kun Li,^{2,†} Jian-dong Zhang,² Xian Chen,^{3,4} Zucheng Gao,⁵ Xin-yi Lin,² and Yi-Ming Hu^{2,‡}

¹*School of Science, Shenzhen Campus of Sun Yat-sen University, Shenzhen 518107, China*
²*MOE Key Laboratory of TianQin Mission, TianQin Research Center for Gravitational Physics & School of Physics and Astronomy, Frontiers Science Center for TianQin, Gravitational Wave Research Center of CNSA, Sun Yat-sen University (Zhuhai Campus), Zhuhai 519082, China*
³*Astronomy Department, School of Physics, Peking University, Beijing 100871, China*
⁴*Kavli Institute for Astronomy and Astrophysics, Peking University, Beijing 100871, China*
⁵*Institute of Astronomy, University of Cambridge, Madingley Road, Cambridge CB3 0HA, UK*
(Dated: February 28, 2024)

The cosmic distance duality relation (CDDR), expressed as $D_L(z) = (1+z)^2 D_A(z)$, plays an important role in modern cosmology. In this paper, we propose a new method of testing CDDR using strongly lensed gravitational wave (SLGW) signals. Under the geometric optics approximation, we calculate the gravitational lens effects of two lens models, the point mass and singular isothermal sphere. We use functions of $\eta_1(z) = 1 + \eta_0 z$ and $\eta_2(z) = 1 + \eta_0 z / (1+z)$ to parameterize the deviation of CDDR. By reparameterizing the SLGW waveform with CDDR and the distance-redshift relation, we include the deviation parameters η_0 of CDDR as waveform parameters. We evaluate the ability of this method by calculating the parameter estimation of simulated SLGW signals from massive binary black holes. We apply the Fisher information matrix and Markov Chain Monte Carlo methods to calculate parameter estimation. We find that with only one SLGW signal, the measurement precision of η_0 can reach a considerable level of 0.5-1.3% for $\eta_1(z)$ and 1.1-2.6% for $\eta_2(z)$, depending on the lens model and parameters.

arXiv:2402.17349v1 [astro-ph.CO] 27 Feb 2024

* corresponding author: huangshj9@mail2.sysu.edu.cn

† corresponding author: lienk@mail.sysu.edu.cn

‡ corresponding author: huyiming@sysu.edu.cn

Ab initio simulations of neutron star oblique electrosphere with realistic neutron star parameters

F. Mottez¹

Laboratoire Univers et Théories, Observatoire de Paris, CNRS, Université PSL, Université Paris Cité, F-92190 Meudon, France
e-mail: fabrice.mottez@obspm.fr

February 28, 2024

ABSTRACT

Context. Electrospheres are environments with the same origin as pulsars, associated with a highly magnetized rotating neutron star. In pulsars, a cascade of electron-positron pair creation enriches the plasma. The plasma surrounding an electrosphere consists only of particles escaped from the neutron star surface. Electrospheres with a magnetic axis aligned with the rotation axis have been well described for decades. Models of electrospheres with oblique magnetic axis relatively to the rotation axis resisted to most theoretical investigations. Some electrospheres and pulsars have been simulated with particle-in-cell codes, but the numerical constraints did not allow the use of realistic neutron star parameters.

Aims. We aimed at developing a numerical simulation code optimized for the understanding the physics of electrospheres and pulsar, with realistic neutron star parameters. As a first step, presented in this paper, we focused on the simulation of oblique electrospheres with realistic physical parameters.

Methods. A specific code is developed for the computation of stationary solutions. The resolution of the Maxwell's equations is based on spectral methods. Particle motion include their finite inertia. No hypothesis is made relative to a force-free behavior of the electrospheric plasma. The numerical code is called *Pulsar ARoMa*, for Pulsar Asymmetric Rotating Magnetosphere.

Results. Various numerical simulation were conducted for neutron star realistic parameters. We find that oblique electrospheres possess the same global structure as for aligned force-free electrosphere, with two domes of electrons and a torus of positively charged particles. The domes are not centered on the magnetic axis, and they are asymmetric. Yet, the solutions do not exhibit a force-free behavior.

Conclusions. The simulations performed with the code *Pulsar ARoMa* require modest resources and little computing time. This code will be upgraded for more ambitious investigations on pulsar physics.

Key words. –neutron stars, electrospheres, numerical methods, magnetic fields

1. Introduction

Since their discovery by Hewish et al. (1969), considerable progress has been made in modeling pulsars. However, considerable progress is also needed to really understand the physical mechanisms governing these highly energetic objects. In this paper, a step forward towards this goal is presented, based on the writing of a new numerical simulation code, named *Pulsar ARoMa* for "Pulsar Asymmetric Rotating Magnetosphere", allowing to solve the fundamental equations governing the electrodynamics of pulsars, in a regime allowing the use of realistic parameters.

As soon as pulsars were recognized as manifestations of neutron stars environments, the problem could be posed physically in a very simple way as that of a magnetized, electrically conductive, rapidly rotating sphere in an initially empty medium. Generally, the magnetic field at the surface of the star is considered as dipolar, but multipolar components are also possible. The symmetry axis of the magnetic field can make any angle with the rotation axis of the neutron star (oblique pulsars), but for computational ease, solutions with a dipole aligned with the rotation axis (aligned pulsars) have been given special attention.

The first step in solving the pulsar problem was the calculation of the electromagnetic field into the vacuum extending around the neutron star. For an oblique dipole, a previous computation by Deutsch (1955) showed that the solution is close to the

dipole solution in the vicinity of the star, but, extends beyond the light cylinder in the form of a wave propagating at the speed of light, whose wave front is deployed along an Archimedes spiral. This wave carries a Poynting flux that corresponds in part with the loss of rotational energy of the pulsar (Gold 1968; Pacini 1967). A vacuum solution with multipolar magnetic field was developed more recently (Bonazzola et al. 2015; Pétri 2015). An important element of the vacuum solution is the fact that the rotating neutron star behaves like a unipolar inductor, generating a large-amplitude electric field at the star's surface.

However, it has been shown in Goldreich & Julian (1969) that the surface electric field repels electrons and ions from the star's surface and accelerates them to very high energies. As a result, the NS is embedded in a plasma, not in an empty region. Goldreich & Julian (1969) applied the concept of unipolar inductor to neutron stars, assuming that the plasma near the star was rotating with it. They then developed the fundamental concept of corotation space charge of the plasma, deduced from the divergence of the corotation electric field. Unlike most astrophysical objects, this charge density is high in the vicinity of neutron stars, due to their high rotation rate and magnetic field. They thus showed that there is a plasma-filled non neutral magnetosphere around neutron stars. The concept of corotation charge cannot be applied at locations near and beyond the light cylinder, but

Nodal precession of a hot Jupiter transiting the edge of a late A-type star TOI-1518

Noriharu WATANABE¹, Norio NARITA,^{2,3,4} and Yasunori HORI^{3,5}

¹Department of Multi-Disciplinary Sciences, Graduate School of Arts and Sciences, The University of Tokyo, 3-8-1 Komaba, Meguro, Tokyo 153-8902, Japan

²Komaba Institute for Science, The University of Tokyo, 3-8-1 Komaba, Meguro, Tokyo 153-8902, Japan

³Astrobiology Center, 2-21-1 Osawa, Mitaka, Tokyo 181-8588, Japan

⁴Instituto de Astrofísica de Canarias (IAC), 38205 La Laguna, Tenerife, Spain

⁵National Astronomical Observatory of Japan, 2-21-1 Osawa, Mitaka, Tokyo 181-8588, Japan

*E-mail: n-watanabe@g.ecc.u-tokyo.ac.jp, narita@g.ecc.u-tokyo.ac.jp, yasunori.hori@nao.ac.jp

Received ; Accepted

Abstract

TOI-1518b, a hot Jupiter around a late A-type star, is one of the few planetary systems that transit the edge of the stellar surface (the impact parameter $b \sim 0.9$) among hot Jupiters around hot stars (Cabot et al. 2021). The high rotation speed of the host star ($\sim 85 \text{ km s}^{-1}$) and the nearly polar orbit of the planet ($\sim 120^\circ$) may cause a nodal precession. In this study, we report the nodal precession undergone by TOI-1518b. This system is the fourth planetary system in which nodal precession is detected. We investigate the time change in b from the photometric data of TOI-1518 acquired in 2019 and 2022 with TESS and from the spectral transit data of TOI-1518b obtained in 2020 with two high-dispersion spectrographs; CARMENES and EXPRES. We find that the value of b is decreasing with $db/dt = -0.0116 \pm 0.0036 \text{ year}^{-1}$, indicating that the transit trajectory is moving toward the center of the stellar surface. We also estimate the minimum value of the quadrupole mass moment of TOI-1518 $J_{2,\text{min}} = 4.41 \times 10^{-5}$ and the logarithm of the Love number of TOI-1518 $\log k_2 = -2.17 \pm 0.33$ from the nodal precession.


Key words: planetary systems — planets and satellites: individual (TOI-1518b) — techniques: spectroscopic — techniques: photometric

1 Introduction

To date, 20 hot Jupiters have been discovered around hot stars whose effective temperatures are above 7,000K. These hot stars have a wide range of obliquities, that is, angles between the stellar rotational and orbital axes. The observed spin-orbit misalignment trends of hot Jupiters around hot stars imply that they did not undergo tidal realignment because of their shallow convective envelopes (Albrecht et al. 2012). Hot stars barely sustain stellar winds that lose their spin angular momentum due to mag-

netic braking. Hot stars tend to rotate rapidly as is known for the Kraft break (Kraft 1967). The oblateness of fast-rotating stars causes nodal precession of hot Jupiters in misaligned orbits. Nodal precession of three hot Jupiters on nearly polar orbits around rapidly rotating hot stars: Kepler-13Ab (Szabó et al. 2012; Szabó et al. 2014; Herman et al. 2018) and WASP-33b (Johnson et al. 2015; Watanabe et al. 2020; Watanabe et al. 2022; Stephan et al. 2022), and KELT-9b (Stephan et al. 2022), were detected. The nodal precession of a planet enables us to restrict the quadrupole mass moment J_2 and the Love number k_2 . J_2 indicates

On the Impact and Utility of Single-Exomoon Modeling for Multi-Moon Systems

Alex Teachey¹ & Garvit Agarwal^{1,2} 

¹Academia Sinica Institute of Astronomy and Astrophysics

11F of AS/NTU Astronomy-Mathematics Building, No.1, Sec. 4, Roosevelt Rd, Taipei 10617, Taiwan, R.O.C.

²Indian Institute of Science Education and Research, Pune

Accepted 2024 February 23. Received 2024 February 20; in original form 2024 January 12

ABSTRACT

The search for exomoons in time-domain photometric data has to-date generally consisted of fitting transit models that are comprised of a planet hosting a single moon. This simple model has its advantages, but it may not be particularly representative, as most of the major moons in our Solar System are found in multi-moon satellite systems. It is critical that we investigate, then, the impact of applying a single-moon model to systems containing multiple moons, as there is the possibility that utilizing an inaccurate or incomplete model could lead to erroneous conclusions about the system. To that end, in this work we produce a variety of realistic multi-moon light curves, perform standard single-moon model selection, and analyze the impacts that this model choice may have on the search for exomoons. We find that the number of moons in a system fit with a single-moon model generally has little impact on whether we find evidence for a moon in that system, and other system attributes are individually not especially predictive. However, the model parameter solutions for the moon frequently do not match any real moon in the system, instead painting a picture of a “phantom” moon. We find no evidence that multi-moon systems yield corresponding multi-modal posteriors. We also find a systematic tendency to overestimate planetary impact parameter and eccentricity, to derive unphysical moon densities, and to infer potentially unphysical limb darkening coefficients. These results will be important to keep in mind in future exomoon search programs.

Key words: exoplanets - planets and satellites: detection

1 INTRODUCTION

Despite a search that has lasted now more than a decade, a clear, unambiguous exomoon discovery remains elusive. To date there are arguably only two transiting exomoon candidates in the literature that have survived a battery of tests to remain viable (Kepler-1625 b-i and Kepler-1708 b-i; Teachey & Kipping 2018; Teachey et al. 2020; Kipping et al. 2022, 2024), and yet even these detections are not without their skeptics (e.g. Kreidberg, Luger, & Bedell 2019; Heller, Rodenbeck, & Bruno 2019; Heller & Hippke 2023). And so the question naturally arises, what is taking so long?

There are a number of key challenges in the detection of exomoons using time-domain photometry. Moons, which are generally expected to be small, and as a rule will be less massive than their host planet, are prone to having their transits buried in the noise. On top of this, their appearance alternately before, after, and during the planet transits can confound simple periodic signal search algorithms such as a box-least squares, and defy easy phase-folding – though methods have been developed to address these issues (e.g. Carter & Agol 2013; Kipping 2021). In addition, exomoon transit

signals may be mimicked by high-frequency, low-amplitude stellar activity (e.g. Kipping et al. 2015), or by planets passing in front of star spots (e.g. Béky et al. 2014). Exomoon transit signals are also vulnerable to removal by detrending algorithms. And to make matters worse, there are allowable and plausible satellite system architectures with inclinations that effectively hide the moons, as the moons can pass above or below the stellar disk for a sizeable fraction of transit epochs and produce no transit signal at all (Martin, Fabrycky, & Montet 2019).

The search for exomoons in time-domain photometry typically consists of fitting at least two competing transit models – a planet-only model, and a planet+moon model – to see which model better explains the data. The model that includes the moon carries several additional free parameters, and so this model is typically penalized for its extra complexity, such that only a significant improvement over the planet-only model will be sufficient to claim evidence of a moon. Photodynamical moon models, produced by algorithms such as LUNA (Kipping 2011), PANDORA (Hippke & Heller 2022), and GEFERA (Gordon & Agol 2022) accurately reproduce the planet and moon transit signals of varying duration, and produce the associated transit timing and duration variations, as well.

These codes support modeling transits of a planet hosting a sin-

* E-mail: amteachey@asiaa.sinica.edu.tw

The candidates of long-periodic variable sources in 6.7 GHz methanol masers associated with four high-mass star-forming regions

Yoshihiro TANABE¹ and Yoshinori YONEKURA¹

¹Center for Astronomy, Ibaraki University, 2-1-1 Bunkyo, Mito, Ibaraki 310-8512, Japan

*E-mail: yoshihiro.tanabe.ap@vc.ibaraki.ac.jp

Received ; Accepted

Abstract

Results of the long-term monitoring observations of the 6.7 GHz Class II methanol masers associated with the four high-mass star-forming regions by Hitachi 32-m radio telescope are presented. We detected periodic flux variability in G06.795–0.257, G10.472+0.027, G12.209–0.102, and G13.657–0.599 with the periods of 968, 1624, 1272, and 1266 d, respectively, although the detected period is tentative due to the short monitoring term relative to the estimated period. The facts that the flux variation patterns show the symmetric sine curves and that the luminosities of the central protostar and periods of maser flux variation are consistent with the expected period-luminosity (PL) relation suggest that the mechanisms of maser flux variability of G10.472+0.027 and G12.209–0.102 can be explained by protostellar pulsation instability. From the PL relation, central stars of these two sources are expected to be very high-mass protostars with a mass of $\sim 40 M_{\odot}$ and to have the mass accretion rate of $\sim 2 \times 10^{-2} M_{\odot} \text{yr}^{-1}$. On the other hand, G06.795–0.257 and G13.657–0.599 have the intermittent variation patterns and have luminosities that are an order of magnitude smaller than those expected from PL relation, suggesting variation mechanisms of these sources originated from binary system. Since almost all the maser features vary with the same period regardless of its geometry, periodic accretion model may be appropriate mechanisms for flux variability in G06.795–0.257 and G13.657–0.599.

Key words: masers — ISM: individual objects — stars: formation — stars: massive

1 Introduction

High-mass stars have significant impact on their surrounding environment and evolution of galaxies through several feedback mechanisms, e.g., stellar winds, ultraviolet radiation, and supernovae. Therefore understanding the processes of the formation and evolution of high-mass stars is one of the most important issues in astronomy. However, our understanding of the formation processes of high-mass stars remains inadequate, hampered by the observational difficulties that they

are born in distant and very deeply embedded in dense gas. Class II methanol maser is a well established tracer of high-mass star-forming regions (HMSFRs) (e.g., Minier et al. 2003; Ellingsen 2006; Pandian et al. 2007; Breen et al. 2013). The strongest methanol maser line is 6.7 GHz the $5_1 - 6_0 A^+$ transition, discovered firstly by Menten (1991) and over 1000 6.7 GHz methanol masers have been discovered by unbiased surveys and targeted observations (e.g., Pestalozzi et al. 2005; Pandian et al. 2007; Caswell et al. 2010, 2011; Green et al. 2010, 2012; Breen et al. 2015; Yang et al. 2017, 2019; Rickert

Magnetic fields in the Southern Coalsack and beyond

M.J.F. VERSTEEG ¹, Y. ANGARITA ¹, A.M. MAGALHÃES ², M. HAVERKORN ¹, C.V. RODRIGUES ³,
R. SANTOS-LIMA ² AND KOJI S. KAWABATA ⁴

¹*Department of Astrophysics/IMAPP, Radboud University, PO Box 9010, 6500 GL Nijmegen, The Netherlands*

²*Depto. de Astronomia, IAG, Universidade de São Paulo, Brazil*

³*Divisão de Astrofísica, Instituto Nacional de Pesquisas Espaciais (INPE/MCTI), Av. dos Astronautas, 1758, São José dos Campos, SP, Brazil*

⁴*Hiroshima Astrophysical Science Center, Hiroshima University, Kagamiyama, Higashi-Hiroshima, Hiroshima, 739-8526, Japan*

ABSTRACT

Starlight polarimetry, when combined with accurate distance measurements, allows for exploration of the three-dimensional structure of local magnetic fields in great detail. We present optical polarimetric observations of stars in and close to the Southern Coalsack, taken from the Interstellar Polarization Survey (IPS). Located in five fields of view approximately 0.3° by 0.3° in size, these data represent the highest density of optical polarimetric observations in the Southern Coalsack to date. Using these data, combined with accurate distances and extinctions based on Gaia data, we are able to characterize the magnetic field of the Coalsack and disentangle contributions to the polarization caused by the Southern Coalsack and a background structure. For the Southern Coalsack, we find an average magnetic field orientation of $\theta \sim 75^\circ$ with respect to the Galactic north pole and an average plane-of-sky magnetic field strength of approximately $B_{POS} = 10 \mu G$, using the Davis-Chandrasekhar-Fermi (DCF) method. These values are in agreement with some earlier estimates of the Coalsack's magnetic field. In order to study the distant structure, we introduce a simple method to separate and isolate the polarization of distant stars from foreground contribution. For the distant structure, which we estimate to be located at a distance of approximately 1.3-1.5 kpc, we find an average magnetic field orientation of $\theta \sim 100^\circ$ and we estimate a field strength of $B_{POS} \sim 10 \mu G$, although this will remain highly uncertain until the precise nature of the distant structure can be uncovered.

1. INTRODUCTION

Optical starlight polarization is a powerful tracer of interstellar material and magnetic fields. (Hall 1949; Hiltner 1949). Asymmetric dust grains in the interstellar medium (ISM) align themselves with the Galactic Magnetic Field (GMF) (see e.g. Lazarian 2007) and subsequently preferentially absorb a fraction of the radiation polarized perpendicularly to the magnetic field lines, see e.g. Clarke (2010); Whittet (2022). Thus, stars that emit unpolarized light may show partial polarization when shining through the dusty ISM. The polarization angle corresponds to the local orientation of the plane-of-sky component of the magnetic field and the degree of polarization may be indicative of the dust conditions along the line of sight (LOS), as well as the magnetic field orientation. In addition, the dispersion of the polarization angles can be used to determine the strength of the GMF, using for example the Davis-Chandrasekhar-Fermi method (Davis 1951; Chandrasekhar & Fermi 1953), hereafter DCF. For a dominating regular magnetic field with an additional, but relatively small tur-

bulent component, the polarization angles would follow a roughly Gaussian distribution, centered around the local orientation of the plane-of-sky component of the magnetic field. Large-scale deviations from a simple Gaussian distribution may be indicative of, for example, changes in a large-scale magnetic field direction along the LOS or the existence of intervening structures such as clouds.

The Southern Coalsack (see also Nyman 2008, for an overview) is a nearby large dark nebula located in the Galactic plane, centered at approximately $l=303^\circ$, $b=0^\circ$ with an on-sky size of about 10 degrees, see Figure 1. It is located at a distance of $d \sim 200$ pc (see e.g. Franco 1989, who finds a distance of $d = 180 \pm 26$ pc, Seidensticker & Schmidt-Kaler 1989 who identify two overlapping clouds with the closest at a distance of $d = 188 \pm 4.1$ pc and Dharmawardena et al. 2023, who place the Coalsack at a distance of approximately $d \sim 150$ pc). The Coalsack has been studied intensively at various wavelengths, in CO by Nyman et al. (1989) and Kato et al. (1999), revealing a large and complex

Distribution of number of peaks within a long gamma-ray burst

C. Guidorzi^{1,2,3}, M. Sartori¹, R. Maccary¹, A. Tsvetkova^{4,3,5}, L. Amati³, L. Bazzanini^{1,3}, M. Bulla^{1,2,6},
A. E. Camisasca¹, L. Ferro^{1,3}, F. Frontera^{1,3}, C. K. Li⁷, S. L. Xiong⁷, and S. N. Zhang^{7,8}

¹ Department of Physics and Earth Science, University of Ferrara, Via Saragat 1, I-44122 Ferrara, Italy

² INFN – Sezione di Ferrara, Via Saragat 1, 44122 Ferrara, Italy

³ INAF – Osservatorio di Astrofisica e Scienza dello Spazio di Bologna, Via Piero Gobetti 101, 40129 Bologna, Italy

⁴ Department of Physics, University of Cagliari, SP Monserrato-Sestu, km 0.7, 09042 Monserrato, Italy

⁵ Ioffe Institute, Politekhnikeskaya 26, 194021 St. Petersburg, Russia

⁶ INAF, Osservatorio Astronomico d’Abruzzo, via Mentore Maggini snc, 64100 Teramo, Italy

⁷ Key Laboratory of Particle Astrophysics, Institute of High Energy Physics, Chinese Academy of Sciences, Beijing 100049, People’s Republic of China

⁸ University of Chinese Academy of Sciences, Beijing 100049, People’s Republic of China

February 28, 2024

ABSTRACT

Context. The variety and complexity of long duration gamma-ray burst (LGRB) light curves (LCs) encode a wealth of information on the way LGRB engines release their energy following the collapse of the progenitor massive star. Thus far, attempts to characterise GRB LCs focused on a number of properties, such as the minimum variability timescale, power density spectra (both ensemble average and individual), or through different definitions of variability. In parallel, a characterisation as a stochastic process was pursued by studying the distributions of waiting times, peak flux, fluence of individual peaks that can be identified within GRB time profiles. Yet, the question remains as to whether the diversity of GRB profiles can be described in terms of a common stochastic process.

Aims. Here we address this issue by extracting and modelling for the first time the distribution of the number of peaks within a GRB profile.

Methods. We analysed four different GRB catalogues: *CGRO/BATSE*, *Swift/BAT*, *BeppoSAX/GRBM*, and *Insight-HXMT*. The statistically significant peaks were identified by means of well tested and calibrated algorithm *MERSA* and further selected by applying a set of thresholds on signal-to-noise ratio. We then extracted the corresponding distributions of number of peaks per GRB.

Results. Among the different models considered (power-law, simple or stretched exponential) only a mixture of two exponentials turned out to model all the observed distributions, suggesting the existence of two distinct behaviours: (i) an average number of 2.1 ± 0.1 peaks per GRB (“peak poor”) and accounting for about 80% of the observed population of GRBs; (ii) an average number of 8.3 ± 1.0 peaks per GRB (“peak rich”) and accounting for the remaining 20% of the observed population.

Conclusions. We associate the class of peak-rich GRBs with the presence of sub-second variability, which instead appears to be absent among peak-poor GRBs. The two classes could result from two different regimes through which GRB inner engines release energy or through which energy is dissipated into gamma-rays.

Key words. (Stars:) Gamma-ray burst: general – Methods: statistical

1. Introduction

Gamma-ray burst (GRB) prompt emission is observed in at least two kinds of explosive transients: (i) the merger of a compact object binary system (Eichler et al. 1989; Paczynski 1991; Narayan et al. 1992; Abbott et al. 2017), (ii) the core collapse of some kinds of massive stars also known as “collapsar” (Woosley 1993; Paczyński 1998; MacFadyen & Woosley 1999; Yoon & Langer 2005). While the prompt emission duration remains the strongest hint on the nature of the progenitor, in a few cases it turned out to be deceitful. To avoid confusion, the two progenitor families (i) and (ii) are often referred to as Type-I and Type-II GRBs, respectively (Zhang 2006). Hereafter, we will consider only the latter class.

Modelling of thousands of GRB prompt emission time-resolved spectra proved that the observed variety is likely the result of different radiative processes in different GRBs, given the variety of spectral components that are observed: the non-thermal

Band function, an occasional quasi-thermal component, and even a broad-band power-law (see Kumar & Zhang 2015 for a review). These processes are possibly related to different dissipation mechanisms taking place at different distances from the progenitor and driven by key properties, such as the ejecta composition of the relativistic jet that is launched by the GRB inner engine.

In parallel, while numerous studies that focused on the temporal properties of GRB time profiles have contributed to characterise their variability, the large variety and highly erratic nature of GRB prompt emission remains mostly unexplained and apparently disconnected from the properties that are inferred from the afterglow modelling, apart from the energetics. Despite being affected by a large scatter, a positive correlation between peak luminosity and variability was found as soon as the number of bursts with measured redshift increased to a dozen or more (Reichart et al. 2001; Fenimore & Ramirez-Ruiz 2000). Variability was defined as the net (that is, removed of the counting statistics noise contribution) variance of the light curve (LC) with respect to a smoothed version of the same. The correlation was

* guidorzi@infn.it

New method for estimating molecular cloud distances based on *Gaia*, 2MASS, and the TRILEGAL galaxy model

Juan Mei (梅娟)^{1,2,3}, Zhiwei Chen (陈志维)^{3*}, Zhibo Jiang (江治波)^{2,3,4}, Sheng Zheng (郑胜)^{1,2}, and Haoran Feng (冯浩然)^{3,4}

¹ Center for Astronomy and Space Sciences, China Three Gorges University, 8 University Road, 443002 Yichang, China

² College of Science, China Three Gorges University, 8 University Road, 443002 Yichang, China

³ Purple Mountain Observatory, Chinese Academy of Sciences, 10 Yuanhua Road, 210023 Nanjing, China
e-mail: zwchen@pmo.ac.cn

⁴ University of Science and Technology of China, Chinese Academy of Sciences, Hefei 230026, China

ABSTRACT

We propose a new method for estimating the distances of molecular clouds traced by CO line emission. Stars from 2MASS and *Gaia* EDR3 are selected as on-cloud stars when they are projected on a cloud. The background on-cloud stars have redder colors on average than the foreground stars. Instead of searching for stars projected away from the cloud, we employed the TRILEGAL galaxy model to mimic the stellar population without cloud extinction along the sightline toward the cloud. Our method does not require an exact boundary of a cloud. The boundaries are highly variable and depend on the sensitivity of the molecular line data. For each cloud, we compared the distributions of on-cloud stars to the TRILEGAL stellar populations in the diagram of $J - K_s$ color versus distance. The intrinsic $J - K_s$ colors of main-sequence and evolved stars from TRILEGAL were considered separately, and they were used as the baseline for subtracting the observed $J - K_s$ colors. The baseline-corrected $J - K_s$ color was deployed with the Bayesian analysis and Markov chain Monte Carlo sampling to determine the distance at which the $J - K_s$ color jump is largest. This method was successfully applied to measure the distances of 27 molecular clouds, which were selected from previously published cloud samples. By replacing TRILEGAL with the GALAXIA galaxy model, we were able to measure the distances for 21 of the 27 clouds. The distances of the 21 clouds based on the GALAXIA model agree well with those based on the TRILEGAL model. The distances of the 27 clouds estimated by this method are consistent with previous estimates. We will apply this new method to a larger region of the gaseous galactic plane, in particular, for the inner galactic region, where a region free of CO emission is hard to separate from the crowded field of clouds.

Key words. Stars: distances - dust, extinction - ISM: clouds

1. Introduction

Molecular clouds are the birthplaces of stars. The distance is an important parameter of a molecular cloud when the intrinsic physical properties (mass and size) are to be estimated. Determining the distances of molecular clouds is crucial for characterizing the initial conditions of star formation (McKee & Ostriker 2007; Kennicutt & Evans 2012; Heyer & Dame 2015) and the gaseous spiral arms of the Milky Way (Dame et al. 2001; Xu et al. 2018).

It is always a challenging task to determine the distances of molecular clouds. Several methods were applied to estimate the distances of molecular clouds. The distances of molecular clouds can be estimated from their radial velocities (V_{lsr}), which are assumed to be attributed to the large-scale rotation of the spiral arms of the Milky Way. The distances estimated from V_{lsr} of molecular clouds are commonly referred to as kinematic distances (Roman-Duval et al. 2009; Reid et al. 2014). The kinematic distances have large uncertainties and ambiguity problems, especially in the inner Galaxy. The cloud distances can also be estimated by identifying objects associated with or within the molecular cloud, such as OB-associations, young open clusters, H II regions, young stellar objects (YSOs), and masers, whose distances are measured from the trigonometric parallaxes

or photometry of stars (Xu et al. 2006; Russeil et al. 2007; Reid et al. 2019; Castro-Ginard et al. 2021; Marton et al. 2022; Zhang 2023). The trigonometric parallaxes measured by *Gaia* (Gaia Collaboration et al. 2016) for stars up to several kiloparsec provide another approach for estimating the distances of molecular clouds by locating the extinction break point along the line of sight (LOS) toward molecular clouds.

The extinction method relies on accurately estimating the distance and extinction of numerous stars. Green et al. (2014) presented a method for deriving reddening and distances of stars from Panoramic Survey Telescope and Rapid Response System (PanSTARRS-1) photometry and produced a three-dimensional (3D) dust map. Based on the technique of Green et al. (2014), Schlafly et al. (2014) simultaneously inferred the reddening and distances of stars. They measured the distances of molecular clouds selected from the catalog of Magnani et al. (1985) by their extinction break point. The release of astrometric data from *Gaia* has brought about significant changes in measuring the distance, as it provides a more precise stellar parallax. Combined with *Gaia* data, several studies presented new 3D extinction maps and have estimated the extinction and distances for millions of stars (Green et al. 2019; Chen et al. 2019; Lallement et al. 2019; Guo et al. 2021; Sun et al. 2021a). One approach involves modeling the dust extinction profiles along different LOS, where the measured cloud is searched for dust clouds from 3D dust structures

* Corresponding author: Zhiwei Chen

The Impact of ionization Morphology and X-ray Heating on the Cosmological 21cm Skew Spectrum

J. H. Cook^{1,2*}, S. Balu^{2,3}, B. Greig^{2,3,4}, C. M. Trott^{1,2}, J. L. B. Line^{1,2}, Y. Qin^{2,3}, J. S. B. Wyithe^{2,4}

¹International Centre for Radio Astronomy Research, Curtin University, Perth, Australia

²ARC Centre of Excellence for All Sky Astrophysics in 3D (ASTRO 3D)

³School of Physics, University of Melbourne, Parkville, VIC 3010, Australia

⁴Research School of Astronomy & Astrophysics, Australian National University, Canberra, ACT 2611, Australia

Accepted XXX. Received YYY; in original form ZZZ

ABSTRACT

The cosmological 21cm signal offers a potential probe of the early Universe and the first ionizing sources. Current experiments probe the spatially-dependent variance (Gaussianity) of the signal through the power spectrum (PS). The signal however is expected to be highly non-Gaussian due to the complex topology of reionization and X-ray heating. We investigate the non-Gaussianities of X-ray heating and reionization, by calculating the skew spectrum (SS) of the 21cm signal using MERAXES, which couples a semi-analytic galaxy population with semi-numerical reionization simulations. The SS is the cross-spectrum of the quadratic temperature brightness field with itself. We generate a set of seven simulations from $z = 30$ to $z = 5$, varying the halo mass threshold for hosting star-formation, the X-ray luminosity per star-formation rate, and the minimum X-ray energy escaping host galaxies. We find the SS is predominantly negative as a function of redshift, transitioning to positive towards the start of reionization, and peaking during the midpoint of reionization. We do not see a negative dip in the SS during reionization, likely due to the specifics of modelling ionization sources. We normalise the SS by the PS during reionization isolating the non-Gaussianities. We find a trough ($k \sim 0.1 \text{ Mpc}^{-1}$) and peak ($k \sim 0.4 - 1 \text{ Mpc}^{-1}$) in the normalised SS during the mid to late periods of reionization. These correlate to the ionization topology, and neutral islands in the IGM. We calculate the cosmic variance of the normalised SS, and find these features are detectable in the absence of foregrounds with the SKA_LOW.

Key words: cosmology: dark ages, reionization, first stars – methods: statistical

1 INTRODUCTION

The cosmological 21cm neutral hydrogen line promises to be an insightful probe of the first luminous sources and the structure of the Universe during early cosmic time. The first luminous sources (stars, galaxies, compact objects) heat and ionize the surrounding intergalactic medium (IGM), through the cumulative emission of ultraviolet (UV) and X-ray photons (see the following review papers: Barkana & Loeb 2001; Morales & Wyithe 2010; Pritchard & Loeb 2012; Furlanetto 2016).¹ These ionized bubbles grow and eventually overlap, culminating in the end of reionization by redshift ~ 5.3 (Bosman et al. 2022). These bubbles encode information about these sources onto the cosmological 21cm temperature brightness signal (Furlanetto & Oh 2005). These luminous sources also heat the neutral hydrogen medium through X-ray emission, which encodes additional information about these sources (Pritchard & Furlanetto 2007; Furlanetto 2016). The cosmological 21cm signal is measured relative to the cosmic microwave background (CMB), and can be either in relative emission or absorption. By measuring the 21cm signal we can construct the spatial, and line of sight distributions of neutral hydrogen. This will allow for the properties of the first luminous

sources to be inferred through their influence on the cosmological 21cm signal.

Most of the focus in the 21cm cosmological community has been on measuring either the one or two-point statistics of the signal. The one point statistic experiments determine the sky averaged quantities (for example the global mean temperature). For example: The Shaped Antenna measurement of the background Radio Spectrum 3 telescope (SARAS3, Nambissan et al. 2021); the Experiment to Detect the Global EoR Signature (EDGES, Bowman et al. 2018). The two point statistic experiments are primarily measured by radio interferometers. The current generation of radio interferometers includes the Murchison Widefield Array (MWA, Tingay et al. 2013; Wayth et al. 2018); Low-Frequency Array (LOFAR, van Haarlem, M. P. et al. 2013); Hydrogen Epoch of Reionization Array (HERA, DeBoer et al. 2017); the New extension in Nancay upgrading LOFAR (NenuFAR, Zarka et al. 2012).

The two point statistic experiments calculate the PS of the 21cm signal which is the Fourier transform of the two point correlation function. This measures the Gaussianity or the variance of the signal as a function of comoving spatial scale. If the signal is entirely Gaussian this would capture all the information about the 21cm signal within cosmic variance². The signal is however expected to

* E-mail: Jaiden.cook@curtin.edu.au

¹ Reionization predominately occurs due to UV photons, with some contribution from X-ray emission (up to ~ 10 percent Mesinger et al. (2013)).

² Since we cannot truly measure the ensemble average power spectrum, we

A chemodynamical analysis of bright metal-poor stars from the HESP-GOMPA survey – Indications of a non-prevailing site for light *r*-process elements

Avrajit Bandyopadhyay,^{1,2,3*} Timothy C Beers^{2,4}, Rana Ezzeddine^{1,2}, Thirupathi Sivarani,³ Prasanta K Nayak,⁵ Jeewan C Pandey,⁶ Pallavi Saraf,^{3,7} and Antony Susmitha³

¹ Department of Astronomy, University of Florida, Gainesville, FL 32601, United States of America

² Joint Institute for Nuclear Astrophysics-Center for the Evolution of the Elements (JINA-CEE), USA

³ Indian Institute of Astrophysics, Koramangala 2nd Block, Bangalore, 560034, India

⁴ Department of Physics and Astronomy, University of Notre Dame, Notre Dame, IN 46556, United States of America

⁵ Instituto de Astrofísica, Pontificia Universidad Católica de Chile, Av. Vicuña MacKenna 4860, 7820436, Santiago, Chile

⁶ Aryabhata Research Institute of Observational Sciences, Nainital 263001, India

⁷ Pondicherry University, R.V Nagar, Kalapet, 605014, Puducherry, India

Accepted 26 February 2024. Received 27 September 2023; in original form 27 September 2023

ABSTRACT

We present a comprehensive analysis of the detailed chemical abundances for a sample of 11 metal-poor, very metal-poor and extremely metal-poor stars ($[\text{Fe}/\text{H}] = -1.65$ to $[\text{Fe}/\text{H}] = -3.0$) as part of the HESP-GOMPA (Galactic survey Of Metal Poor stArs) survey. The abundance determinations encompass a range of elements, including C, Na, Mg, Al, Si, Ca, Sc, Ti, Cr, Mn, Fe, Co, Ni, Cu, Zn, Sr, and Ba, with a subset of the brighter objects allowing for the measurement of additional key elements. Notably, the abundance analysis of a relatively bright highly *r*-process-enhanced (*r*-II) star (SDSS J0019+3141) exhibits a predominantly main *r*-process signature and variations in the lighter *r*-process elements. Moreover, successful measurements of thorium in this star facilitate stellar age determinations. We find a consistent odd-even nucleosynthesis pattern in these stars, aligning with expectations for their respective metallicity levels, thus implicating Type II supernovae as potential progenitors. From the interplay between the light and heavy *r*-process elements, we infer a diminishing relative production of light *r*-process elements with increasing Type II supernova contributions, challenging the notion that Type II supernovae are the primary source of these light *r*-process elements in the early Milky Way. A chemodynamical analysis based on Gaia astrometric data and our derived abundances indicates that all but one of our program stars are likely to be of accreted origin. Additionally, our examination of α -poor stars underscores the occurrence of an early accretion event from a satellite on a prograde orbit, similar to that of the Galactic disc.

Key words: techniques: spectroscopic - Galaxy: formation – stars: abundances – stars: atmospheres – stars: fundamental parameters

1 INTRODUCTION

Extremely metal-poor (EMP; $[\text{Fe}/\text{H}] \leq -3.0$) stars are believed to be the immediate descendants of the first stars in the Galactic halo (Bromm & Larson 2004; Naoz et al. 2006; Yoshida et al. 2012; Lazar & Bromm 2022; Klessen & Glover 2023; Ji et al. 2024). The evolution and subsequent explosions of these first stars, which were also massive, played a pivotal role in the genesis of all elements heavier than Li in the early Universe. The very metal-poor (VMP; $[\text{Fe}/\text{H}] \leq -2.0$) stars also carry important imprints of the early stellar populations and are likely to be formed in the first epochs of the Universe (Cayrel et al. 2004; Beers & Christlieb 2005; Bonifacio

et al. 2007; Bromm et al. 2009; Cooke & Madau 2014; Frebel & Norris 2015a; Frebel 2018).

The primordial supernovae from these early stars had profound effects on the dynamics and chemical evolution of the surrounding interstellar medium (Denissenkov & Weiss 1996; Sbordone et al. 2010; Chiaki et al. 2017). Subsequent generations of stars and their host galaxies are expected to bear the signatures of nucleosynthesis events originating from these Population III stars, e.g., as explored by Nakamura et al. (1999), Frebel & Norris (2015b), Sharma et al. (2018), and Koutsouridou et al. (2023). The wide diversity in the chemical composition of metal-poor stars has led to predictions and theoretical modelling regarding the possible nature and contributions from the progenitor populations (Heger & Woosley 2002; Nomoto et al. 2013; Rossi et al. 2023). The production sites of the different elements are largely decoupled from each other, and

* E-mail: abandyopadhyay@ufl.edu

The Optical to Infrared 0.6 – 5.3 μm Dust Extinction Law of the Milky Way with JWST NIRSpec: Westerlund 2

SHU WANG¹ AND XIAODIAN CHEN^{1,2,3}

¹CAS Key Laboratory of Optical Astronomy, National Astronomical Observatories, Chinese Academy of Sciences, Beijing 100101, China

²Institute for Frontiers in Astronomy and Astrophysics, Beijing Normal University, Beijing 102206, China

³School of Astronomy and Space Science, University of the Chinese Academy of Sciences, Beijing 101408, China

ABSTRACT

The interstellar extinction law is important for interpreting observations and inferring the properties of interstellar dust grains. Based on the 993 prism/CLEAR spectra from the James Webb Space Telescope (JWST), we investigate 0.6 – 5.3 μm interstellar dust extinction law. We propose a pair method to obtain the reddening curves based only on JWST observed spectra. Most of the high extinction sources are toward the young star cluster Westerlund 2. The infrared (IR) 1.0 – 5.3 μm reddening curves agree with the power-law $A_\lambda \propto \lambda^{-\alpha}$ well. We determine an average value of $\alpha = 1.98 \pm 0.15$, which is consistent with the average value of the Galaxy. We find that α may be variable and independent of R_V . With the derived α , we convert the reddening curves into the extinction curves and establish the non-parameterized α -dependent extinction curves in the wavelength range of 0.6–5.3 μm . At $\lambda < 1 \mu\text{m}$, the derived extinction law is not well described by the parameterized power-law type curve. Our non-parameterized α -dependent extinction curves are suitable for the extinction correction of JWST-based photometry and spectra measurements at 0.6 – 5.3 μm . We also provide the extinction coefficients for the JWST NIRCcam bandpasses with different α .

Keywords: Interstellar dust extinction (837); Interstellar reddening (853); Reddening law (1377); Interstellar extinction (841); Star clusters (1567);

1. INTRODUCTION

With the increasing wealth of optical spectroscopic, astrometric, and photometric data, the optical extinction law has been relatively well understood in recent years (Schlafly et al. 2016; Fitzpatrick et al. 2019; Wang & Chen 2019; Gordon et al. 2023; Li et al. 2023; Wang & Chen 2023; Zhang et al. 2023). However, the infrared (IR) extinction law is not well understood and is still controversial. In the last century, it has been reported that the near-IR extinction curve of 0.9 to 3 μm can be approximately characterized by a universal power-law $A_\lambda \propto \lambda^{-\alpha}$ with $\alpha \approx 1.6 - 1.8$ (Rieke & Lebofsky 1985; Cardelli et al. 1989; Draine 1989; Martin & Whittet 1990; Whittet et al. 1993; He et al. 1995). However, a large number of steeper near-IR extinction curves with $\alpha > 1.9$ or even ~ 2.6 have been reported in different lines of sight in the

last two decades (Messineo et al. 2005; Nishiyama et al. 2006, 2009; Gosling et al. 2009; Stead & Hoare 2009; Schödel et al. 2010; Fritz et al. 2011; Wang & Jiang 2014; Alonso-García et al. 2017; Chen et al. 2018; Nogueras-Lara et al. 2019; Maíz Apellániz et al. 2020). In addition, several studies argued that the power-law index α depends on the wavelength region (e.g. Schödel et al. 2010; Nogueras-Lara et al. 2019). Based on these different α values, the resultant near-IR relative extinction A_J/A_{K_s} values are from 2.5 to 3.5 with an uncertainty of at least 20%.

Whether near-IR extinction curve varies with sightlines or the optical extinction is also controversial. Some studies support no significant variation (Indebetouw et al. 2005; Stead & Hoare 2009; Wang & Jiang 2014; Wang et al. 2015a; Nogueras-Lara et al. 2019; Maíz Apellániz et al. 2020). In contrast, some studies found that the near-IR extinction curve changes from one sightline to another (Nishiyama et al. 2006; Gosling et al. 2009; Alonso-García et al. 2017; Declair et al. 2022). The IR extinction laws are important for constraining

Reverse Shock Emission in an Off-axis Top-hat Jet Model for Gamma-Ray Bursts

Sen-Lin Pang¹ and Zi-Gao Dai^{1,2}★

¹*Department of Astronomy, University of Science and Technology of China, Hefei 230026, China*

²*School of Astronomy and Space Science, University of Science and Technology of China, Hefei 230026, China*

Accepted XXX. Received YYY; in original form ZZZ

ABSTRACT

The afterglow of a gamma-ray burst (GRB) has been widely argued to arise from the interaction of a relativistic outflow with its ambient medium. During such an interaction, a pair of shocks are generated: a forward shock that propagates into the medium, and a reverse shock that propagates into the outflow. Extensive studies have been conducted on the emission from the forward shock viewed off-axis. Furthermore, the observation of a reverse shock in an on-axis short GRB suggests that the reverse shock can produce an electromagnetic counterpart to a gravitational wave-detected merger. In this paper, we investigate the contribution of the reverse shock to the afterglow from a top-hat jet viewed off-axis, and apply our model to some short GRBs previously modeled by an off-axis emission. We employ the Markov Chain Monte Carlo (MCMC) method to get the model parameters (i.e., the jet's half-opening angle θ_j , the viewing angle θ_{obs} , the initial Lorentz factor Γ_0 , and the isotropic energy E_{iso}). Our model successfully reproduces off-axis afterglow emission without a structured jet. In addition, our calculations suggest that the reverse shock may produce a prominent feature in an early afterglow, which can be potentially observed in an orphan optical afterglow.

Key words: gamma-ray bursts: general – stars: jet – relativistic processes

1 INTRODUCTION

Gamma-ray bursts (GRBs) are the most energetic explosions in the universe. It is widely believed that GRBs originate from the death of massive stars (Woolsey & Bloom 2006; Cano et al. 2017) or the merger of two compact objects, such as two neutron stars (NS-NS) (Thompson 1994; Metzger et al. 2011), one neutron star and one stellar-mass black hole (NS-BH) (Narayan et al. 1992), or one neutron star and one white dwarf (Zhong et al. 2023). There are mainly two phases in GRBs (Kumar & Zhang 2015): prompt gamma-ray emission and longer-lasting broadband afterglow emission. The prompt emission typically lasts for a timescale of a few milliseconds to a few thousands of seconds while the afterglow can persist for a period ranging from days to years. According to the internal-external shock model (Sari & Piran 1997; Piran 2005), the prompt emission is produced by internal shocks within relativistic outflows, and the afterglow is produced by external shocks between this outflow and its circum-burst medium (CBM).

The external shock model describes the interaction of a relativistic GRB jet with its circum-burst medium. This interaction naturally gives rise to a pair of shocks (Mészáros & Rees 1999; Sari & Piran 1999; Kobayashi & Zhang 2002; Shao & Dai 2005). A long-lived forward shock (FS) sweeps up the CBM, while a short-lived reverse shock (RS) propagates into the jet and sweeps through the jet itself. Both forward and reverse shocks can accelerate electrons through stochastic processes (Blandford & Eichler 1987), and these

non-thermal electrons release their energy through synchrotron radiation and inverse-Compton scattering (Sari et al. 1998; Sari & Esin 2001). The dynamics and radiation processes of this FS-RS system have been widely studied. Sari & Piran (1995) proposed the standard FS-RS model. Dai & Lu (1998), Chevalier & Li (1999) and Wu et al. (2003) investigated the FS-RS system in a stellar wind environment, and obtained analytical solutions in the cases of an ultra-relativistic reverse shock (RRS) and a Newtonian reverse shock (NRS). Beloborodov & Uhm (2006) developed the mechanical model by applying conservation laws for the energy-momentum tensor and the mass flux to the FS-RS system. Zhang et al. (2022) presented a semi-analytical solution for the FS-RS system by considering a power-law density profile of CBM. In this paper, we utilize the semi-analytical solution proposed by Zhang et al. (2022) to describe the evolution of RS. Once the RS crosses the shell, we employ a generic dynamical model proposed by Huang et al. (1999) can describe the evolution of the FS.

The investigation of off-axis jets in the context of GRBs has been extensive (Woods & Loeb 1999; Granot 2005; Lamb & Kobayashi 2017; Gill & Granot 2018; Beniamini et al. 2020), but the consideration of RS emission from such off-axis jets has been relatively rare. Fraija et al. (2019) conducted a modeling study on the off-axis emission of GW 170817/GRB 170817A and demonstrated that the γ -ray flux could be consistent with a synchrotron self-Compton (SSC) RS model. Lamb & Kobayashi (2019) performed calculations on the RS emission from a structured jet observed from an off-axis perspective, and suggested that the pre-peak afterglow exhibits a distinctive feature originating from the RS. In this paper, we calculate the emission of the FS-RS system from a top-hat jet viewed off-axis in a strati-

★ E-mail: daizg@ustc.edu.cn

Constraining Planetary Formation Models Using Conditional Occurrences of Various Planet Types

Sridhar Gajendran¹, Ing-Guey Jiang^{1*}, Li-Chin Yeh², and Devesh P. Sariya¹

¹*Department of Physics and Institute of Astronomy, National Tsing Hua University, Hsin-Chu 30013, Taiwan*

²*Institute of Computational and Modeling Science, National Tsing Hua University, Hsin-Chu 30013, Taiwan*

Accepted XXX. Received YYY; in original form ZZZ

ABSTRACT

We report the conditional occurrences between three planetary types: super-Earths ($m \sin i < 10 M_{\oplus}$, $P < 100$ days), warm Jupiters ($m \sin i > 95 M_{\oplus}$, $10 < P < 100$ days), and cold Jupiters ($m \sin i > 95 M_{\oplus}$, $P > 400$ days) for sun-like stars. We find that while the occurrence of cold Jupiters in systems with super-Earths is $22.2^{+8.3}_{-5.4}\%$, compared to 10% for the absolute occurrence rate of cold Jupiters, the occurrence of super-Earths in systems with cold Jupiters is $66.0^{+18.0}_{-16.0}\%$, compared to 30% for the absolute occurrence rate of super-Earths for sun-like stars. We find that the enhancement of super-Earths in systems with cold Jupiters is evident for sun-like stars, in agreement with several previous studies. We also conduct occurrence studies between warm Jupiters and super-Earths, and between warm Jupiters and cold Jupiters, to consolidate our methods. We conduct an independent observational test to study the effects of cold Jupiters against the inner multiplicity using the well-established giant planet host star metallicity correlation for all transiting planets found to date. The conditional occurrences we find here can be used to constrain the validity of various planetary formation models. The extremely interesting correlations between the super-Earths, cold Jupiters, and warm Jupiters can also be used to understand the formation histories of these planetary types.

Key words: exoplanets – planets and satellites: formation – planets and satellites: general – methods: statistical

1 INTRODUCTION

The abundance of extrasolar planets discovered in recent years has created a renewed interest in planetary sciences. In particular, the multitude of extrasolar multiple planetary systems has given us an excellent opportunity to verify the validity of various planetary formation models. Even though planet formation is a complicated process involving various parameters, the continuity in the data of discovered exoplanets clearly implies that, in general, several common mechanisms play a part in the formation of generic planetary systems. The abundance of extrasolar multiple planetary systems has also given us an opportunity to explore the various planetary types and their effects in their respective planetary systems. One of the major discerning factors between different planetary formation models is their ability to explain the fraction of planets of different masses (i.e. different types) in a planetary system.

Super-Earths, a planet type whose formation is not well explained by any planetary formation models (Ida & Lin 2004; Mordasini et al. 2009; Morbidelli & Raymond 2016), are nearly ubiquitous among the discovered planets. In particular, close-in or hot super-Earths, defined as a planet of around $1-10 M_{\oplus}$ or $1-4 R_{\oplus}$ and orbital period $P < 100$ days (Mayor et al. 2011; Fressin et al. 2013; Schlichting 2018), present a challenge to most planetary formation models. The two major models explaining their formation, namely, the in situ and inward migration models give rise to several contradicting conclusions. The numerical simulations reported in Izidoro et al. (2015)

suggest that super-Earths are explained well by the inward migration model. However, their study also concludes that such planets will play a major role in defining the planetary composition of their respective systems and, in particular, would present an anti-correlation with giant planets. Consequently, Izidoro et al. (2015), proposed that in systems with hot (close-in) super-Earths, the presence of gas giants should be rare. Schlaufman (2014) used the metallicity scaling of giant planet occurrence with small planet occurrence rates to note that close-in multi-planetary systems suggest formation from high mass disks and that migration is important.

However, gas giants, particularly cold giants, are also known to be relatively abundant around sun-like stars. Using the ELODIE survey, Naef et al. (2005) first estimated a value of $7.5 \pm 1.5\%$ for the giant planet occurrence rate. Cumming et al. (2008) arrived at a value of $12.6 \pm 1.6\%$ from the Keck survey. Several follow-up studies (Zechmeister et al. 2013; Wittenmyer et al. 2016, 2020; Fulton et al. 2021) found a value of $\approx 10\%$ to be consistent for the occurrence rate of giant planets around sun-like stars. More recently, Bonomo et al. (2023) derived an occurrence rate of $9.3^{+7.7}_{-2.9}\%$. Given their overwhelming numbers, it would appear highly unlikely that these two planetary types, super-Earths and gas giants, would be anti-correlated. Moreover, if the super-Earths really are dominant and prevent gas giants from forming in their systems, this would show up as a paucity of massive planets with short orbital periods. This, however, is not found to be true, as the period-ratio and mass-ratio of adjacent planets in multi-planet systems have been verified to present a positive correlation, suggesting that multi-planet systems with a large period ratio (and therefore a large orbital-radius ratio)

* jiang@phys.nthu.edu.tw

Prediction of the SYM-H Index Using a Bayesian Deep Learning Method with Uncertainty Quantification

Yasser Abdouallah^{1,2}, Khalid A. Alobaid^{1,2,3}, Jason T. L. Wang^{1,2}
 Haimin Wang^{1,4,5}, Vania K. Jordanova⁶, Vasyl Yurchyshyn⁵
 Huseyin Cavus^{7,8}, Ju Jing^{1,4,5}

¹Institute for Space Weather Sciences, New Jersey Institute of Technology, Newark, NJ 07102, USA

²Department of Computer Science, New Jersey Institute of Technology, Newark, NJ 07102, USA

³College of Applied Computer Sciences, King Saud University, Riyadh 11451, Saudi Arabia

⁴Center for Solar-Terrestrial Research, New Jersey Institute of Technology, Newark, NJ 07102, USA

⁵Big Bear Solar Observatory, New Jersey Institute of Technology, Big Bear City, CA 92314, USA

⁶Space Science and Applications, Los Alamos National Laboratory, Los Alamos, NM 87545, USA

⁷Department of Physics, Canakkale Onsekiz Mart University, 17110 Canakkale, Turkey

⁸Harvard-Smithsonian Center for Astrophysics, 60 Garden Street, Cambridge, MA 02138, USA

Key Points:

- SYMHnet is a novel deep learning method for making short-term predictions of the SYM-H index (1 or 2 hours in advance).
- With Bayesian inference, SYMHnet can quantify both aleatoric (data) and epistemic (model) uncertainties in making its prediction.
- SYMHnet generally performs better than related machine learning methods for SYM-H forecasting.

Corresponding author: Jason T. L. Wang, wangj@njit.edu

–1–

Abstract

We propose a novel deep learning framework, named SYMHnet, which employs a graph neural network and a bidirectional long short-term memory network to cooperatively learn patterns from solar wind and interplanetary magnetic field parameters for short-term forecasts of the SYM-H index based on 1-minute and 5-minute resolution data. SYMHnet takes, as input, the time series of the parameters' values provided by NASA's Space Science Data Coordinated Archive and predicts, as output, the SYM-H index value at time point $t + w$ hours for a given time point t where w is 1 or 2. By incorporating Bayesian inference into the learning framework, SYMHnet can quantify both aleatoric (data) uncertainty and epistemic (model) uncertainty when predicting future SYM-H indices. Experimental results show that SYMHnet works well at quiet time and storm time, for both 1-minute and 5-minute resolution data. The results also show that SYMHnet generally performs better than related machine learning methods. For example, SYMHnet achieves a forecast skill score (FSS) of 0.343 compared to the FSS of 0.074 of a recent gradient boosting machine (GBM) method when predicting SYM-H indices (1 hour in advance) in a large storm (SYM-H = -393 nT) using 5-minute resolution data. When predicting the SYM-H indices (2 hours in advance) in the large storm, SYMHnet achieves an FSS of 0.553 compared to the FSS of 0.087 of the GBM method. In addition, SYMHnet can provide results for both data and model uncertainty quantification, whereas the related methods cannot.

Plain Language Summary

In the past several years, machine learning and its subfield, deep learning, have attracted considerable interest. Computer vision, natural language processing, and social network analysis make extensive use of machine learning algorithms. Recent applications of these algorithms include the prediction of solar flares and the forecasting of geomagnetic indices. In this paper, we propose an innovative machine learning method that utilizes a graph neural network and a bidirectional long short-term memory network to cooperatively learn patterns from solar wind and interplanetary magnetic field parameters to provide short-term predictions of the SYM-H index. In addition, we present techniques for quantifying both data and model uncertainties in the output of the proposed method.

1 Introduction

Geomagnetic activities and events are known to have a substantial impact on the Earth. They can damage and affect technological systems such as telecommunication networks, power transmission systems, and spacecraft (Ayala Solares et al., 2016; Jordanova et al., 2020). These activities are massive and scale on orders of magnitude (Newell et al., 2007). It may take a few days to recover from the damage, depending on its severity. These activities and events cannot be ignored regardless of whether they are in regions at high, medium, or low latitudes (Carter et al., 2016; Gaunt & Coetzee, 2007; Moldwin & Tsu, 2016; Tozzi et al., 2019; Viljanen et al., 2014). Therefore, several activity indices have been developed to measure the intensity of the geomagnetic effects. These indices characterize the magnitude of the disturbance over time. Modeling and forecasting these geomagnetic indices have become a crucial area of study in space weather research.

Some indices, such as Kp, describe the overall level of geomagnetic activity while others, such as the disturbance storm time (Dst) index (Woodroffe et al., 2016), describe a specific area of geomagnetic activity. The Dst index has been used to classify a storm based on its intensity (Bala & Reiff, 2012; Gruet et al., 2018; Lazzús et al., 2017; Lu et al., 2016; Xu et al., 2023). The storm is intense when Dst is less than -100 nT, moderate when Dst is between -100 nT and -50 nT, and weak when Dst is greater than -50 nT (Gruet et al., 2018; Nuraeni et al., 2022). Another important index is the sym-

–2–

The *XMM-Newton* Line Emission Analysis Program (X-LEAP) I: Emission Line Survey of O VII, O VIII, and Fe L-Shell Transitions

ZEYANG PAN ^{1,2} ZHIJIE QU ³ JOEL N. BREGMAN ⁴ AND JIFENG LIU^{1,2,5,6}

¹*Key Laboratory of Optical Astronomy, National Astronomical Observatories, Chinese Academy of Sciences, 20A Datun Road, Beijing, 100101, People's Republic of China*

²*School of Astronomy and Space Science, University of Chinese Academy of Sciences, Beijing, 100049, People's Republic of China*

³*Department of Astronomy & Astrophysics, The University of Chicago, Chicago, IL 60637, USA*

⁴*Department of Astronomy, University of Michigan, Ann Arbor, MI 48109, USA*

⁵*Institute for Frontiers in Astronomy and Astrophysics, Beijing Normal University, Beijing, 102206, People's Republic of China*

⁶*New Cornerstone Science Laboratory, National Astronomical Observatories, Chinese Academy of Sciences, Beijing, 100012, People's Republic of China*

ABSTRACT

The *XMM-Newton* Line Emission Analysis Program (X-LEAP) is designed to study diffuse X-ray emissions from the Milky Way (MW) hot gas, as well as emissions from the foreground solar wind charge exchange (SWCX). This paper reports an all-sky survey of spectral feature intensities corresponding to the O VII, O VIII, and iron L-shell (Fe-L) emissions. These intensities are derived from 5418 selected *XMM-Newton* observations with long exposure times and minimal contamination from point or extended sources. For 90% of the measured intensities, the values are within $\approx 2\text{--}18$ photons $\text{cm}^{-2} \text{s}^{-1} \text{sr}^{-1}$ (line unit; L.U.), $\approx 0\text{--}8$ L.U., and $\approx 0\text{--}9$ L.U., respectively. We report long-term variations in O VII and O VIII intensities over 22 years, closely correlating with the solar cycle and attributed to SWCX emissions. These variations contribute $\sim 30\%$ and $\sim 20\%$ to the observed intensities on average and peak at ≈ 4 L.U. and ≈ 1 L.U. during solar maxima. We also find evidence of short-term and spatial variations in SWCX, indicating the need for a more refined SWCX model in future studies. In addition, we present SWCX- and absorption-corrected all-sky maps for a better view of the MW hot gas emission. These maps show a gradual decrease in oxygen intensity moving away from the Galactic center and a concentration of Fe-L intensity in the Galactic bubbles and disk.

Keywords: Milky Way Galaxy (1054); Diffuse x-ray background (384); Circumgalactic medium (1879); Solar wind (1534)

1. INTRODUCTION

The circumgalactic medium (CGM) is a diffuse, multi-phase gas surrounding the galaxy. It plays an important role in the formation, evolution, and interactions of galaxies (see the reviews Tumlinson et al. 2017; Donahue & Voit 2022). In particular, the CGM encodes the feedback materials, metals, and energy ejected from the galaxy disk, as well as the accreted gas from the intergalactic medium (IGM). Studying the properties and distribution of the CGM provides valuable constraints on these uncertain processes.

Over the last two decades, the multi-phase CGM in the Milky Way (MW) has been extensively explored using multi-wavelength observations (see the review Putman et al. 2012). X-ray observations reveal that the hot CGM ($T \gtrsim 10^6$ K) is a massive component in the multi-phase medium (e.g., Snowden et al. 1995; Henley & Shelton 2010, 2012). Notably, the stars and interstellar medium (ISM) in the MW only account for $\approx 30\text{--}50\%$ of the baryons, expected from the cosmic average baryonic fraction (e.g., Sommer-Larsen 2006; McGaugh et al. 2010). This discrepancy suggests a deficit of $\approx 3 \times 10^{11} M_{\odot}$ (Anderson & Bregman 2010), positioning the hot CGM as a principal candidate for the “missing baryons”.

FORECASTOR – II. Simulating Galaxy Surveys with the Cosmological Advanced Survey Telescope for Optical and UV Research

MADÉLINE A. MARSHALL ¹, LAURIE AMEN ^{1,2}, TYRONE E. WOODS ^{1,3}, PATRICK CÔTÉ ¹, L. Y. AARON YUNG ^{4,5},
MELISSA AMÉNOUCHE ¹, EMILY K. PASS ^{6,7}, MICHAEL BALOGH ^{8,7}, SAMIR SALIM ⁹, AND THIBAUD MOUTARD ^{10,11}

¹*National Research Council of Canada, Herzberg Astronomy & Astrophysics Research Centre,
5071 West Saanich Road, Victoria, BC V9E 2E7, Canada*

²*Department of Physics and Trottier Space Institute, McGill University, 3600 University Street, Montréal, QC H3A 2T8, Canada*

³*Department of Physics and Astronomy, Allen Building, 30A Sifton Rd, University of Manitoba, Winnipeg, MB R3T 2N2, Canada*

⁴*Astrophysics Science Division, NASA Goddard Space Flight Center, 8800 Greenbelt Rd, Greenbelt, MD 20771, USA*

⁵*Space Telescope Science Institute, 3700 San Martin Drive, Baltimore, MD 21218, USA*

⁶*Center for Astrophysics | Harvard & Smithsonian, 60 Garden Street, Cambridge, MA 02138, USA*

⁷*University of Waterloo, Waterloo, Ontario, N2L 3G1 Canada*

⁸*Waterloo Centre for Astrophysics, Waterloo, Ontario, N2L 3G1 Canada*

⁹*Department of Astronomy, Indiana University, Bloomington, IN 47405, USA*

¹⁰*European Space Agency (ESA), European Space Astronomy Centre (ESAC), Camino Bajo del Castillo s/n, 28692 Villanueva de la Cañada, Madrid, Spain*

¹¹*Aix Marseille Univ, CNRS, CNES, LAM, Marseille, France*

ABSTRACT

The Cosmological Advanced Survey Telescope for Optical and UV Research (CASTOR) is a planned flagship space telescope, covering the blue-optical and UV part of the spectrum. Here we introduce the CASTOR image simulator, a Python GalSim package-based script capable of generating mock CASTOR images from an input catalogue. We generate example images from the CASTOR Wide, Deep, and Ultra-Deep surveys using simulated light-cones from the Santa Cruz Semi-Analytic Model. We make predictions for the performance of these surveys by comparing galaxies that are extracted from each image using Source Extractor to the input catalogue. We find that the Wide, Deep, and Ultra-Deep surveys will be complete to ~ 27 , 29 and 30 mag, respectively, in the UV, u, and g filters, with the UV-split and u-split filters reaching a shallower depth. With a large area of ~ 2200 deg², the Wide survey will detect hundreds of millions of galaxies out to $z \sim 4$, mostly with $M_* \gtrsim 10^9 M_\odot$. The Ultra-Deep survey will probe to $z \sim 5$, detecting a large fraction of $M_* \simeq 10^8 M_\odot$ galaxies. These powerful samples will enable precision measurements of the distribution of star formation in the cosmic web, connecting the growth of stellar mass to the assembly of dark matter halos over two thirds of the history of the Universe, and other core goals of CASTOR’s legacy surveys. These image simulations and the tools developed to generate them will be a vital planning tool to estimate CASTOR’s performance and iterate the telescope and survey designs prior to launch.

Keywords: Space telescopes(1547); Ultraviolet astronomy(1736); Ultraviolet surveys(1742); Galaxy evolution(594); Star formation(1569); Astronomical simulations(1857)

1. INTRODUCTION

Space astronomy has entered an extraordinary era of deep, high-resolution capabilities across the optical–infrared, with the high resolution of the James Webb Space Telescope (JWST; Gardner et al. 2006, 2023; McElwain et al. 2023) complemented by new wide field optical–infrared observatories, including ESA’s new Euclid mission (Laureijs et al. 2011; Racca et al. 2016)

and NASA’s upcoming Roman Space Telescope (Spergel et al. 2013, 2015). However, long term astronomical planning exercises around the world (e.g., Astro2020, LRP2020, Voyage 2050; National Academies of Sciences Engineering, and Medicine 2021; Gaensler & Barmby 2020; Tacconi et al. 2021) have identified a looming gap in the astronomical community’s space-based ultraviolet and blue-optical capability. To avoid astronomy’s capacity to observe in the UV lagging far behind other

The Composition and Chemistry of Titan's Atmosphere [†]

Conor A Nixon*

*Planetary Systems Laboratory, NASA Goddard Space Flight Center
8800 Greenbelt Road, Greenbelt, MD 20771*

E-mail: conor.a.nixon@nasa.gov

Phone: +1 301 286-6757

Abstract

In this article I summarize the current state of knowledge about the composition of Titan's atmosphere, and our current understanding of the suggested chemistry that leads to that observed composition. I begin with our present knowledge of the atmospheric composition, garnered from a variety of measurements including *Cassini-Huygens*, the *Atacama Large Millimeter/submillimeter Array (ALMA)*, and other ground and space-based telescopes. This review focuses on the typical vertical profiles of gases at low latitudes, rather than global and temporal variations. The main body of the paper presents a chemical description of how complex molecules are believed to arise from simpler species, considering all known 'stable' molecules – those that have been uniquely identified in the neutral atmosphere. The last section of the paper is devoted to the gaps in our present knowledge of Titan's chemical composition and how further work may fill those gaps.

[†]Keywords: Titan; Astrochemistry; Astrobiology; Atmospheres; Photochemistry

The *Fermi*-LAT view of the changing-look blazar OQ 334

S.S. Ren¹, R.X. Zhou², Y.G. Zheng^{1,*}, S.J. Kang^{3,*}, and Q. Wu⁴

¹ Department of Physics, Yunnan Normal University, Kunming, 650092, China
e-mail: ynzyg@ynu.edu.cn

² Institute of Space Sciences, Shandong University, Weihai, Shandong, 264209, People's Republic of China

³ School of Physics and Electrical Engineering, Liupanshui Normal University, Liupanshui, Guizhou 553004, China
e-mail: kangshiju@alumni.hust.edu.cn

⁴ Department of Astronomy, School of Physics, Huazhong University of Science and Technology, Wuhan, Hubei, 430074, China.

February 28, 2024

ABSTRACT

Context. Unusually, there are still certain characteristics of the changing-look (CL) active galactic nuclei (AGNs) that remain undetected. Consequently, the trigger mechanism behind the CL phenomenon observed in partial AGNs remains unknown.

Aims. We explore the light curve and spectral energy distribution (SED) of the CL blazar OQ 334 as obtained by *Fermi*-LAT.

Methods. By examining the variability of the equivalent width (EW), we categorise the *Fermi*-LAT light curves of OQ 334 during the epoch of MJD 54628–58677 into seven distinct epochs, including the flat spectrum radio quasar (FSRQ) state, the transition state, and the BL Lac state. We obtained both a *Fermi*-LAT SED and a multi-wavelength SED for each of these distinct epochs.

Results. The source exhibits a transformation from a quiescent state to a highly active state, as evidenced by the variability of the EW. The multi-wavelength SEDs display a prominent external Compton characteristic, even though the *Fermi*-LAT SED reveals both a FSRQ and a BL Lac state across the seven different epochs. To gain further insights, we employed a leptonic model that takes into account the soft photon fields originating from both synchrotron radiation and the external environment. By simulating the multi-wavelength SEDs for each epoch, we uncover the following results. Firstly, the energy density of the external photon fields evolves in an oscillatory manner over the seven different epochs. Also, the energy density of the external photon fields in the BL Lac state is lower than that in the FSRQ state.

Conclusions. These findings suggest that the CL blazar represents a unique phase in the blazar sequence. Considering that the energy density of the external photon fields is proportional to the accretion rate, we propose that evidence for the interconversion of advection-dominated accretion flow (ADAF) discs and standard Shakura-Sunyaev discs (SSDs), — as variations in accretion modes in the CL blazar — can be obtained through observations by *Fermi*-LAT.

Key words. galaxies: active - quasars: emission lines - accretion, accretion discs

1. Introduction

Blazars, a subclass of active galactic nuclei (AGNs), exhibit a peculiar characteristic where the angle between the jet direction of the blazar and the line of sight is extremely small. The multi-wavelength spectral energy distribution (SED) serves as a representation of the energy-flux density of blazars across different frequencies. The SED prominently displays two distinct humps. The first hump, known as the low-energy hump, is typically observed within the optical to X-ray wavelength range. The second hump, referred to as the high-energy hump, is usually observed between X-ray and γ -ray. The generation of the lower energy hump in blazars is widely accepted as being a result of the relativistic electron synchrotron (Syn) radiation occurring within the jet (Urry 1998). However, the mechanism behind the generation of the high-energy hump is still a subject of controversy, with two main explanations being the leptonic model and the hadronic model. In the leptonic model, the second hump is typically attributed to inverse Compton (IC) scattering. Specifically, when the low photon involved in the IC (Maraschi et al. 1992) originates from low-energy Syn radiation, the high-energy hump is generated through synchrotron self-Compton (SSC) radiation (Marscher & Gear 1985). Additionally, when the low-

energy photons for the IC come from outside of the jet, the high-energy hump is generated through external Compton (EC) radiation. The external photon field has four main sources: (1) photons emitted from the accretion disc (Dermer et al. 1992; Sikora et al. 1994); (2) photons originating from the broad-line region (BLR) (Sikora et al. 1994; Blandford & Levinson 1995; Ghisellini & Madau 1996; Bednarek 1998); (3) photons derived from infrared radiation emitted by the dust torus (DT) outside the jet zone, and microwave background radiation (Wagner & Witzel 1995).

The SSC model has been widely employed to fit the multi-wavelength SED of BL Lacertae (BL Lacs) (Krawczynski et al. 2004; Zhang et al. 2012), while a combination of SSC and EC is often used to describe flat-spectrum radio quasars (FSRQs) more accurately (Böttcher & Chiang 2002; Ghisellini et al. 2011; Yan et al. 2014; Zhang et al. 2014; Hovatta & Lindfors 2019). Blazars can also be categorised based on the peak frequency of their low-energy Syn radiation: low-synchrotron-peaked objects (LSP, $v_{peak}^{syn} < 10^{14}$ Hz), intermediate-synchrotron-peaked objects (ISP, 10^{14} Hz $< v_{peak}^{syn} < 10^{15}$ Hz), and high-synchrotron-peaked objects (HSP, $v_{peak}^{syn} > 10^{15}$ Hz) (Abdo et al. 2010a). Another categorisation of blazars is based on the equivalent width (EW) of their emission lines (Stocke et al. 1991; Urry &

Send offprint requests to: Y.G. Zheng

KINDLING THE FIRST STARS II: DEPENDENCE OF THE PREDICTED PISN RATE ON THE POP III INITIAL MASS FUNCTION

ALESSA IBRAHIM WIGGINS¹, MIA SAUDA BOVILL², LOUIS-GREGORY STROLGER³, MASSIMO STIAVELLI³, AND CORA BOWLING¹

¹Department of Physics and Astronomy, Texas Christian University, Fort Worth, TX

²Department of Astronomy, University of Maryland, College Park, College Park, MD and

³Space Telescope Science Institute, Baltimore, MD

Version February 28, 2024

ABSTRACT

Population III (Pop III) stars formed out of metal free gas in minihalos at $z > 20$. While their ignition ended the Dark Ages and begin enrichment of the IGM, their mass distribution remains unconstrained. To date, no confirmed Pop III star has been observed and their direct detection is beyond the reach of the James Webb Space Telescope (JWST) without gravitational lensing. However, a subset of massive Pop III stars end their lives in pair instability supernova (PISN). With typical energies of $\sim 10^{53}$ erg, PISN light curve peaks are bright enough to be detectable by JWST and the Roman Space Telescope. The fundamental question of this work is whether or not observed PISN can be used as a diagnostic of the Pop III IMF. In this work, we use a model of the formation of the first stars to determine the dependence of PISN rates at $z > 5$ for a range of Pop III power law IMFs ($\alpha = 0.2 - 2.35$) and, critically, the method by which the IMF is populated. At $z > 15$, we predict typical rates of $10^{-2} - 10^2$ per deg² per year which will produce $10^{-3} - 0.1$ /year in a single NIRC₂ pointing and $0.003 - 30$ /year in a single Roman pointing with $0.1 - 1000$ per year detected in the HLTDS. Our work highlights that theoretical modeling of PISN rates is required if upcoming PISN studies with JWST and Roman are going to constrain the Pop III IMF.

1. INTRODUCTION





Population III (Pop III) stars are a theoretical population of metal-free stars. It is normally assumed that they formed in dark matter minihalos with masses of $10^5 - 10^6 M_{\odot}$ at $z > 30$ (Abel et al. 2002). Their ignition ended the Cosmic Dark Ages, and their supernovae explosions enriched the interstellar and intergalactic mediums (Jaacks et al. 2018). However, to date, no confirmed Pop III star or star cluster has been observed, and without gravitational lensing, those at high- z remain beyond the reach of JWST (Gardner et al. 2006; Bovill et al. 2024).

Due to the inefficiency of the cooling of molecular hydrogen, Pop III stars are thought to be more massive than enriched Pop II and Pop I stars. Although it is widely agreed that typical Pop III stars are more massive compared to their enriched Pop II or Pop I counterparts, the precise mass distribution of Pop III stars remains uncertain. Certain investigations propose initial mass function upper limits reaching $1000 M_{\odot}$ or even higher (Bromm et al. 1999; Abel et al. 2000; Ohkubo et al. 2009). Conversely, other theoretical studies propose that Population III stars could exhibit a broad range of masses, potentially extending down to a solar mass or below (Stacy et al. 2016; Prole et al. 2022; Latif et al. 2022; Wollenberg et al. 2020; Sugimura et al. 2020; Clark et al. 2011; Greif et al. 2011; Susa 2013; Yoshida et al. 2006; Park et al. 2021a,b). Consequently, our understanding of both the shape of the Pop III stellar initial mass function (IMF) and the maximum mass for a Pop III star remain elusive. While their formation and evolution are likely distinct from that of enriched stars in the local Universe, they remain observationally unconstrained.

Directly detecting Pop III stars or Pop III star clusters at high- z is challenging as their magnitudes are too faint for even the deepest JWST observations (Rydberg et al. 2013; Bovill et al. 2024). Nevertheless, utilizing gravitational lensing shows promise, and has been studied with a focus on magnification in known lensing clusters (Zackrisson et al. 2015; Windhorst et al. 2018). Detecting Pop III stars through gravitational lensing necessitates accurate lensing models, which are available for various lensing clusters (Lam et al. 2014; Diego et al. 2016, 2015; Jauzac et al. 2015a,b). Additionally, individual stars magnified up to 10,000 times have been observed in caustics (Vanzella et al. 2020; Welch et al. 2022), providing evidence that these high-redshift stars could have masses exceeding $> 50 M_{\odot}$ (Welch et al. 2022). The volume probed by very high magnification lensing clusters is modest, which may make the direct observation of a Population III star unlikely.

Consequently, one of the most favorable methods to detect the earliest stars is indirectly through their supernovae. Specifically, a subgroup of Pop III stars with masses ranging from $140 - 260 M_{\odot}$ undergo what is known as a pair instability supernova (PISN) (Fowler & Hoyle 1964; Barkat et al. 1967; Rakavy et al. 1967). These explosive events release energy, perhaps exceeding 10^{53} erg, making them more than a hundred times more energetic than a typical core collapse supernova, although see Schulze et al. (2023) and Gal-Yam et al. (2009) for a highly likely candidates

Up around the bend: a multi-wavelength view of the quasar 3C 345

Jan Röder ^{1,*}, Eduardo Ros ¹, Frank K. Schinzel ², and Andrei P. Lobanov ¹

¹ Max-Planck-Institut für Radioastronomie, Auf dem Hügel 69, D-53121 Bonn, DE
e-mail: jroeder.astro@gmail.com

² National Radio Astronomy Observatory, P.O. Box O, Socorro, NM 87801, USA

Received 20 December, 2023; accepted 19 Feb, 2024

ABSTRACT

Context. The flat-spectrum radio quasar 3C 345 has been showing gamma-ray activity since the mid-2000s along with activity across the electromagnetic spectrum. A gamma-ray burst in 2009 was successfully linked to relativistic outflow in 43 GHz very long baseline interferometry (VLBI) observations and has since been analyzed also using single dish measurements. A multi-wavelength follow-up VLBI observation to the 2009 flare in conjunction with 43 GHz catalogue data from the VLBA-BU-BLAZAR and BEAM-ME programs are analyzed in this study in the context of the long-term evolution of the source.

Aims. We aim to probe the innermost few milli-arcseconds of the ultracompact 3C 345 jet. In the process, we analyze the long-term kinematics of the inner jet and discuss the magnetic field morphology at different scales, as well as the origin of the gamma-ray emission.

Methods. New observations at 23, 43, and 86 GHz took place on ten epochs between 2017 and 2019. We calibrate the 30 data sets using the rPicard pipeline, image them in Difmap and carry out polarization calibration using the GPCAL pipeline. We complement our VLBI data with single-dish lightcurves as well as ancillary VLBI maps at multiple frequencies. This data is then complemented by 43 GHz observation carried out in the framework of the BEAM-ME and VLBA-BU-BLAZAR monitoring programs.

Results. We find multiple distinct component paths in the inner jet, forming a helical geometry. The helix is anchored at a stationary feature some 0.16 mas from the 43 GHz VLBI core and has a timescale of about 8 years. The characteristic bends in the jet morphology are caused by variations in the component ejection angle. We confirm the result of previous studies that the gamma-ray emission is produced (or caused) by relativistic outflow and violent interactions within the jet.

Key words. galaxies: active – galaxies: jets – quasars: individual: 3C 345 – magnetic fields – polarization – hydrodynamics

1. Introduction

In recent years, very long baseline interferometry (VLBI) observations with a variety of telescope arrays have enabled us to study the formation and evolution of relativistic jets in great detail (e.g. Kim et al. 2020b; Issaoun et al. 2022; Jorstad et al. 2022; Lee 2013, 2014; Lee et al. 2016a,b; Nair et al. 2019). Among others, the flat-spectrum quasar 3C 345 is one of the most extensively studied active galactic nuclei (AGN) (e.g., Wittels et al. 1976a,b; Shapiro et al. 1979; Biretta et al. 1983, 1986; Cohen et al. 1981, 1983; Unwin & Wehrle 1992; Zensus et al. 1995; Gabuzda et al. 1999; Klare et al. 2001; Lobanov & Zensus 1999; Lobanov & Roland 2005; Ros et al. 2000; Schinzel et al. 2011). 3C 345 is monitored in the MOJAVE 15 GHz (Lister et al. 2021), VLBA-BU-BLAZAR & BEAM-ME 43 GHz and SMA calibrator 230 GHz programs (Gurwell et al. 2007), as well as by the FERMI/LAT gamma ray telescope (Kocevski & Fermi Large Area Telescope Collaboration 2021; Abdollahi et al. 2023).

At radio frequencies, 3C 345 is known to show a characteristic core-jet structure with a notable persistent bend changing the jet direction from west to north-west at some 4 mas from the core (Schinzel et al. 2010). The compact jet between the central engine and the northward bend consists of both stationary and moving shocks with transverse magnetic field orientation.

The downstream shocks are frequently observed moving at apparent superluminal speeds (e.g., Zensus et al. 1995; Lister et al. 2019, 2021; Weaver et al. 2022) and show a typical transverse magnetic field as expected from shock compression. At 15 GHz, the magnetic field is longitudinal, indicative of a shear layer that is resolved out at higher frequencies (see Sec. 3.7). The VLBI core keeps its transverse magnetic field in this frequency range. Lobanov & Zensus (1999) have postulated a ~ 7.5 year activity cycle in 3C 345, which for the most part has served somewhat accurate predictions of flares.

The relativistic parsec-scale outflow has been identified as a source of the observed γ -ray emission in 3C 345 (Schinzel et al. 2011, 2012), as well as other AGN (MacDonald et al. 2017; Angioni et al. 2019, 2020; Kim et al. 2020a, 2022; Rösch et al. 2022). Specifically, they showed a correlation between a newly ejected component passing through a stationary feature near the 43 GHz core, and a spike in the γ -ray flux. This discovery prompted the proposal for the multi-frequency follow-up observations analyzed in this paper.

Following Pötzl et al. (2021), we adopt a flat Λ CDM cosmology where $\Omega_M = 0.3$, $\Omega_\Lambda = 0.7$ and $H_0 = 70 \text{ km s}^{-1} \text{ Mpc}^{-1}$. At a redshift $z = 0.593$, this yields a linear scale of 6.65 pc mas^{-1} and a proper motion scale of 1 mas yr^{-1} corresponding to $34.5 c$. The paper is organized as follows: In section 2, the multi-frequency VLBA observations and data reduction are described. Section 3 is split into an analysis of the total intensity jet morphology, its kinematics, and its polarized structure. We discuss and summarize the results in section 4.

* Member of the International Max Planck Research School (IMPRS) for Astronomy and Astrophysics at the Universities of Bonn and Cologne

The Interstellar Medium in Dwarf Irregular Galaxies

Deidre A. Hunter,¹ Bruce G. Elmegreen,² and Suzanne C. Madden³

¹Lowell Observatory, Flagstaff, USA, 86001; email: dah@lowell.edu; ORCID 0000-0002-3322-9798

²IBM Research, T.J. Watson Research Center, 1101 Kitchawan Road, Yorktown Heights, NY 10598; email: belmegreen@gmail.com; ORCID 0000-0002-1723-6330

³Université Paris Cité, Université Paris-Saclay, CEA, CNRS, AIM, F-91191, Gif-sur-Yvette Cedex, France; email: suzanne.madden@cea.fr; ORCID 0000-0003-3229-2899

Ann. Rev. Astronomy and Astrophysics
2024. 62:1–44

[https://doi.org/10.1146/\(\(article doi\)\)](https://doi.org/10.1146/((article doi)))

Copyright © 2024 by the author(s).
All rights reserved

Keywords

dwarf irregular galaxies, interstellar medium, atomic gas, molecular gas, CO-dark gas, dust

Abstract

Dwarf irregulars (dIrrs) are among the most common type of galaxy in the Universe. They typically have gas-rich, low surface-brightness, metal-poor, and relatively-thick disks. Here we summarize the current state of our knowledge of the interstellar medium (ISM), including atomic, molecular and ionized gas, along with their dust properties and metals. We also discuss star formation feedback, gas accretion, and mergers with other dwarfs that connect the ISM to the circumgalactic and intergalactic media. We highlight one of the most persistent mysteries: the nature of pervasive gas that is yet undetected as either molecular or cold hydrogen, the “dark gas”. Here are a few highlights:

- Significant quantities of H I are in far-outer gas disks.
- Cold H I in dIrrs would be molecular in the Milky Way, making the chemical properties of star-forming clouds significantly different.
- Stellar feedback has a much larger impact in dIrrs than in spiral galaxies.
- The escape fraction of ionizing photons is significant, making dIrrs a plausible source for reionization in the early Universe.
- Observations suggest a significantly higher abundance of hydrogen (H₂ or cold H I) associated with CO in star-forming regions than that traced by the CO alone.

Magnetic filaments: formation, stability, and feedback

Evgeny A. Kuznetsov^{1,2,3,4}, Evgeny A. Mikhailov^{1,2,5}

¹*P.N.Lebedev Physical Institute, 119991 Moscow, Russia*

²*Skolkovo Institute of Science and Technology, 121205 Moscow, Russia*

³*L.D.Landau Institute for Theoretical Physics, 142432 Chernogolovka, Russia*

⁴*Space Research Institute, 117997 Moscow, Russia*

⁵*M.V.Lomonosov Moscow State University, 119991 Moscow, Russia*

e-mail: kuznetso@itp.ac.ru, ea.mikhajlov@physics.msu.ru

As well known, magnetic fields in space are distributed very inhomogeneously. Some-times field distributions have forms of filaments with high magnetic field values. As many observations show, such a filamentation takes place in convective cells in the Sun and other astro-physical objects. This effect is associated with the frozenness of the magnetic field into a medium with high conductivity that leads to compression of magnetic field lines and forming magnetic filaments. We show analytically, based on the general analysis, that the magnetic field intensifies in the regions of downward flows in both two-dimensional and three-dimensional convective cells. These regions of the hyperbolic type for magnetic fields play a role of a specific attractor. This analysis was confirmed by numerical simulations for 2D convective cells of the roll-type. Without dissipation the magnetic field grows exponentially in time and does not depend on the aspect ratio between horizontal and vertical scale of the cell. An increase due to compression in the magnetic field in the high conductive plasma is saturated due to the natural limitation associated with dissipative effects when the maximum magnitude of the magnetic field is of the order of the root of the magnetic Reynolds number Rem . For the solar convective zone the mean kinetic energy density exceeds mean magnetic energy density at least for two orders of magnitude that allows one to use the kinematic approximation for the MHD induction equation. In this paper based on the stability analysis we explain why downward flows influence magnetic filaments from making them more flat with orientation along interfaces between convective cells.

Keywords: magnetohydrodynamics, convective cells, magnetic field, filaments, feedback

1. Introduction

The phenomenon of collapse plays a significant role in terms of understanding how turbulence, convection and other similar phenomena operate in fluids. The collapse is understood as a process of formation of singularities in a finite time for smooth initial conditions. Such processes have been widely studied for quite a long time. According to classical concepts of the Kolmogorov - Obukhov theory [1, 2] in the case of a low viscosity limit, the vorticity fluctuations in the inertial interval with a scale λ behave proportionally to $\lambda^{-2/3}$. This means that in the limit of small λ we will have infinite amplitudes of fluctuations, which may indicate that classical turbulence is closely related to the occurrence of collapse. At the same time, when highly accurate numerical modeling of such problems became possible, it turned out that in fact collapse was not observed in such cases [3] (see also the review paper [4] devoted to this subject). Nevertheless, the tendency for vorticity enhancement remains but without blow-up behavior. At the same time, for two-dimensional hydrodynamics in the ideal case, solutions associated with collapse are forbidden [5, 6, 7]. In the 2D case this, however, does not exclude the existence of infinite exponential growth [8]. In the 3D hydrodynamics, the generation of the pancake-type structures was numerically observed, when the pancake thickness decreases with time according to an exponential law due to compressible character of the vorticity field [9]. It is important to note that the appearance of such structures in the three-dimensional case is associated with the vorticity frozenness into a fluid [10]. It should be noted that in two-dimensional ideal flows, the vorticity rotor (called divorticity) is also a frozen vector field [8]. This means that not only vorticity, but also any other fields frozen into a medium should be compressible and all arguments about collapse given above are applicable to them. Compressible feature of such fields is a sequence of their frozenness.

Another classical example of frozen fields is a magnetic field in the ideal magnetohydrodynamics (MHD) [11]. In this case, we may expect that the magnetic field should evolve by the same laws as the vorticity in ideal fluids and consequently compress into localized magnetic structures [12]. But, unlike fluids, the MHD operates with two vector fields, namely, velocity and magnetic field. If kinetic energy density sufficiently exceeds magnetic energy density we can consider evolution of the magnetic field in a given velocity distribution and ignore the influence of the growing magnetic field on velocity flows. Such a situation is realized in the convective zone of the Sun where the ratio between mean kinetic energy density and magnetic pressure at least consists of two orders of magnitude. Indeed, in this case, the size of magnetic distributions has a tendency to decrease exponentially in time

Meridional Circulation Streamlined

Deepayan Banik* and Kristen Menou*†‡

*Department of Physics, University of Toronto, 60 St George Street, Toronto, Ontario, M5S 1A7, Canada

† Physics & Astrophysics Group, Dept. of Physical & Environmental Sciences, University of Toronto Scarborough, 1265 Military Trail, Toronto, Ontario, M1C 1A4, Canada

‡ David A. Dunlap Department of Astronomy & Astrophysics, University of Toronto. 50 St. George Street, Toronto, Ontario, M5S 3H4, Canada

(Received 00 Month 20xx; final version received 00 Month 20xx)

Time-dependent meridional circulation and differential rotation in radiative zones are central open issues in stellar evolution theory. We streamline this challenging problem using the ‘downward control principle’ of atmospheric science, under a geostrophic f-plane approximation. New insights emerge from this simplified approach, using pressure as the vertical coordinate. We recover the known stellar physics result that the steady-state meridional circulation decays on the length scale $(N/2\Omega \times \sqrt{Pr})H$, assuming molecular viscosity is the dominant drag mechanism. Prior to steady-state, the meridional circulation and the zonal wind (= differential rotation) spread together via radiative diffusion, under thermal wind balance. The corresponding (4th-order) hyperdiffusion process is reasonably well approximated by regular (2nd-order) diffusion on scales of order a pressure scale-height. We derive an inhomogeneous diffusion (equiv. advection-diffusion) equation for the zonal flow which admits closed-form time-dependent solutions in a finite depth domain, allowing rapid prototyping of the meridional circulation pattern. In the weak drag limit, we find that the time to rotational steady-state can be longer than the Eddington-Sweet time and be instead determined by the longer drag time. Unless strong enough drag operates, the internal rotation of main-sequence stars may thus never reach steady-state. Streamlined meridional circulation solutions provide leading-order internal rotation profiles for studying the role of fluid/MHD instabilities (or waves) in redistributing angular momentum in the radiative zones of stars. Despite clear geometrical limitations and simplifying assumptions, one might expect our thin-layer geostrophic approach to offer qualitatively useful results to understand deep meridional circulation in stars.

Keywords: Differential rotation; Radiative zone; Downward Control Principle; Hyperdiffusion; Time-dependent penetration

1. Introduction

Meridional circulation (Hanasoge 2022) in stars is important for several reasons, including solar activity cycles and dynamo models (Choudhuri *et al.* 1995, Spruit 2002, Weiss and Thompson 2009, Charbonneau 2020), latitudinal distribution of sunspots (Nandy and Choudhuri 2002), advection of angular momentum (Miesch 2000), *tachocline* dynamics (Spiegel and Zahn 1992, Rempel 2005, Garaud and Brummell 2008, Garaud and Arreguin 2009) and the radial transport of chemical species (Elliott and Gough 1999). Even then, it remains poorly understood and crudely treated in state-of-the-art stellar evolution codes such as a MESA (Paxton *et al.* 2010).

Helioseismology (Christensen-Dalsgaard 2002) shows that the outer convective envelope of the Sun ($0.7 - 1 R_{\odot}$), is rotating differentially (Schou *et al.* 1998), while the radiative zone ($0.2 - 0.7 R_{\odot}$) is in approximate solid body rotation (Brown *et al.* 1989, Goode *et al.* 1991). The differential rotation in the convective zone is attributed to different processes like varying

*Corresponding author. Email: deepayan.banik@mail.utoronto.ca

X-Shooting ULLYSES: Massive Stars at low metallicity^{★,★★}

II. DR1: Advanced optical data products for the Magellanic Clouds.

H. Sana¹, F. Tramper¹, M. Abdul-Masih^{2,3,4}, R. Blomme⁵, K. Dsilva^{1,6}, G. Maravelias^{7,8}, L. Martins⁹, A. Mehner², A. Wofford¹⁰, G. Banyard¹, C.L. Barbosa¹¹, J. Bestenlehner¹², C. Hawcroft^{1,14}, D. John Hillier¹⁵, H. Todt¹⁶, C.J.K. Larkin^{17,18}, L. Mahy⁵, F. Najarro¹⁹, V. Ramachandran¹⁷, M.C. Ramírez-Tannus²⁰, M.M. Rubio-Díez²¹, A.A.C. Sander¹⁷, T. Shenar²², J.S. Vink²³, F. Backs^{22,1}, S. A. Brands²², P. Crowther¹², L. Decin¹, A. de Koter^{22,1}, W.-R. Hamann¹⁶, C. Kehrig²⁴, R. Kuiper²⁵, L. Oskinova¹⁶, D. Pauli¹⁶, J. Sundqvist¹, O. Verhamme¹, and the XSHOOT-U collaboration

(Affiliations can be found after the references)

Received September 15, 1996; accepted March 16, 1997

ABSTRACT

Context. The XShootU project aims to obtain ground-based optical to near-infrared spectroscopy of all targets observed by the *Hubble Space Telescope* (HST) under the Director’s Discretionary program ULLYSES. Using the medium resolution spectrograph X-shooter, spectra of 235 OB and Wolf-Rayet (WR) stars in sub-solar metallicity environments have been secured. The bulk of the targets belong to the Large and Small Magellanic Clouds, with the exception of three stars in NGC 3109 and Sextans A.

Aims. This second paper of the series focuses on the optical observations of Magellanic Clouds targets. It describes the uniform reduction of the UVB (300 – 560 nm) and VIS (550 – 1020 nm) XShootU data as well as the preparation of advanced data products that are suitable for homogeneous scientific analyses.

Methods. The data reduction of the RAW data is based on the ESO CPL X-shooter pipeline. We paid particular attention to the determination of the response curves. This required equal flat-fielding of the science and flux standard star data and the derivation of improved flux standard models. The pipeline products were then processed with our own set of routines to produce a series of advanced data products. In particular, we implemented slit-loss correction, absolute flux calibration, (semi-)automatic rectification to the continuum, and a correction for telluric lines. The spectra of individual epochs were further corrected for the barycentric motion, re-sampled and co-added, and the spectra from the two arms were merged into a single flux calibrated spectrum covering the entire optical range with maximum signal-to-noise ratio.

Results. We identify and describe an undocumented recurrent ghost visible on the RAW data. We present an improved flat-fielding strategy that limits artefacts when the SCIENCE and FLUX standard stars are observed on different nights. The improved FLUX standard models and the new grid of anchor points allow to limit artefacts of the response curve correction on, e.g., the shape of the wings of the Balmer lines, from a couple of per cent of the continuum level to less than 0.5%. We confirm the presence of a radial velocity shift of about 3.5 km s⁻¹ between the UVB and the VIS arm of X-shooter and that there is no short term variations impacting the RV measurements. RV precision better than 1 km s⁻¹ can be obtained on sharp telluric lines while RV precision of the order of 2 to 3 km s⁻¹ are obtained on data with the best S/N.

Conclusions. For each target observed by XShootU, we provide three types of data products: (i) two-dimensional spectra for each UVB and VIS exposure before and after correction for the instrument response; (ii) one-dimensional UVB and VIS spectra as produced by the X-shooter pipeline before and after response-correction, as well as after applying various processing, including absolute flux calibration, telluric removal, normalisation and barycentric correction; and (iii) co-added flux-calibrated and rectified spectra over the full optical range, for which all available XShootU exposures were combined. For the large majority of the targets, the final signal-to-noise ratio per resolution element is above 200 in both the UVB and the VIS co-added spectra. The reduced data and advanced scientific data products are made available to the community. Together with the HST UV ULLYSES data, they should enable various science goals, from detailed stellar atmosphere and stellar wind studies, to empirical libraries for population synthesis, to study of the local nebular environment and feedback of massive stars in sub-solar metallicity environments.

Key words. Atlases – Magellanic Clouds – Stars: early-type – Stars: massive – Techniques: spectroscopic

1. Introduction

Low-metallicity massive stars remain poorly understood. The lack of detailed understanding of the global, photospheric and wind properties of these massive stars, and of the physical mechanisms operating in their interiors and atmospheres directly propagate to topics as diverse and important as the Universe’s chemical enrichment in heavy elements (Kobayashi et al. 2006;

Hansen et al. 2014), the formation of high-ionization emitting gas (Kashino et al. 2023), the feedback of massive stars on the local environment (Doran et al. 2013), hosts galaxies and reionization of the early Universe (Codoreanu et al. 2018), as well as on the astrophysical interpretation of gravitational wave detections (Belczynski et al. 2010; Abbott et al. 2020). One of the reasons of the current limitations stems from the lack of a sufficiently high-quality observational database of a broad set of massive stars in various low-metallicity environments.

With typical metallicities of 0.5 Z_⊙ (Hunter et al. 2009) and 0.2 Z_⊙, respectively, (Bouret et al. 2003; Rickard et al. 2022), the Large and Small Magellanic Clouds (LMC, SMC) are our closest

* Based on observations collected at the European Southern Observatory under ESO program ID 106.211Z.001.

** Tables 1, 2 and A.1 are only available in electronic form at the CDS via anonymous ftp to cdsarc.u-strasbg.fr (130.79.128.5) or via <http://cdsweb.u-strasbg.fr/cgi-bin/qcat?J/A+A/>.

The Gasing Pangkah Collaboration: I. Asteroseismic Identification and Characterisation of a Rapidly-Rotating Engulfment Candidate*

J. M. JOEL ONG (王加冕)^{1,2,†} MARC TENG YEN HON^{1,2,†} MELINDA SOARES-FURTADO^{3,4,2,†} ALEXANDER P. STEPHAN^{5,6,†} JENNIFER VAN SADERS,¹ JAMIE TAYAR,⁷ BENJAMIN SHAPPEE,¹ DANIEL R. HEY,¹ LYRA CAO,⁵ MUTLU YILDIZ,⁸ ZEYNEP ÇELİK ORHAN,⁸ SİBEL ÖRTEL,⁸ BENJAMIN MONTET,^{9,10} THOMAS W.-S. HOLOIEN,¹¹ JOSS BLAND-HAWTHORN,^{12,13} SVEN BUDER,^{14,13} GAYANDHI M. DE SILVA,^{15,16,13} KEN C. FREEMAN,^{14,13} SARAH L. MARTELL,^{9,13} GERAINT F. LEWIS,¹² SANJIB SHARMA,¹⁷ AND DENNIS STELLO^{9,12,13,18}

¹*Institute for Astronomy, University of Hawai'i, 2680 Woodlawn Drive, Honolulu, HI 96822, USA*

²*NASA Hubble Fellow*

³*Department of Astronomy, University of Wisconsin-Madison, 475 N. Charter St., Madison, WI 53703, USA*

⁴*MIT Kavli Institute for Astrophysics and Space Research, 77 Massachusetts Ave., Cambridge, MA 02139, USA*

⁵*Department of Astronomy, The Ohio State University, Columbus, OH 43210, USA*

⁶*Center for Cosmology and Astroparticle Physics, The Ohio State University, Columbus, OH 43210, USA*

⁷*Department of Astronomy, University of Florida, Bryant Space Science Center, Stadium Road, Gainesville, FL 32611, USA*

⁸*Department of Astronomy and Space Sciences, Science Faculty, Ege University, 35100, Bornova, İzmir, Turkey*

⁹*School of Physics, University of New South Wales, Sydney, NSW 2052, Australia*

¹⁰*UNSW Data Science Hub, University of New South Wales, Sydney, NSW 2052, Australia*

¹¹*Carnegie Observatories, 813 Santa Barbara Street, Pasadena, CA 91101 USA*

¹²*Sydney Institute for Astronomy, School of Physics, A28, The University of Sydney, NSW 2006, Australia*

¹³*ARC Centre of Excellence for All Sky Astrophysics in 3 Dimensions (ASTRO 3D), Australia*

¹⁴*Research School of Astronomy and Astrophysics, Australian National University, Canberra, ACT 2611, Australia*

¹⁵*School of Mathematical and Physical Sciences, Macquarie University, Sydney, NSW 2109, Australia*

¹⁶*Australian Astronomical Optics, Macquarie University, 105 Delhi Rd, North Ryde, NSW 2113, Australia*

¹⁷*Space Telescope Science Institute, 3700 San Martin Drive, Baltimore, MD, 21218, USA*

¹⁸*Stellar Astrophysics Centre, Aarhus University, Ny Munkegade 120, DK-8000 Aarhus C, Denmark*

(Received June 30, 2023; Revised February 23, 2024; Accepted February 26, 2024)

Submitted to ApJ

ABSTRACT

We report the discovery and characterisation of TIC 350842552 (“Zvrk”), an apparently isolated, rapidly-rotating ($P_{\text{rot}} \sim 99$ d) red giant observed by TESS in its Southern Continuous Viewing Zone. The star’s fast surface rotation is independently verified by the use of p-mode asteroseismology, strong periodicity in TESS and ASAS-SN photometry, and measurements of spectroscopic rotational broadening. A two-component fit to APOGEE spectra indicates a coverage fraction of its surface features consistent with the amplitude of the photometric rotational signal. Variations in the amplitude of its photometric modulations over time suggest the evolution of its surface morphology, and therefore enhanced magnetic activity. We further develop and deploy new asteroseismic techniques to characterise radial differential rotation, and find weak evidence for rotational shear within Zvrk’s convective envelope. This feature, in combination with such a high surface rotation rate, is incompatible with models of angular-momentum transport in single-star evolution. Spectroscopic abundance estimates also indicate a high lithium abundance, among other chemical anomalies. Taken together, all of these suggest a planet-ingestion scenario for the formation of this rotational configuration, various models for which we examine in detail.

Keywords: Asteroseismology (73), Red giant stars (1372), Stellar rotation (1629), Star-planet interactions (2177)

1. INTRODUCTION

As stars evolve up the red giant branch (RGB), their radiative cores contract (and spin up) while their convective envelopes expand (and slow down in their rotation). While seismic rotational measurements with evolved stars indicate that subgiant convective envelopes rotate faster than strict angular momentum conservation would suggest (e.g. Mosser et al. 2012;

Corresponding author: Joel Ong
joelong@hawaii.edu

* *Gasing pangkah* is a traditional Malay competitive game of fighting spinning tops, whose name we adopt as the name of our collaboration.

† The *Gasing Pangkah* Collaboration

arXiv:2402.16971v1 [astro-ph.SR] 26 Feb 2024

Imaging Spectropolarimetry – A New Observing Mode on the Hubble Space Telescope’s Advanced Camera for Surveys

NIMISH P. HATHI ¹, DEAN C. HINES ¹, YOTAM COHEN,¹ NORMAN A. GROGIN ¹ AND MARCO CHIABERGE¹

¹*Space Telescope Science Institute*

3700 San Martin Drive, Baltimore, MD 21218, USA

ABSTRACT

Imaging spectropolarimetry is a new observing mode on the Advanced Camera for Surveys (ACS) aboard the Hubble Space Telescope (HST) that was commissioned in Cycle 30 and is available to HST observers starting in Cycle 31 (i.e., from 2023). It is a technique that is accessible from ground-based observatories, but the superb spatial resolution afforded by HST/ACS combined with the slitless nature of HST/ACS grism spectroscopy opens up the possibility of studying polarized extended emission in a way that is not currently possible even with Adaptive Optics facilities on the ground. This mode could help to study interesting targets including (but not limited to) QSOs, AGN and Radio Galaxies, ISM Dust Properties, Pre-Planetary Nebulae, Proto-Planetary and Debris Disks, Supernovae/Supernova Remnants, and Solar System objects. This research note presents the preliminary results from the calibration programs used to calibrate imaging spectropolarimetry on HST/ACS.

1. INTRODUCTION

The polarization state of light observed from astrophysical sources can provide information otherwise unobtainable from intensity alone. Examples of such information include (but are not limited to): The origin of emission (direct vs. scattered); Nature of emitting or scattering particles (e.g., rela-

Winds of change: the nuclear and galaxy-scale outflows and the X-ray variability of 2MASS 0918+2117

P. Baldini^{1,2,3}, G. Lanzuisi², M. Brusa^{1,2}, A. Merloni³, K. Gkimisi¹, M. Perna⁴, I.E. López^{1,2}, E. Bertola^{5,1,2}, Z. Igo^{3,6}, S. Waddell³, B. Musiimenta^{1,2}, C. Aydar³, R. Arcodia^{*7,3}, G. A. Matzeu^{1,2,8}, A. Luminari^{9,10}, J. Buchner³, C. Vignali^{1,2}, M. Dadina², A. Comastri², G. Cresci⁵, S. Marchesi^{1,2,11}, R. Gilli², F. Tombesi^{12,13,14}, and R. Serafinelli⁹

¹ Dipartimento di Fisica e Astronomia “Augusto Righi”, Università di Bologna, via Gobetti 93/2, 40129 Bologna, Italy
e-mail: pietro.baldini@studio.unibo.it

² INAF – Osservatorio di Astrofisica e Scienza dello Spazio di Bologna, via Gobetti 93/3, 40129 Bologna, Italy

³ Max-Planck-Institut für extraterrestrische Physik, Giessenbachstraße 1, D-85748 Garching bei München, Germany

⁴ Centro de Astrobiología (CAB), CSIC-INTA, Ctra. de Ajalvir km 4, Torrejón de Ardoz, E-28850, Madrid, Spain.

⁵ INAF – Osservatorio Astrofisico di Arcetri, Largo Enrico Fermi 5, I-50125 Firenze, Italy

⁶ Exzellenzcluster ORIGINS, Boltzmannstr. 2, 85748, Garching, Germany

⁷ MIT Kavli Institute for Astrophysics and Space Research, 70 Vassar Street, Cambridge, MA 02139, USA.

⁸ Quasar Science Resources SL for ESA, European Space Astronomy Centre (ESAC), Science Operations Department, 28692, Villanueva de la Cañada, Madrid, Spain

⁹ INAF—Istituto di Astrofisica e Planetologia Spaziali, Via del Fosso del Cavaliere 100, I-00133 Roma, Italy.

¹⁰ INAF—Osservatorio Astronomico di Roma, Via Frascati 33, I-00078 Monte Porzio Catone Roma, Italy.

¹¹ Department of Physics and Astronomy, Clemson University, Kinard Lab of Physics, Clemson, SC 29634, USA.

¹² Department of Astronomy, University of Maryland, College Park, MD 20742, USA.

¹³ Dipartimento di Fisica, Università degli Studi di Roma ‘Tor Vergata’, Via della Ricerca Scientifica 1, I-00133 Roma, Italy.

¹⁴ Istituto Nazionale di Fisica Nucleare, Sezione di Roma ‘Tor Vergata’, Via della Ricerca Scientifica 1, I-00133 Roma, Italy.

ABSTRACT

Context. Powerful outflows from active galactic nuclei (AGN) can significantly impact the gas reservoirs of their host galaxies. However, it is still unclear how these outflows can propagate from the very central regions of galaxies to their outskirts, and whether nuclear winds can be driven by and/or be responsible for drastic spectral transitions.

Aims. In this work we test feedback propagation models on the case test of 2MASS 0918+2117 (2M0918), a $z=0.149$ X-ray variable AGN, which showed tentative evidence for nuclear ultra-fast outflows (UFOs) in a 2005 *XMM-Newton* observation. We also investigate whether UFOs can be related to the observed X-ray variability.

Methods. We observed 2M0918 with *XMM-Newton* and *NuSTAR* in 2020 to confirm the presence and characterize the UFOs. We perform a kinematic analysis of the publicly available 2005 SDSS optical spectrum to reveal and measure the properties of galaxy-scale ionized outflows. Furthermore, we construct 20-year-long lightcurves of observed flux, line-of-sight column density, and intrinsic accretion rate from the spectra of the first 4 *SRG/eROSITA* all-sky surveys and archival observations from *Chandra* and *XMM-Newton*.

Results. We significantly detect UFOs with $v \sim 0.16c$ and galaxy-scale ionized outflows with velocities of ~ 700 km/s. We also find that the drastic X-ray variability (factors > 10) can be explained both in terms of variable obscuration and variable intrinsic luminosity.

Conclusions. Comparing the energetics of the two outflow phases, 2M0918 is consistent with momentum-driven wind propagation. 2M0918 expands the sample of AGN with both UFOs and ionized gas winds from 5 to 6, and brings the sample of AGN hosting multiscale outflows to 19, contributing to a clearer picture of feedback physics. From the variations in accretion rate, column density, and ionization level of the obscuring medium, we propose a scenario that connects obscurers, an accretion enhancement, and the emergence of UFOs.

Key words. galaxies: active - galaxies: nuclei - X-rays: galaxies - ISM: jets and outflows

1. Introduction















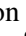

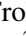

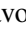



Most massive galaxies host at least one supermassive black hole (SMBH) in their inner regions. These SMBHs are known to be the engine of the powerful emitters known as active galactic nuclei (AGN), as they accrete gas in their vicinity. In the past 20 years, observational evidence of tight correlations between the properties of the host-galaxy and the SMBH (e.g Magorrian et al. 1998; Ferrarese & Merritt 2000; Gebhardt et al. 2000; Häring & Rix 2004), as well as theoretical arguments (e.g Silk & Rees 1998) have led the astronomical community to believe that the

assembly of the SMBH and the galaxy are connected (see Kormendy & Ho 2013 for a review).

In the AGN/galaxy coevolution framework, the enormous amount of energy that the AGN releases through accretion can severely impact the gas reservoirs of the host galaxy, possibly quenching or triggering star-formation (e.g Harrison 2017). The so-called AGN “feedback” is now included in most cosmological simulations (e.g. Di Matteo et al. 2005; Sijacki et al. 2015; Pillepich et al. 2021), as it is a necessary ingredient to prevent the formation of galaxies of extreme stellar masses ($M_{\star} > 10^{12-13} M_{\odot}$), which are indeed extremely rare in the universe.

* NASA Einstein fellow

Searching for late-time interaction signatures in Type Ia supernovae from the Zwicky Transient Facility

Jacco H. Terwel ^{1,2}, Kate Maguire ¹, Georgios Dimitriadis ¹, Mat Smith ^{3,4}, Simeon Reusch ^{5,6}, Leander Lacroix ^{7,8}, Lluís Galbany ^{9,10}, Umut Burgaz ¹, Luke Harvey ¹, Steve Schulze ⁸, Mickael Rigault ⁴, Steven L. Groom ¹¹, David Hale¹², Mansi M. Kasliwal ¹³, Young-Lo Kim ³, Josiah Purdum ¹², Ben Rusholme ¹¹, Jesper Sollerman ¹⁴, Joseph P. Anderson ^{15,16}, Ting-Wan Chen ¹⁷, Christopher Frohmaier ¹⁸, Mariusz Gromadzki ¹⁹, Tomás E. Müller-Bravo ^{9,10}, Matt Nicholl ²⁰, Shubham Srivastav ²⁰, and Maxime Deckers ¹

¹ School of Physics, Trinity College Dublin, The University of Dublin, Dublin 2, Ireland
e-mail: terwel.j@tcd.ie

² Isaac Newton Group (ING), Apt. de correos 321, E-38700, Santa Cruz de La Palma, Canary Islands, Spain

³ Department of Physics, Lancaster University, Lancs LA1 4YB, UK

⁴ Université de Lyon, Université Claude-Bernard Lyon 1, CNRS/IN2P3, IP2I Lyon, 69622 Villeurbanne, France

⁵ Deutsches Elektronen Synchrotron DESY, Platanenallee 6, D-15738 Zeuthen, Germany

⁶ Institut für Physik, Humboldt-Universität zu Berlin, D-12489 Berlin, Germany

⁷ LPNHE, CNRS/IN2P3, Sorbonne Université, Université Paris-Cité, Laboratoire de Physique Nucléaire et de Hautes Énergies, 75005 Paris, France

⁸ Oskar Klein Centre, Department of Physics, Stockholm University, Albanova University Center, SE-106 91, Stockholm, Sweden

⁹ Institute of Space Sciences (ICE-CSIC), Campus UAB, Carrer de Can Magrans, s/n, E-08193 Barcelona, Spain.

¹⁰ Institut d'Estudis Espacials de Catalunya (IEEC), E-08034 Barcelona, Spain.

¹¹ IPAC, California Institute of Technology, 1200 E. California Blvd, Pasadena, CA 91125, USA

¹² Caltech Optical Observatories, California Institute of Technology, Pasadena, CA 91125

¹³ Division of Physics, Mathematics, and Astronomy, California Institute of Technology, Pasadena, CA 91125, USA

¹⁴ Oskar Klein Centre, Department of Astronomy, Stockholm University, Albanova University Center, SE-106 91, Stockholm, Sweden

¹⁵ European Southern Observatory, Alonso de Córdova 3107, Casilla 19, Santiago, Chile

¹⁶ Millennium Institute of Astrophysics MAS, Nuncio Monsenor Sotero Sanz 100, Off. 104, Providencia, Santiago, Chile

¹⁷ Graduate Institute of Astronomy, National Central University, 300 Zhongda Road, 32001 Zhongli, Taiwan

¹⁸ School of Physics and Astronomy, University of Southampton, Highfield, Southampton SO17 1BJ, UK

¹⁹ Astronomical Observatory, University of Warsaw, Al. Ujazdowskie 4, 00-478 Warszawa, Poland

²⁰ Astrophysics Research Centre, School of Mathematics and Physics, Queens University Belfast, Belfast BT7 1NN, UK

Received XXX; accepted YYY

ABSTRACT

The nature of the progenitor systems and explosion mechanisms that give rise to Type Ia supernovae (SNe Ia) are still debated. The interaction signature of circumstellar material (CSM) being swept up by the expanding ejecta can constrain the type of system from which it was ejected. However, most previous studies have focused on finding CSM ejected shortly before the SN Ia explosion, which still resides close to the explosion site resulting in short delay times until the interaction starts. We use a sample of 3 627 SNe Ia from the Zwicky Transient Facility that were discovered between 2018 and 2020 and search for interaction signatures greater than 100 days after peak brightness. By binning the late-time light curve data to push the detection limit as deep as possible, we identify potential late-time rebrightening in three SNe Ia (SN 2018grt, SN 2019ldf, and SN 2020tfc). The late-time optical detections occur between 550 and 1450 d after peak brightness, have mean absolute r -band magnitudes of -16.4 to -16.8 mag and last up to a few hundred days, which is significantly brighter than the late-time CSM interaction discovered in the prototype, SN 2015cp. The late-time detections in the three objects all occur within 0.8 kpc of the host nucleus and are not easily explained by nuclear activity, another transient at a similar sky position, or data quality issues. This is suggestive of environment or specific progenitor characteristics playing a role in the production of potential CSM signatures in these SNe Ia. Through simulating the ZTF survey, we estimate that <0.5 per cent of normal SNe Ia display late-time (> 100 d post peak) strong $H\alpha$ -dominated CSM interaction. This is equivalent to an absolute rate of 8^{+20}_{-4} to 54^{+91}_{-26} $\text{Gpc}^{-3} \text{yr}^{-1}$ assuming a constant SN Ia rate of $2.4 \times 10^{-5} \text{Mpc}^{-3} \text{yr}^{-1}$ for $z \leq 0.1$. Weaker interaction signatures of $H\alpha$ emission, more similar to the strength seen in SN 2015cp, could be more common but are difficult to constrain with our survey depth.

Key words. supernovae: general – supernovae: individual: SN 2018grt, SN 2019ldf, SN 2020tfc – circumstellar matter

1. Introduction

Type Ia supernovae (SNe Ia) span a range of peak absolute magnitudes that can be standardised using properties of their light

curves around peak (e.g. Phillips 1993; Phillips et al. 1999). However, besides normal SNe Ia, there are also events that are spectroscopically and/or photometrically different, creating their own subclasses and that can not be standardised in the normal

An Eccentric Planet Orbiting the Polar V808 Aurigae

McKENNA LEICHTY,¹ PETER GARNAVICH,¹ COLIN LITTLEFIELD,^{1,2} AXEL SCHWOPE,³ JAN KURPAS,^{3,4} PAUL A. MASON,^{5,6} AND KLAUS BEUERMANN⁷

¹*Department of Physics and Astronomy, University of Notre Dame, Notre Dame, IN 46556, USA*

²*Bay Area Environmental Research Institute, Moffett Field, CA 94035 USA*

³*Leibniz-Institut für Astrophysik Potsdam (AIP), An der Sternwarte 16, 14482 Potsdam, Germany*

⁴*Potsdam University, Institute for Physics and Astronomy, Karl-Liebknecht-Straße 24/25, 14476 Potsdam, Germany*

⁵*New Mexico State University, MSC 3DA, Las Cruces, NM, 88003, USA*

⁶*Picture Rocks Observatory, 1025 S. Solano Dr. Suite D., Las Cruces, NM 88001, USA*

⁷*Institut für Astrophysik, Georg-August-Universität, Friedrich-Hund-Platz 1, 37077 Göttingen, Germany*

ABSTRACT

We analyze 15 years of eclipse timings of the polar V808 Aur. The rapid ingress/egress of the white dwarf and bright accretion region provide timings as precise as a few tenths of a second for rapid cadence photometric data. We find that between 2015 and 2018, the eclipse timings deviated from a linear ephemeris by more than 30 s. The rapid timing change is consistent with the periastron passage of a planet in an eccentric orbit about the polar. The best fit orbital period is 11 ± 1 yr and we estimate a projected mass of $M \sin(i) = 6.8 \pm 0.7$ Jupiter masses. We also show that the eclipse timings are correlated with the brightness of the polar with a slope of 1.1 s/mag. This is likely due to the change in the geometry of the accretion curtains as a function of the mass transfer rate in the polar. While an eccentric planet offers an excellent explanation to the available eclipse data for V808 Aur, proposed planetary systems in other eclipsing polars have often struggled to accurately predict future eclipse timings.

Keywords: cataclysmic variables—AM Herculis stars—exoplanet detection methods—eclipsing minima timing methods—stellar magnetic fields

1. INTRODUCTION

The precise timing of short-period eclipsing binaries provides a sensitive method to search for planets or substellar companions orbiting the system (e.g. [Beuermann et al. 2010](#)). Over an orbit, a planet shifts the center of mass of the close pair resulting in variations in the eclipse times due to the light-travel time effect. The very small physical size of white dwarfs (WD) means that an eclipse in a cataclysmic variable (CV) or pre-CV systems can be measured with excellent precision. Polars (AM Her stars) are CVs where a magnetic field from the WD disrupts the formation of an accretion disk. Gas donated from the secondary is funneled to the vicinity of the magnetic poles of the WD, generating a very bright and compact emission region. Thus, eclipsing polars are excellent systems to search for planets or additional stellar components.

Caution is required in interpreting changes in eclipse timings in magnetic CVs. Eclipse timings from the polar HU Aqr initially suggested multiple planet candidates orbiting the close binary ([Qian et al. 2011](#)). However, extending the observation baseline revealed timing variations that could not be explained solely by a multiple planet hypothesis

([Schwope & Thinius 2014, 2018](#)). The source of this timing variability remains uncertain.

Here, we investigate the eclipse timings of the polar V808 Aur (aka CSS081231:071126+440405; [Thorne et al. 2010](#)). V808 Aur is a polar with observational properties that are similar to HU Aqr. Both systems show deep primary eclipses and sometimes pre-eclipse “dips” caused by the self-eclipse of a magnetic accretion curtain. Both polars have orbital periods very close to two hours. HU Aqr and V808 Aur display large variations in their mass transfer rate on time scales of weeks to months ([Schwope et al. 2015](#)).

A study of eclipse timings in V808 Aur by [Schwope et al. \(2015\)](#) did not detect significant variations in data obtained between 2008 and 2015. Here, we analyze a new set of very precise eclipse times obtained between 2008 to 2023.

2. DATA

The times of photometric measurements are referenced to the center of the exposure and converted to BJD (Barycentric Julian Day in the Barycentric Dynamical Time (TDB) system). In our analysis, we include 11 eclipse measurements from [Schwope et al. \(2015\)](#) that had estimated timing errors

The outskirts of M33: Tidally induced distortions versus signatures of gas accretion

Edvige Corbelli¹ and Andreas Burkert²

¹ INAF-Osservatorio Astrofisico di Arcetri, Largo E. Fermi, 5, 50125 Firenze, Italy
e-mail: edvige.corbelli@inaf.it

² Universitäts-Sternwarte, Ludwig-Maximilians-Universität München, Scheinerstr. 1, D-81679 Munich, Germany
e-mail: burkert@usm.uni-muenchen.de

Received; accepted

ABSTRACT

Context.

Aims. We investigate a possible close encounter between M33 and M31 in the past to understand the role of galaxy-galaxy interactions in shaping the matter distribution in galaxy outskirts.

Methods. By examining a variety of initial conditions, we recovered possible orbital trajectories of M33, M31 and the Milky Way in the past, which are compatible with the Early Third Data Release of the *Gaia* mission and with mass estimates of Local Group spirals. Using test-particle simulations we explored if the M33 warp and its dark satellite distribution have been induced by a past M33-M31 encounter along these orbits, after tuning mass losses and the dynamical friction term with the help of N-body numerical simulations.

Results. A close encounter of M33 and M31 in the past has a low but non-negligible probability. If the two galaxies had been closer in the past, their minimum distance would be of the order of 100 kpc or larger, and this happened earlier than 3 Gyr ago. During this encounter, 35-40% of the dark matter mass of M33 might have been removed from the halo due to tidal stripping. A detailed comparison of the results of test-particle simulations with the observed disk warp or with the spatial distribution of candidate dark satellites of M33 suggests that a closer passage of M33 around M31 cannot, however, be responsible for the observed morphological features. We suggest that more recent gas accretion events, possibly from a cosmic filament, might cause the misalignment of the outer disk of M33 after the rapid inner disk formation.

Key words. Galaxies: individual (M33,M31) – Galaxies: dynamics –

1. Introduction

The relevance of galaxy outskirts for understanding galaxy formation and evolution is fully recognised today because numerical simulations and observations show that galaxies do not evolve as close boxes but through a continuous exchange of radiation and matter with the environment, cosmic filaments, clusters, and groups where galaxies reside (Dekel & Birnboim 2006; Cen & Ostriker 2006; Kereš & Hernquist 2009; Boselli et al. 2009). Depending upon cosmic time, the cosmic web as well as galaxy encounters might trigger or stop gas accretion, driving internal processes such as the rate of star formation and galaxy growth (Kennicutt et al. 1987; Larson 2002; Dekel & Mandelker 2014). Evidence of gas accretion from the cosmic web, today or at earlier cosmic times, is still controversial since direct imaging of cosmic filament flows is difficult due to the low matter density and to projection effects. There is only indirect evidence that this is effectively taking place (Sánchez Almeida et al. 2014; Cooper et al. 2015). Galaxy outskirts are excellent places where one can search for signs of recent gas accretion or tidal disturbances because of their low baryonic content and shallower potential well than the brighter inner regions.

Local Group galaxies offer a unique opportunity to search for signatures of these processes because of the high spatial resolution and sensitivity available (Braun & Thilker 2004; Braun 2004; Grossi et al. 2008; Putman et al. 2009; Wolfe et al. 2013; Kerp et al. 2016; Wolfe et al. 2016). In the Local Group, how-

ever, the evidence of intergalactic cold gas accretion into its more massive members, the Milky Way (hereafter MW), M31, and M33, has to face another difficulty. Internal cycling such as galactic fountains or cosmic web accretion can produce cold gas clouds above the MW disk, also known as high velocity clouds (HVCs), with systemic velocities close to that of M31 or M33. This makes it difficult to distinguish MW clouds lying in projection towards M31 or M33 from more massive and distant clouds effectively orbiting these galaxies. Gas clouds that show a rotational pattern are likely to be associated with M31 or M33 (Thilker et al. 2004; Westmeier et al. 2005; Grossi et al. 2008). These clouds at the distance of M31 and M33 can be a sign of gas accretion or the baryonic counterparts of dark satellites orbiting M31 or M33, alleviating the missing satellite problem, which is very severe in the case of M33 (Grossi et al. 2011; Keenan et al. 2016; Patel et al. 2018; Martínez-Delgado et al. 2022).

The outer disk of M33 has a well-defined orientation established through a tilted ring model fit to the velocity field of the 21-cm line (Corbelli & Schneider 1997; Corbelli et al. 2014). The presence of a warp in the outer disk can be a sign of a recent interaction but also of slow gas and dark matter accretion at later times than the inner disk formation epoch, which causes an infall-driven reorientation of the outer parts of virialised haloes and disks (Jiang & Binney 1999). In this paper we examine, in detail, the possible origins of the disk warp and of the non-isotropic distribution of possible dark satellites, as traced by HI gas clouds in the proximity of M33 (Grossi et al. 2008; Corbelli

Discovery of Globular Cluster Candidates in the Dwarf Irregular Galaxy IC 2574 Using HST/ACS Imaging

Noushin Karim¹, Michelle L. M. Collins¹, Duncan A. Forbes² and Justin I. Read¹

¹*Physics Department, University of Surrey, Guildford, GU2 7XH, UK*

²*Centre for Astrophysics and Supercomputing, Swinburne University, Hawthorn, VIC 3122, Australia*

28 February 2024

ABSTRACT

We report the discovery of 23 globular cluster (GC) candidates around the relatively isolated dwarf galaxy IC 2574 within the Messier 81 (M81) group, at a distance of 3.86 Mpc. We use observations from the HST Advanced Camera for Surveys (ACS) to analyse the imaging in the F814W and F555W broadband filters. Our GC candidates have luminosities ranging from $-5.9 \geq M_V \geq -10.4$ and half-light radii of $1.4 \leq r_h \leq 11.5$ pc. We find the total number of GCs ($N_{GC} = 27 \pm 5$) after applying completeness corrections, which implies a specific frequency of $S_N = 4.0 \pm 0.8$, consistent with expectations based on its luminosity. The GC system appears to have a bimodal colour distribution, with 30% of the GC candidates having redder colours. We also find 5 objects with extremely blue colours that could be young star clusters linked to an intense star formation episode that occurred in IC 2574 ~ 1 Gyr ago. We make an independent measurement of the halo mass of IC 2574 from its kinematic data, which is rare for low mass galaxies, and find $\log M_{200} = 10.93 \pm 0.08$. We place the galaxy on the well-known GC system mass-halo mass relation and find that it agrees well with the observed near-linear relation. IC 2574 has a rich GC population for a dwarf galaxy, which includes an unusually bright ω Cen-like GC, making it an exciting nearby laboratory for probing the peculiar efficiency of forming massive GCs in dwarf galaxies.

Key words: galaxies: clusters: general – galaxies: formation – galaxies: dwarf – galaxies: individual: IC 2574

1 INTRODUCTION

Globular clusters (GCs) are among the oldest astronomical objects to exist, providing a unique probe into the early Universe and the conditions under which the first galaxies formed, making them reliable tracers of galaxy formation and evolution (Puzia et al. 2005; Strader et al. 2005; Kruijssen 2014; Orkney et al. 2019; Beasley 2020). GCs are composed of a homogeneous stellar population with similar ages, metallicities and chemical compositions, although they do show interesting spreads and correlations in their light element abundances (Osborn & Schmitt 1971; Shetrone 1996; Ivans et al. 1999; Yong et al. 2003; Gratton et al. 2004; Piotto et al. 2007; D’Antona & Caloi 2007; Carretta et al. 2009; Marino et al. 2012; Mészáros et al. 2015; Bastian & Lardo 2018; Nataf et al. 2019, and references therein). Despite complex galaxy evolution through mergers and interactions, high density GC cores can remain largely intact and retain unique characteristics of the environment in which they were born (Peñarrubia et al. 2009; Mucciarelli et al. 2021, and references therein). This makes them a promising way to gauge the evolution of galaxies over their lifetimes (Kissler-Patig 2000). The properties of GC systems as a whole have a remarkable story to tell in this context. The number of GCs (N_{GC}) in a system allow us to make an estimate of the GC system mass (M_{GC}) (e.g. McLaughlin & van der Marel 2005; Spitler & Forbes 2009), which is found to follow tight scaling relations with the halo mass and total luminosity of the host galaxy. This physical link between the properties of the GC system and the host galaxy was first established by Blakeslee et al. (1997), and has grown in to

a rich topic of study using various host galaxy properties (Santiago & Djorgovski 1993; Zepf & Ashman 1993; Peng et al. 2008; Spitler & Forbes 2009; Georgiev et al. 2010; Harris et al. 2013, 2015; Hudson et al. 2014; Forbes et al. 2018b; Forbes & Remus 2018; Burkert & Forbes 2020; Beasley 2020; Eadie et al. 2022; Dornan & Harris 2023). These scaling relations suggest that GCs formed in the smallest proto-galactic building blocks (e.g. Boley et al. 2009) and therefore accurately track the assembly history of galaxies thereafter (Harris 1991; Ashman & Zepf 1998; El-Badry et al. 2019; Beasley 2020). N_{GC} , M_{GC} , the luminosity, size and colour distribution all offer insightful clues about the history of their host galaxies (Kissler-Patig 2000; Spitler & Forbes 2009; Georgiev et al. 2010; Hudson et al. 2014; Harris et al. 2017; Amorisco et al. 2018; Forbes et al. 2018b; Prole et al. 2019; Beasley 2020; Doppel et al. 2021; Trujillo-Gomez et al. 2021, and references therein).

M_{GC} is found to have an empirical, near-linear correlation with M_{200} across 7 orders of magnitude (Spitler & Forbes 2009; Georgiev et al. 2010; Hudson et al. 2014; Harris et al. 2017; Forbes et al. 2018b). Populating the $M_{GC} - M_{200}$ relation with observed galaxy data is vital to build a complete picture, however measuring the halo mass of individual galaxies is difficult and relies on kinematic data from the galaxy. A review by Courteau et al. (2014) discusses the variety and reliability of mass estimator techniques in detail. However, each of these have their own limitations (Courteau et al. 2014; Coles et al. 2014; Read et al. 2017), and often require expensive and targeted follow-up observations to determine precision

The Sun Remains Relatively Refractory Depleted: Elemental Abundances for 17,412 Gaia RVS Solar Analogs and 50 Planet Hosts

RAYNA RAMPALLI,^{1,*} MELISSA K. NESS,^{2,3,4} GRAHAM H. EDWARDS,^{5,1} ELISABETH R. NEWTON,¹ AND MEGAN BEDELL⁴

¹*Department of Physics and Astronomy, Dartmouth College, Hanover, NH 03755, USA*

²*Research School of Astronomy & Astrophysics, Australian National University, Canberra, ACT 2611, Australia*

³*Department of Astronomy, Columbia University, 550 West 120th Street, New York, NY, 10027, USA*

⁴*Center for Computational Astrophysics, Flatiron Institute, 162 Fifth Avenue, New York, NY 10010, USA*

⁵*Department of Earth Sciences, Dartmouth College, Hanover, NH 03755, USA*

(Accepted February 23, 2024)

Submitted to ApJ

ABSTRACT

The element abundances of stars, particularly the refractory elements (e.g., Fe, Si, Mg), play an important role in connecting stars to their planets. Most Sun-like stars do not have refractory abundance measurements since obtaining a large sample of high-resolution spectra is difficult with oversubscribed observing resources. In this work we infer abundances for C, N, O, Na, Mn, Cr, Si, Fe, Ni, Mg, V, Ca, Ti, Al, and Y for solar analogs with Gaia RVS spectra ($R=11,200$) using the Cannon, a data-driven method. We train a linear model on a reference set of 34 stars observed by Gaia RVS with precise abundances measured from previous high resolution spectroscopic efforts ($R > 30,000 - 110,000$). We then apply this model to several thousand Gaia RVS solar analogs. This yields abundances with average upper limit precisions of 0.04–0.1 dex for 17,412 stars, 50 of which are identified planet (candidate) hosts. We subsequently test the relative refractory depletion of these stars with increasing element condensation temperature compared to the Sun. The Sun remains refractory depleted compared to other Sun-like stars regardless of our current knowledge of the planets they host. This is inconsistent with theories of various types of planets locking up or sequestering refractories. Furthermore, we find no significant abundance differences between identified close-in giant planet hosts, giant planet hosts, and terrestrial/small planet hosts and the rest of the sample within our precision limits. This work demonstrates the utility of data-driven learning for future exoplanet composition and demographics studies.

Keywords: stars: abundances, stars: solar-type - sun: abundances – techniques: spectroscopic – exoplanet: formation - solar system: formation

1. INTRODUCTION

Know thy star, know thy planet: planets can reflect chemical properties of their host star because they are formed from the same molecular cloud. Studying star-planet connections of other planetary systems using their host star chemistry can answer open questions we have about our own solar system. The Sun shows a

trend of relative depletion in refractory elements¹ (Na, Mn, Cr, Si, Fe, Ni, Mg, V, Ca, Ti, Al, Y) with increasing condensation temperature compared to 80% of its Sun-like counterparts (Bedell et al. 2018), but the source of this relative depletion is unknown. Early work from Meléndez et al. (2009); Ramírez et al. (2009) posits that the terrestrial planets have locked up these refractory elements. More recently, Booth & Owen (2020)

Corresponding author: Rayna Rampalli
raynarampalli@gmail.com

* NSF GRFP Fellow

¹ We define an element as “refractory” if its 50% condensation temperature from Lodders (2003) > 900 K following Flores et al. (2023).

The rate of extreme coronal line emitting galaxies in the Sloan Digital Sky Survey and their relation to tidal disruption events

J. Callow¹*, O. Graur^{1,2}, P. Clark¹, A. Palmese³, J. Aguilar⁴, S. Ahlen⁵, S. BenZvi⁶, D. Brooks⁷, T. Claybaugh⁴, A. de la Macorra⁸, P. Doel⁷, J. E. Forero-Romero^{9,10}, E. Gaztañaga^{11,12}, S. Gontcho A Gontcho⁴, A. Lambert⁴, M. Landriau⁴, M. Manera^{13,14}, A. Meisner¹⁵, R. Miquel^{16,14}, J. Moustakas¹⁷, J. Nie¹⁸, C. Poppett^{4,19,20}, F. Prada²¹, M. Rezaie²², G. Rossi²³, E. Sanchez^{16,24}, J. Silber⁴, G. Tarlé²⁵, B. A. Weaver¹⁵ and Z. Zhou¹⁸

¹ Institute of Cosmology & Gravitation, University of Portsmouth, Dennis Sciama Building, Portsmouth, PO1 3FX, UK

² Department of Astrophysics, American Museum of Natural History, New York, NY 10024, USA

³ Department of Physics, Carnegie Mellon University, 5000 Forbes Avenue, Pittsburgh, PA 15213, USA

⁴ Lawrence Berkeley National Laboratory, 1 Cyclotron Road, Berkeley, CA 94720, USA

⁵ Physics Dept., Boston University, 590 Commonwealth Avenue, Boston, MA 02215, USA

⁶ Department of Physics & Astronomy, University of Rochester, 206 Bausch and Lomb Hall, P.O. Box 270171, Rochester, NY 14627-0171, USA

⁷ Department of Physics & Astronomy, University College London, Gower Street, London, WC1E 6BT, UK

⁸ Instituto de Física, Universidad Nacional Autónoma de México, Cd. de México C.P. 04510, México

⁹ Departamento de Física, Universidad de los Andes, Cra. 1 No. 18A-10, Edificio Ip, CP 111711, Bogotá, Colombia

¹⁰ Observatorio Astronómico, Universidad de los Andes, Cra. 1 No. 18A-10, Edificio H, CP 111711 Bogotá, Colombia

¹¹ Institut d'Estudis Espacials de Catalunya (IEEC), 08034 Barcelona, Spain

¹² Institute of Space Sciences, ICE-CSIC, Campus UAB, Carrer de Can Magrans s/n, 08913 Bellaterra, Barcelona, Spain

¹³ Departament de Física, Serra Hünter, Universitat Autònoma de Barcelona, 08193 Bellaterra (Barcelona), Spain

¹⁴ Institut de Física d'Altes Energies (IFAE), The Barcelona Institute of Science and Technology, Campus UAB, 08193 Bellaterra Barcelona, Spain

¹⁵ NSF's NOIRLab, 950 N. Cherry Ave., Tucson, AZ 85719, USA

¹⁶ Institució Catalana de Recerca i Estudis Avançats, Passeig de Lluís Companys, 23, 08010 Barcelona, Spain

¹⁷ Department of Physics and Astronomy, Siena College, 515 Loudon Road, Loudonville, NY 12211, USA

¹⁸ National Astronomical Observatories, Chinese Academy of Sciences, A20 Datun Rd., Chaoyang District, Beijing, 100012, P.R. China

¹⁹ Space Sciences Laboratory, University of California, Berkeley, 7 Gauss Way, Berkeley, CA 94720, USA

²⁰ University of California, Berkeley, 110 Sproul Hall #5800 Berkeley, CA 94720, USA

²¹ Instituto de Astrofísica de Andalucía (CSIC), Glorieta de la Astronomía, s/n, E-18008 Granada, Spain

²² Department of Physics, Kansas State University, 116 Cardwell Hall, Manhattan, KS 66506, USA

²³ Department of Physics and Astronomy, Sejong University, Seoul, 143-747, Korea

²⁴ CIEMAT, Avenida Complutense 40, E-28040 Madrid, Spain

²⁵ University of Michigan, Ann Arbor, MI 48109, USA

Accepted XXX. Received YYY; in original form ZZZ

ABSTRACT

Strong high-ionization iron coronal lines (CLs) are a rare phenomenon observed in galaxy and quasi-stellar object spectra that are thought to be created as a result of tidal disruption event (TDE) flares. To test whether these CLs are the result of TDE activity, we search for extreme coronal line emitting galaxies (ECLEs) in the Sloan Digital Sky Survey (SDSS), measure their rate, and compare it to TDE rates from the literature. We detect sufficiently strong CLs in 14 objects, doubling the number previously found in SDSS. Using follow-up spectra from the Dark Energy Spectroscopic Instrument and Gemini Multi-Object Spectrograph, *Wide-field Infrared Survey Explorer* mid-infrared observations, and Liverpool Telescope optical photometry, we find that of the seven new objects, only one evolves in a manner consistent with that of the five previously discovered variable ECLEs. Using this new sample of six variable ECLEs, we calculate the galaxy-normalised rate of ECLEs in SDSS to be $R_G = 2.2^{+1.3}_{-0.8}$ (statistical) $^{+0.0}_{-1.3}$ (systematic) $\times 10^{-5}$ galaxy⁻¹ year⁻¹. The mass-normalised rate is $R_M = 1.9^{+1.1}_{-0.7}$ (statistical) $^{+0.0}_{-1.1}$ (systematic) $\times 10^{-16}$ M_⊙⁻¹ year⁻¹ and the volumetric rate is $R_V = 6.9^{+5.6}_{-2.1}$ (statistical) $^{+0.0}_{-3.9}$ (systematic) $\times 10^{-8}$ Mpc⁻³ year⁻¹. Our rates are comparable to TDE rates from the literature, supporting the suggestion that the CLs in variable ECLEs are the product of TDEs.

Key words: transients: tidal disruption events – galaxies: active – galaxies: nuclei

Eccentric Mergers in AGN Discs: Influence of the Supermassive Black-Hole on Three-body Interactions

Gaia Fabj,¹* Johan Samsing¹

¹*Niels Bohr International Academy, The Niels Bohr Institute, Blegdamsvej 17, 2100 Copenhagen, Denmark*

Accepted XXX. Received YYY; in original form ZZZ

ABSTRACT

There are indications that stellar-origin black holes (BHs) are efficiently paired up in binary black holes (BBHs) in Active Galactic Nuclei (AGN) disc environments, which can undergo interactions with single BHs in the disc. Such binary-single interactions can potentially lead to an exceptionally high fraction of gravitational-wave mergers with measurable eccentricity in LIGO/Virgo/KAGRA. We here take the next important step in this line of studies, by performing post-Newtonian N-body simulations between migrating BBHs and single BHs set in an AGN disc-like configuration with a consistent inclusion of the central supermassive black hole (SMBH) in the equations of motion. With this setup, we study how the fraction of eccentric mergers varies in terms of the initial size of the BBH semi-major axis relative to the Hill sphere, as well as how it depends on the angle between the BBH and the incoming single BH. We find that the fraction of eccentric mergers is still relatively large, even when the interactions are notably influenced by the gravitational field of the nearby SMBH. However, the fraction as a function of the BBH semi-major axis does not follow a smooth functional shape, but instead shows strongly varying features that originate from the underlying phase-space structure. The phase-space further reveals that many of the eccentric mergers are formed through prompt scatterings. Finally, we present the first analytical solution to how the presence of an SMBH in terms of its Hill sphere affects the probability for forming eccentric BBH mergers through chaotic three-body interactions.

Key words: stars: kinematics and dynamics – galaxies: active – accretion, accretion discs – galaxies: nuclei – stars: black holes – gravitational waves

1 INTRODUCTION

The observations of gravitational-wave (GW) sources with LIGO/Virgo/KAGRA (LVK) is ongoing and have to date revealed sources of both binary black holes (BBHs) (Abbott et al. 2016b,c,a, 2017a,b; Venumadhav et al. 2020a,b), binary neutron stars (BNSs) (Abbott et al. 2017c), as well as possible black hole-neutron star mergers (Abbott et al. 2023; Hamers et al. 2021; Vynatheya & Hamers 2022). However, how and where these sources form in our Universe are still major unsolved problems. Many formation channels have been proposed, including field binaries (Dominik et al. 2012, 2013, 2015; Kinugawa et al. 2014; Belczynski et al. 2016b,a; Silsbee & Tremaine 2017; Murguia-Berthier et al. 2017; Rodriguez & Antonini 2018; Schröder et al. 2018), dense stellar clusters (Portegies Zwart & McMillan 2000; Lee et al. 2010; Banerjee et al. 2010; Tanikawa 2013; Bae et al. 2014; Rodriguez et al. 2015, 2016a,b,b; Askar et al. 2017; Park et al. 2017; Samsing 2018; D’Orazio & Samsing 2018; Samsing & D’Orazio 2018; Samsing et al. 2020; Rozner & Perets 2022), active galactic nuclei (AGN) accretion discs (Bartos et al. 2017; Stone et al. 2017; McKernan et al. 2018; Tagawa et al. 2019; Rozner et al. 2023), galactic nuclei (GN) (O’Leary et al. 2009; Hong & Lee 2015; VanLandingham et al. 2016; Antonini & Rasio 2016; Stephan et al. 2016; Hoang et al. 2018; Hamers et al. 2018), very

massive stellar mergers (Loeb 2016; Woosley 2016; Janiuk et al. 2017; D’Orazio & Loeb 2018), and single-single GW captures of primordial black holes (Bird et al. 2016; Cholis et al. 2016; Sasaki et al. 2016; Carr et al. 2016). To disentangle these different scenarios using GWs, we have to understand how the observable parameters differ between the different channels. For example, studies indicate that one can distinguish dynamically induced mergers from isolated binaries, by analyzing the the relative spin orientation of the merging black-holes (BHs) (Rodriguez et al. 2016c), the orbital eccentricity at some reference GW frequency (Gültekin et al. 2006; Samsing et al. 2014; Samsing & Ramirez-Ruiz 2017; Samsing & Ilan 2018; Samsing et al. 2018a; Samsing 2018; Samsing et al. 2018b; Samsing & D’Orazio 2018; Rodriguez et al. 2018; Zevin et al. 2019; Samsing et al. 2019b, 2020), as well as the mass spectrum (Zevin et al. 2017). The environment in which the BBH was formed and merged can also be imprinted in the GW form, showing up as e.g. a GW phase-shift (e.g. Inayoshi et al. 2017; D’Orazio & Loeb 2020, Samsing & Hendriks (in prep.)). Other probes of formation include e.g. stellar tidal disruptions (e.g. Samsing et al. 2019a; Lopez et al. 2019; Kremer et al. 2019b). From these studies it generally follows that dynamically formed mergers tend to have mass ratios near one (e.g. Rodriguez et al. 2018), random spin orientations (e.g. Rodriguez et al. 2016c), as well as a non-negligible fraction of sources with measurable eccentricity in LISA (Samsing & D’Orazio 2018; D’Orazio & Samsing 2018; Kremer et al. 2019a), DECIGO/Tian-Qin (e.g. Chen & Amaro-

* E-mail: gaia.fabj@nbi.ku.dk

Excess cataloged X-ray and radio sources at galaxy-cluster virial shocks

Gideon Ilani,^{*} Kuan-Chou Hou,[†] and Uri Keshet[‡]

Physics Department, Ben-Gurion University of the Negev, POB 653, Be'er-Sheva 84105, Israel

We detect a highly significant excess of X-ray (2RXS) and radio (NVSS, GMRT, VLSSr) catalog sources when stacked around MCXC galaxy clusters and groups, narrowly confined within $\lesssim 100$ kpc of the $\sim 2.4R_{500}$ virial shock radius (inferred from continuum stacking), with similar X-ray ($\sim 4\sigma$ for 443 clusters) and radio ($\sim 4\sigma$ for 485 clusters) characteristics ($> 5\sigma$ joint). The excess sources show 10–100 kpc scales, $L_X(0.1\text{--}2.4\text{ keV}) \simeq 10^{42\text{--}43}\text{ erg s}^{-1}$ or $\nu L_\nu(\nu = 1.4\text{ GHz}) \simeq 10^{40\text{--}41}\text{ erg s}^{-1}$ luminosities, and a preferentially radial radio-polarization. The narrow localization and properties of the excess identify these sources not as AGN, often invoked speculatively for excess X-ray sources at cluster outskirts, but rather as infalling gaseous clumps interacting with the virial shock, probably galactic halos and possibly outflow remnants. The local excess of such discrete, radio-to- γ -ray sources around an object can probe its virial shock also at high redshifts and sub-cluster scales.

1. INTRODUCTION

Several studies have reported a radially-broad excess of X-ray sources in the outskirts of galaxy clusters. These include a $\gtrsim 5\sigma$ excess at $1.5 \lesssim r \lesssim 3$ Mpc radii in stacked *Chandra* data around 24 relaxed, redshift $0.3 < z < 0.7$ MACS clusters [1], a $\sim 4\sigma$ excess at $2 \lesssim r \lesssim 3$ Mpc in stacked *XMM-Newton* data around 22 luminous, $0.9 < z \lesssim 1.6$ clusters [2], and a statistically significant excess at normalized, $2 < \tau \equiv r/R_{500} < 4$ radii in stacked *XMM-LSS* field data around 19 clusters of $0.14 < z < 0.35$ [3]. Here, the subscript 500 refers (henceforth) to the radius around the center of a cluster enclosing a mass density ρ that is 500 times larger than the critical mass density of the Universe. The excess sources were usually assumed to be associated with active galactic nuclei (AGN). Their excess at the cluster periphery was tentatively attributed to an enhanced rate of major galaxy mergers [*e.g.*, 1, 4, and references therein]. Part of the excess was speculated to arise from gravitational lensing of background quasi-stellar objects [3] or from foreground structures [2].

In contrast, other analyses, including larger studies, have found no excess of peripheral sources. In particular, no X-ray source excess was found beyond $r = 1$ Mpc using *Chandra* data around 27 disturbed, $0.3 < z < 0.7$ MACS clusters [1] or 148 clusters of $0.1 < z < 0.9$ [5], and no excess of optical, IR or radio-selected cataloged AGN was found at the outskirts of 2300 infrared-selected clusters [6]. Searches for a source excess performed after normalizing distances to typical cluster scales such as R_{500} did not show a consistent signal, either; for example, a local deficit of X-ray sources was found at $2 < \tau < 3$ around 14 clusters of $0.43 < z < 1.05$ [3].

More recently, a $\sim 3\sigma$ excess of *Chandra* X-ray sources was reported [7] in a fairly narrow, $2 < \tau < 2.5$ range of

normalized radii around a small sample of five $z \sim 1$, mostly disturbed clusters. This signal is dominated by two clusters, each with about ten excess $2.0 < \tau < 2.5$ sources with respect to neighbouring bins. The excess sources show $10^{42.5}\text{ erg s}^{-1} \lesssim L_{0.5\text{ keV}}^{8.0\text{ keV}} \lesssim 10^{44}\text{ erg s}^{-1}$ luminosities, where energy or frequency subscripts (super-scripts) denote low (high) band limits, henceforth. These sources were again attributed to enhanced AGN activity, due to excessive galaxy mergers or gas stripping.

However, an excess of AGN over such a narrow range of radii at the outskirts of clusters would be unnatural, especially taking into account projection (and, in other studies, also stacking) effects. Indeed, the rate of galaxy mergers is thought to evolve quite gradually, rising well before the accreted galaxies reach the cluster outskirts, and remaining high after pericentric crossing [*e.g.*, 8]. AGN activity can be affected by the intracluster medium (ICM) through several channels, notably, in this context, by ram pressure stripping of hot halo gas [*e.g.*, 9], but these processes are thought to be important only once the galaxy approaches the central, $r \lesssim 1$ Mpc region of the cluster [8, and references therein].

Therefore, a sharp spike in the density of sources would indicate a localized, sudden change in the environment. Interestingly, the structure formation, or virial, shock of a galaxy cluster, long anticipated to lie in the $2 < \tau < 3$ range according to cosmological simulations [*e.g.*, 10, 11], provides a natural candidate for such a sharp environmental transition. Indeed, as an infalling object crosses the virial shock (VS), it should see the ambient pressure suddenly jump by orders of magnitude as the infalling surrounding plasma is violently slowed down and heated, accompanied by the generation of magnetic fields and shock-accelerated relativistic particles (cosmic rays, CRs) carrying a substantial fraction of the elevated thermal energy. While crossing a VS is unlikely to trigger an AGN, and the processes by which it could lead to the emergence of bright excess X-ray or radio sources may be a-priori unclear, the VS could explain at least the position and sharpness of the signal.

Moreover, recent studies have identified stacked VS signals in precisely the same $2 < \tau < 2.5$ region harboring the excess [7] X-ray sources. Such stacking analyses in-

^{*} Posthumously. Gideon Ilani was killed in action on December 10, 2023. This paper is based on his research.

[†] Institute of Astronomy and Astrophysics, Academia Sinica, PO Box 23-141, Taipei 10617, Taiwan

[‡] keshet.uri@gmail.com

An attractive model: simulating fuzzy dark matter with attractive self-interactions

Connor A. Painter¹, Michael Boylan-Kolchin¹, Philip Mocz^{2,3}, and Mark Vogelsberger⁴

¹*Department of Astronomy, The University of Texas at Austin, 2515 Speedway, Stop C1400, Austin, TX 78712-1205, USA*

²*Lawrence Livermore National Laboratory, 4 Ivy Lane, 7000 East Ave, Livermore, CA 94550, USA*

³*Department of Astrophysical Sciences, Princeton University, 4 Ivy Lane, Princeton, NJ 08544, USA*

⁴*Department of Physics, Kavli Institute for Astrophysics and Space Research, M.I.T., Cambridge, MA 02139, USA*

Accepted XXX. Received YYY; in original form ZZZ

ABSTRACT

Fuzzy Dark Matter (FDM) comprised of ultralight ($m \sim 10^{-22}$ eV) boson particles has received significant attention as a viable alternative to Cold Dark Matter (CDM), as it approximates CDM on large scales ($\gtrsim 1$ Mpc) while potentially resolving some of its small-scale problems via kiloparsec-scale quantum interference. However, the most basic FDM model, with one free parameter (the boson mass), is subject to a tension: small boson masses yield the desired cores of dwarf galaxies but underpredict structure in the Lyman- α forest, while large boson masses render FDM effectively identical to CDM. This *Catch-22* problem may be alleviated by considering an axion-like particle with attractive particle self-interactions. We simulate an idealized FDM halo with self-interactions parameterized by an energy decay constant $f \sim 10^{15}$ GeV related to the axion symmetry-breaking conjectured to solve the strong-CP problem in particle physics. We observe solitons, a hallmark of FDM, condensing within a broader halo envelope, and find that the density profile and soliton mass depend on self-interaction strength. We propose generalized formulae to extend those from previous works to include self-interactions. We also investigate a critical mass threshold predicted for strong interactions at which the soliton collapses into a compact, unresolved state. We find that the collapse happens quickly and its effects are initially contained to the central region of the halo.

Key words: galaxies: formation – galaxies: high-redshift – dark matter – cosmology: theory

1 INTRODUCTION

The particle nature of cosmological dark matter is still one of the most pressing unknowns in modern astrophysics. For decades, Cold Dark Matter (CDM) has prevailed as the leading theory, stating that dark matter particles are non-relativistic, collisionless, and dissipationless. CDM, as part of the Λ CDM paradigm, has reproduced observations of the Cosmic Microwave Background (Aghanim et al. 2020; Alam et al. 2021) and large-scale structure remarkably well (Vogelsberger et al. 2014a,b, 2020; Schaye et al. 2014; Springel et al. 2017). However, the simplest CDM simulations admit puzzling discrepancies with observations on the scale of dwarf galaxies (Bullock & Boylan-Kolchin 2017; Del Popolo & Le Delliou 2017; Sales et al. 2022). Problems actively debated in the literature include missing satellites (Klypin et al. 1999; Moore et al. 1999), density profile cores versus cusps (Moore 1994; Flores & Primack 1994; de Blok 2010), dark matter halos “too big to fail” to produce stars (Boylan-Kolchin et al. 2011; Garrison-Kimmel et al. 2014), and overly diverse galaxy rotation curves (Oman et al. 2015). Even though baryonic feedback has shown promise to remedy many of the inconsistencies when incorporated into Λ CDM simulations, the most commonly considered CDM particle candidates, Weakly In-

teracting Massive Particles (WIMPs) on the mass scale of GeV, have so far evaded discovery (Roszkowski et al. 2018). Small-scale inconsistencies along with non-detections of plausible particle candidates have fueled a search for alternative models.

A popular alternative to CDM is dark matter in the form of ultra-light boson particles of mass $m \sim 10^{-22}$ eV (Hu et al. 2000; Guzmán & Ureña-López 2003; Hui et al. 2017; Mocz et al. 2019; Burkert 2020; Niemeyer 2020; Hui 2021). This so-called Fuzzy Dark Matter (FDM) model approximates CDM on large scales (Widrow & Kaiser 1993; Kopp et al. 2017), but small-scale structure is altered by a “quantum pressure” tensor in the momentum equation (Schive et al. 2014a). The dark matter clusters under self-gravity with fluid-like properties, and dark waves generated on the de Broglie scale $\lambda_{dB} \equiv \frac{h}{mv} \sim \text{kpc}$ interfere to smooth over small-scale structure. This smoothing cuts off the dark matter power spectrum above a certain wavenumber (Hu et al. 2000), offering a natural explanation for the missing satellites predicted by CDM-only simulations. FDM also naturally addresses the cusp-core discrepancy: halos are characterized by cored central structures called *solitons* (Schive et al. 2014a,b) enveloped by a broader NFW-like power law drop-off in density (Navarro et al. 1996; Marsh & Pop 2015; Mocz et al. 2017). Further-

The LOFAR - eFEDS survey: The incidence of radio and X-ray AGN and the disk-jet connection*

Z. Igo^{1,2†}, A. Merloni¹, D. Hoang³, J. Buchner^{1,2}, T. Liu^{1,4}, M. Salvato^{1,2}, R. Arcodia⁵, S. Bellstedt⁶, M. Brüggen³, J. H. Croston⁷, F. de Gasperin^{3,8}, A. Georgakakis⁹, M. J. Hardcastle¹⁰, K. Nandra¹, Q. Ni¹, T. Pasini^{3,8}, T. Shimwell^{11,12}, J. Wolf¹³

¹ Max-Planck-Institut für Extraterrestrische Physik (MPE), Giessenbachstrasse 1, 85748 Garching bei München, Germany

² Exzellenzcluster ORIGINS, Boltzmannstr. 2, 85748, Garching, Germany

³ Hamburger Sternwarte, Gojenbergsweg 112, 21029 Hamburg, Germany

⁴ University of Science and Technology of China, No.96, JinZhai Road Baohe District, Hefei, Anhui, 230026, P.R.China

⁵ MIT Kavli Institute for Astrophysics and Space Research, Massachusetts Institute of Technology, Cambridge, MA 02139, USA

⁶ ICRAR, The University of Western Australia, 35 Stirling Highway, Crawley, WA 6009, Australia

⁷ School of Physical Sciences, The Open University, Walton Hall, Milton Keynes, MK7 6AA, United Kingdom

⁸ Istituto di Radioastronomia IRA-INAF, via Gobetti 101, 40129 Bologna, Italy

⁹ Institute for Astronomy and Astrophysics, National Observatory of Athens, V. Paulou and I. Metaxa, 11532, Greece

¹⁰ Centre for Astrophysics Research, University of Hertfordshire, College Lane, Hatfield AL10 9AB, UK

¹¹ ASTRON, the Netherlands Institute for Radio Astronomy, Oude Hoogeveensedijk 4, 7991 PD Dwingeloo, The Netherlands

¹² Leiden Observatory, Leiden University, PO Box 9513, NL-2300 RA, Leiden, The Netherlands

¹³ Max-Planck Institut für Astronomie, Königstuhl 17, 69117 Heidelberg

ABSTRACT

Context. Radio jets are present in a diverse sample of AGN. However, the mechanisms of jet powering are not fully understood, and it is yet unclear to what extent they obey mass-invariant scaling relations, similar to those found for the triggering and fuelling of X-ray selected AGN.

Aims. This work uses the multi-wavelength data in the eFEDS field observed by eROSITA/*Spectrum-Roentgen-Gamma* (SRG) and LOFAR to study the incidence of X-ray and radio AGN as a function of several stellar mass (M_*) normalised AGN power indicators.

Methods. A new sample of radio AGN from the LOFAR - eFEDS survey, with host galaxy counterparts from Legacy Survey DR9, is defined via a radio-excess relative to the star formation rates in their hosts. We further subdivide the sample into compact and complex radio morphologies. The subset matching to the well-characterised, highly complete spectroscopic GAMA09 galaxies ($0 < z < 0.4$) is used in this work. We release this value-added LOFAR-eFEDS catalogue*. The fraction of GAMA09 galaxies hosting radio, X-ray and both radio and X-ray AGN are calculated as a function of the specific black hole kinetic (λ_{jet}) and radiative (λ_{Edd}) power.

Results. Despite the soft-X-ray eROSITA selected sample, the incidence of X-ray AGN as a function of λ_{Edd} shows the same mass-invariance and power-law slope of -0.65 as found in past studies, once corrected for completeness. Across the M_* range probed, the incidence of compact radio AGN as a function of λ_{jet} is described by a power-law with constant slope, showing that it is not only high mass galaxies hosting high power jets and vice versa. This slope is steeper than that of the X-ray incidence, with a value around -1.5 . Furthermore, higher mass galaxies are more likely to host radio AGN across the λ_{jet} range, indicating some residual mass dependence of jet powering. Upon adding complex radio morphologies, including 34 FRIIs, three of which are giant radio galaxies, the incidence not only shows a larger mass dependence but also a jet power dependence, being clearly boosted at high λ_{jet} values. Importantly, the latter effect cannot be explained by such radio AGN residing in more dense environments (or more massive dark matter haloes). The similarity in the incidence of quiescent and star-forming radio AGN reveals that radio AGN are not only found in ‘red and dead’ galaxies. Overall, our incidence analysis reveals some fundamental statistical properties of radio AGN samples, but highlights a number of open questions on the use of a single radio luminosity–jet power conversion. We explore how different mass and accretion rate dependencies of the incidence can explain the observed results for varying disk-jet coupling models.

Key words. Accretion, accretion disks – Black hole physics – Galaxies: jets

1. Introduction

It is now widely accepted that supermassive black holes (SMBHs) populate the centres of galaxies and co-evolve with their hosts, undergoing different stages of feeding and feedback.




























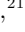

The sub-population of SMBHs which are actively accreting matter from the surrounding gas, usually in the form of an accretion disk, are called active galactic nuclei (AGN). Depending on their accretion rate, AGN exhibit different observational properties which we observe over more than ten decades of frequency from radio to gamma ray wavelengths (e.g. Alexander & Hickox 2012; Heckman & Best 2014; Hardcastle & Croston 2020, and references therein).

For highly accreting systems, with Eddington ratios ≥ 0.01 – 1, the situation is often thought to be well described in terms of

* The source catalogue is available at the CDS via anonymous ftp to cdsarc.u-strasbg.fr (130.79.128.5) or via <http://cdsweb.u-strasbg.fr/cgi-bin/qcat?J/A+A/> or on the LOFAR Surveys DR website: <https://lofar-surveys.org/efeds.html>

† e-mail: zigo@mpe.mpg.de

A NIRC*am*-dark galaxy detected with the MIRI/F1000W filter in the MIDIS/JADES Hubble Ultra Deep Field

PABLO G. PÉREZ-GONZÁLEZ ¹, PIERLUIGI RINALDI ², KARINA I. CAPUTI ², JAVIER ÁLVAREZ-MÁRQUEZ ¹,
MARIANNA ANNUNZIATELLA ¹, DANIAL LANGEROODI ³, THIBAUD MOUTARD ⁴, LEINDERT BOOGAARD ⁵,
EDOARDO IANI ², JENS MELINDER ⁶, LUCA COSTANTIN ¹, GÖRAN ÖSTLIN ⁶, LUIS COLINA ¹,
THOMAS R. GREVE ^{7,8,9}, GILLIAN WRIGHT ¹⁰, ALMUDENA ALONSO-HERRERO ¹¹, ARJAN BIK ⁶,
SARAH E. I. BOSMAN ^{12,13}, ALEJANDRO CRESPO GÓMEZ ¹, DANIEL DICKEN ¹⁰, ANDREAS ECKART ¹⁴,
MACARENA GARCÍA-MARÍN ¹⁵, STEVEN GILLMAN ^{7,8}, MANUEL GÜDEL ^{16,17}, THOMAS HENNING ⁵, JENS HJORTH ³,
IRIS JERMANN ^{7,8}, ÁLVARO LABIANO ¹⁸, ROMAIN A. MEYER ¹⁹, FLORIAN PEIßKER ¹⁴, JOHN P. PYE ²⁰,
THOMAS P. RAY ²¹, TUOMO TIKKANEN ²², FABIAN WALTER ⁵, AND PAUL P. VAN DER WERF ²³

¹Centro de Astrobiología (CAB), CSIC-INTA, Ctra. de Ajalvir km 4, Torrejón de Ardoz, E-28850, Madrid, Spain

²Kapteyn Astronomical Institute, University of Groningen, P.O. Box 800, 9700 AV Groningen, The Netherlands

³DARK, Niels Bohr Institute, University of Copenhagen, Jagtvej 155, 2200 Copenhagen, Denmark

⁴European Space Agency (ESA), European Space Astronomy Centre (ESAC), Camino Bajo del Castillo s/n, 28692 Villanueva de la Cañada, Madrid, Spain

⁵Max Planck Institut für Astronomie, Königstuhl 17, D-69117, Heidelberg, Germany

⁶Department of Astronomy, Stockholm University, Oscar Klein Centre, AlbaNova University Centre, 106 91 Stockholm, Sweden

⁷Cosmic Dawn Center (DAWN), Denmark

⁸DTU Space, Technical University of Denmark, Elektrovej, Building 328, 2800, Kgs. Lyngby, Denmark

⁹Dept. of Physics and Astronomy, University College London, Gower Street, London WC1E 6BT, United Kingdom

¹⁰UK Astronomy Technology Centre, Royal Observatory Edinburgh, Blackford Hill, Edinburgh EH9 3HJ, UK

¹¹Centro de Astrobiología (CAB), CSIC-INTA, Camino Bajo del Castillo s/n, E-28692 Villanueva de la Cañada, Madrid, Spain

¹²Institute for Theoretical Physics, Heidelberg University, Philosophenweg 12, D-69120, Heidelberg, Germany

¹³Max-Planck-Institut für Astronomie, Königstuhl 17, 69117 Heidelberg, Germany

¹⁴I. Physikalisches Institut der Universität zu Köln, Zùlpicher Str. 77, 50937 Köln, Germany

¹⁵European Space Agency, Space Telescope Science Institute, Baltimore, Maryland, USA

¹⁶Dept. of Astrophysics, University of Vienna, Türkenschanzstr 17, A-1180 Vienna, Austria

¹⁷ETH Zürich, Institute for Particle Physics and Astrophysics, Wolfgang-Pauli-Str. 27, 8093 Zürich, Switzerland

¹⁸Telespazio UK for the European Space Agency, ESAC, Camino Bajo del Castillo s/n, 28692 Villanueva de la Cañada, Spain

¹⁹Department of Astronomy, University of Geneva, Chemin Pegasi 51, 1290 Versoix, Switzerland

²⁰School of Physics & Astronomy, Space Research Centre, Space Park Leicester, University of Leicester, 92 Corporation Road, Leicester, LE4 5SP, UK

²¹Dublin Institute for Advanced Studies, 31 Fitzwilliam Place, D02 XF86, Dublin, Ireland

²²School of Physics & Astronomy, Space Research Centre, Space Park Leicester, University of Leicester, 92 Corporation Road, Leicester, LE4 5SP, UK

²³Leiden Observatory, Leiden University, P.O. Box 9513, 2300 RA Leiden, The Netherlands

ABSTRACT

We report the discovery of *Cerberus*, an extremely red object detected with the MIRI Deep Imaging Survey (MIDIS) observations in the F1000W filter of the Hubble Ultra Deep Field. The object is detected at $S/N \sim 6$, with F1000W ~ 27 mag, and it is extremely faint in both the NIRC*am* data gathered by the JWST Advanced Deep Extragalactic Survey, JADES, with ~ 30.5 mag 5σ upper limits in individual bands, as well as in the MIDIS F560W ultra deep data (~ 29 mag, 5σ). Analyzing the spectral energy distribution built with individual (low S/N) optical-to-mid-infrared filters and ($S/N \sim 5$) stacks, we discuss the possible nature of this red NIRC*am*-dark source using a battery of codes. We discard the possibility of *Cerberus* being a Solar System body based on the $< 0''.016$ proper motion in the 1-year apart JADES and MIDIS observations. A sub-stellar Galactic nature is deemed unlikely, given that the *Cerberus*' relatively flat NIRC*am*-to-NIRC*am* and very red NIRC*am*-to-MIRI flux ratios are not consistent with any brown dwarf model. The extragalactic nature of *Cerberus* offers 3 possibilities: (1) A $z \sim 0.4$ galaxy with strong emission from polycyclic aromatic hydrocarbons; the

Effects of anisotropy in an anisotropic extension of w CDM model

Vikrant Yadav,^{1,*} Santosh Kumar Yadav,^{2,†} and Rajpal^{1,‡}

¹*School of Basic and Applied Sciences, Raffles University, Neemrana - 301705, Rajasthan, India*

²*School of CS & AI, SR University, Warangal-506371, Telangana, India*

In this paper, we derive observational constraints on an anisotropic w CDM model from observational data including Baryonic Acoustic Oscillations (BAOs), Cosmic Chronometer (CC), Big Bang Nucleosynthesis (BBN), Pantheon Plus (PP) compilation of Type Ia supernovae, and SH0ES Cepheid host distance anchors. We find that anisotropy is of the order 10^{-13} , and its presence in the w CDM model reduces H_0 tension by $\sim 2\sigma$ and $\sim 1\sigma$ in the analyses with BAO+CC+BBN+PP and BAO+CC+BBN+PPSH0ES data combinations, respectively. In both analyses, the quintessence form of dark energy is favored at 95% CL.

I. INTRODUCTION

Our Universe is expanding with accelerated rate of expansion as observed from type Ia supernovae (SNe Ia) observations [1, 2]. Later on, various other observations such as the large scale structure (LSS), the Baryonic Acoustic Oscillations (BAOs) and the cosmic microwave background (CMB) supported this observation. A number of cosmological models have been proposed/investigated in the literature to help us comprehend the dynamics of the universe. But, among all cosmological models, Λ CDM has proven to be the simplest mathematical model which has widely been accepted by the cosmological community and referred to as the standard cosmological model of cosmology. Basically, this model is composed of two main parts: cold (non-relativistic) dark matter (CDM) which is the reason behind the structure formation, and dark energy (DE) in the form of cosmological constant (Λ) which causes the late time accelerated expansion of Universe. The Λ CDM model provides an excellent fit across a broad range of scales and epochs [3–7], and successfully describes late-time accelerated expansion of the Universe [8, 9]. Despite the excellent fit to the current available cosmological observations, the model faces several theoretical and observational challenges. For instance, the nature of DE is not known accurately so far, and within the Λ CDM paradigm, DE is regarded as the cosmological constant in its most basic form, lacking any solid physical foundation. Except for its typical gravitational interactions with other components, the exact nature of dark matter remains unknown. Also, there is no concrete explanation of ‘coincidence problem’ stating why, despite having very distinct cosmic evolutions, do the dark matter densities and the DE have the same order? Is this coincidence indicating the possibility for interaction between the dark sector components? Up to what extent the cosmological principle has been tested? Is the Universe homogeneous and isotropic at cosmic scales?

Further, a few indications in the observations point towards the need to expand the Λ CDM model in order to account for the growing conflicts between measurements made at early (high redshifts) and late (low redshifts) Universe [10, 11]. The Hubble constant, H_0 , which represents the Universe’s current rate of expansion, has the greatest statistically significant tension. The Hubble tension appears when we compare the value of H_0 predicted by CMB measurements within the Λ CDM framework and the direct local distance ladder measurements, that is, the one estimated by the Cepheid calibrated supernovae SNe Ia. In particular, the Hubble tension is referred to as the disagreement at 5σ between the latest SH0ES (Supernovae and H_0 for the equation of state (EoS) of DE) collaboration [12] constraint, $H_0^{\text{R}22} = (73.04 \pm 1.04) \text{ km s}^{-1} \text{ Mpc}^{-1}$ at 68% confidence level (CL), based on the supernovae calibrated by Cepheids, and the *Planck* collaboration [3] value, $H_0 = (67.27 \pm 0.60) \text{ km s}^{-1} \text{ Mpc}^{-1}$ at 68% CL. The Hubble tension may be defined as a difference between the observed value of H_0 from two sets of observations: (i) all of the direct late time Λ CDM independent measurements, and (ii) all of the indirect model dependent estimations at early times. In general, the value of H_0 obtained at late times is greater than the one obtained at early times.

This disparity could indicate the existence of novel physics outside of the Λ CDM cosmology [13–18]. In the literature, a number of extensions of Λ CDM have been suggested to resolve the H_0 tension. These extensions include but not limited to: DM-DE interactions [19–25]; decaying DM [26–29]; introducing Early DE [30–34]; and introducing a sign-switching DE at intermediate redshifts ($z \sim 2$) [35–39]. The current status on H_0 tension and possible solutions can be found in recent review articles [40–43].

The Cosmological Principle (CP), which asserts that the Universe is statistically homogenous and isotropic in space and matter on vast scales (100Mpc), is one of the fundamental tenets of Λ CDM cosmology. Mathematically, such a universe is described by the Friedmann-Lemaître-Robertson-Walker (FLRW) space-time metric, in which all three of the metric’s spatial orthogonal components are functions of cosmic time (t) exclusively. This is the primary space-time metric that facilitates the cre-

* vikuyd@gmail.com

† sky91bbaulko@gmail.com

‡ rajpal05041985@gmail.com